TEMPERATURE AND PRESSURE EFFECTS ON TISSUE SEALING AND PROTEIN DENATURATION

A THESIS
SUBMITTED TO THE FACULTY OF THE
UNIVERSITY OF MINNESOTA
BY

JOEL ROSS SCHEUMANN

IN PARTIAL FULFILLMENT OF THE REQUIREMENTS
FOR THE DEGREE OF
MASTER OF SCIENCE IN MECHANICAL ENGINEERING

JOHN C. BISCHOF, ADVISER

MAY 2016

ACKNOWLEDGEMENTS

My labmates in the Bio Heat and Mass Transfer Lab: Yiru Wang, Kanav Khosla, Shaunak Phatak, Zhe Gao, Qi Shao, Feng Liu, Navid Manuchehrabadi, Li Zhan, Priyatanu Roy, Dushyant Mehra, Jeunghwan Choi, Michael Etheridge, Connie Chung, and Zhengpeng Qin. I am thankful for your encouragement, teaching, and friendship during my time in the lab.

I am thankful for Dr. Victor Barocas for collaborating with the Ethicon project on the mechanical properties of the tissue. His students, Hallie Wagner and Nathan Cal, were quite beneficial in teaching me how to prepare samples and thinking about the project. Additionally, I am thankful for Dr. Paul Iazzio's leadership in the Visible Heart Lab which provided carotid arteries for useful measurements. I am thankful for constructive conversations with Dr. Durfee in development of the electrical component of the Thermal Jig. Also, I am thankful for the coordination from Brenda Konair, Christina Larson, and Nicholas Burrows who helped me get rat tails from the Research Animal Resources (RAR) facility. In addition to the RAR, Qi Shao helped me get rat tails from the Cancer Animal Core. Thank you for your provision.

Also, former UMN Prof. Jeff Vogel was instrumental in talking with me about pursuing further schooling. For that, I am thankful.

Also, I am thankful for Ethicon and representatives Peter Shires and Mark Davison for their collaboration, support, and useful discussion. Mark reliably coordinated valuable tissue shipments for measurements which enables many experiments.

I am thankful for Bing Luo who provided insight into FTIR and helped me make initial measurements at the Characterization Facility in Shepherd Labaortories. Also, I am thankful for Wim Wolkers who helped me figure out how to calculate protein denaturation and helped me process many runs of denaturation measurements. Thanks to Minsoo Kim who helped me develop a standard operating procedure for the FTIR procedure and a protein denaturation MATLAB script. Also, I am thankful for Mike Jensen who provided useful tips in developing the design of the mechanical portion of the Thermal Jig.

Additionally, it has been a blessing to have Dr. Bischof as my adviser for my time at UMN. He has pushed me to pursue excellence and diligence both in my research and studies. Many conversations have encouraged me to pursue ventures without fear of making mistakes.

Finally, I am thankful for my parents, Leroy and Joyce Scheumann, and my siblings, Joshua, Julianna, Jonathan, Jeremiah, Joseph, Jesse, and Josiah, who have been a continual encouragement to me throughout my life.

ABSTRACT

Tissue sealing is an attractive method for tissue sealing in laparoscopic (minimally invasive) surgeries as it does not leave any materials in a patient's body. Most of the research for tissue sealing has been concerned on the end-goal results of burst pressure, and not as much time has been spent investigating the more fundamental properties of tissue sealing which include temperature, pressure, time, vessel composition, disease state, and sealing modality (i.e., thermal, radiofrequency, and ultrasonic). This work investigates temperature and pressure by studying how these parameters affect collagen denaturation and burst pressure. Ethicon provided carotid arteries that were sealed under controlled temperature and pressure with a constructed Thermal Jig. Additionally, denaturation of collagen was studied with the use of carotid arteries and rat tail tendons with the use of FTIR spectroscopy under temperature and pressure control from an ATR accessory. From the research, it was determined that the burst pressure was highest with the temperature of 140ºC. Changing the weight from 20lb to 50lb did not yield any significant difference. The results for burst pressure from the treatments of 100ºC;80psi;30s, 100ºC;330psi;30s, 140ºC;80psi;30s, and 140ºC;330psi;30s were 188.4 ± 55.3mm Hg, 439.9 ± 232.6mm Hg, 647.3 ± 241.3mm Hg, and 678.1 ± 153.7mm Hg, respectively. Denaturation onset was observed to be delayed with the application of pressure. For rat tail tendon, denaturation onset was observed to be 58.0 ± 2.5ºC and 60.1 ± 4.9ºC for loads of 0N and 2N, respectively. For carotid artery, the denaturation onset was observed to be 59.8 ± 0.7ºC, 59.8 ± 1.9ºC, 79.1 ± 4.3ºC, indeterminable, and indeterminable for loads of 0N, 2N, 10N, 20N, and 50N, respectively. To form an effective seal one must increase the temperature above 100ºC. Additionally, the denaturation was delayed significantly as the load was increased. This mechanical pressure correlates with results from osmotic pressure that also cause a delay in protein denaturation. Future work should investigate protein denaturation to higher temperature and tissue fusion by varying disease state of arteries, tissue composition (i.e., collagen and elastin content), and sealing time.

TABLE OF CONTENTS

LIST OF TABLES

LIST OF FIGURES

Temperature and Pressure Effects on Tissue Denaturation and Artery Sealing

1. INTRODUCTION

Tissue sealing is an attractive option for laparoscopic surgeries as opposed to using suture, clips, or staples. Additionally, laparoscopic surgery has faster healing times than open surgery. Tissue sealing devices have been developed despite a lack of understanding the mechanisms of action in the sealing process. This study is divided into two parts. The first part will test the optimal conditions for artery sealing by varying temperature and pressure. The second part will investigate how protein denaturation in collagen is affected by heat and pressure.

1.1 Tissue Sealing Overview

Tissue sealing is some combination of forcing tissue together, heating the tissue up, maintaining both temperature and pressure over a certain amount of time and then removing the pressure and temperature. What remains is a permanent seal of tissue. Many companies are around that make similar kinds of devices. The main companies are Medtronic (LigaSure^{TM}), Ethicon (ENSEAL^{TM}), and Gyrus (Gyrus^{TM}). These companies make a variety of tissue sealing devices which include bipolar and ultrasound energy sources. Table 1 shows a summary of these sealing modalities.

Table 1: Summary of Tissue Sealing Modalities

Tissue Sealing Modality	Description of Modality	Advantage	Disadvantage	Cost
Mechanical	Mechanical methods can be broken up into three main categories: collagen-based, suture-based, and staples and clips [1]	Clips are effective in providing a strong seal [2]	Applying these mechanical means can be tedious [3] and they may migrate after placement [4, 5]	Stapler: $300/each; Cartridge: $100/each [6]
Bipolar	A bipolar device uses two electrodes for focusing the radiofrequency energy by having the tissue clamped by both electrodes. The energy passes from one electrode to the other, and the tissue heats up due to its impedance. The generator of the bipolar device monitors this tissue impedance and changes the energy output based its algorithm in order to provide an effective seal [7]	Thermal spread is less in bipolar than monopolar systems [8]	Bipolar devices have the added danger of sticking to adjacent tissue because of the hot bipolar device [9]	LigaSure device ($506) Force Triad Generator (with LigaSure): $36,050 ENSEAL device: $425 ENSEAL Generator: $11,500 [10]
Ultrasonic	Harmonic scalpels simultaneous cut and seal vessels by breaking up hydrogen bonds in tissue proteins with a vibrating titanium blade at 55,000 Hz [10-12]	Leaves small thermal spread after closing vessels [13]	Can only transect vessels up to 5mm [14]	Harmonic ACE device ($482) Harmonic Generator: $15,750 [10]

A summary of the burst pressure literature values of the HarmonicACE, ENSEAL, and LigaSure devices are shown in Figure 1 below.

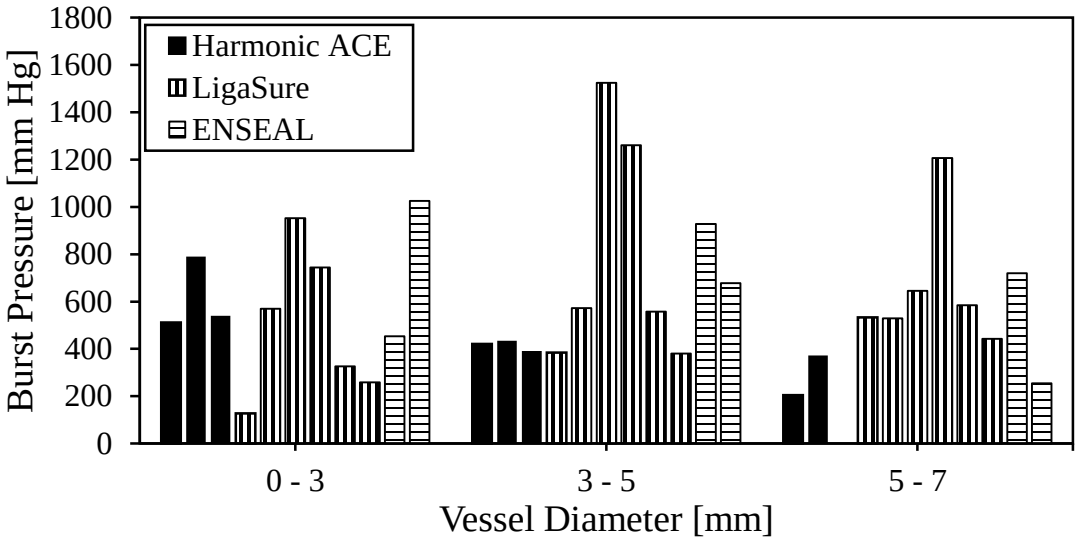

Figure 1: Review of Burst Pressure from Common Devices where each of the bars correspond to a separate study [2, 14-21]

Additionally, these tissue sealing devices have been used in a number of surgeries which include cholecystectomy, hysterectomy, bullectomy, and splenectomy. Table 2 shows the surgeries that have been used with each device.

Table 2: Summary of Surgeries performed with Various Sealing Devices

Manufacturer	Device Name	Surgery Performed
Ethicon (Cincinnati, OH, USA)	Harmonic ACE™	Bullectomy [22, 23] Cystic Duct Closure [24] Cholecystectomy [25, 26] Thyroidectomy [27, 28] Gastrectomy [29] Radical Prostatectomy [30]
Medtronic (Dublin, Ireland)	LigaSure™	Hemorrhoidectomy [31] Colectomy [32] Radical Prostatectomy [33] Cystic Duct Closure [24, 34, 35] Hysterectomy [36, 37] Splenectomy [5, 38] Liver Resection [39, 40] Pulmonary Resection [22, 23]
ERBE (Tübingen, Germany)	BiClamp™	Hysterectomy [41, 42] Thyroidectomy [43] Pulmonary Resection [44] Tonsillectomy [45]
Ethicon (Cincinnati, OH, USA)	ENSEAL™	Cholecystectomy [46] Cryptorchidectomy and ovariectomy [47] Nephrectomy [48] Hysterectomy [49] Colectomy [50]

The above table shows many surgeries that remove either partial or whole organs. Arteries and veins sustain organs by transporting blood to them. These arteries need to be cut and sealed shut when extracting the organ. Thus, the need arises for a device to both seal (i.e., close off the vessel and sustain a pressure level more than normal blood pressure) and cut the arteries. Figure 2 shows a simple diagram of an organ connected to blood vessels.

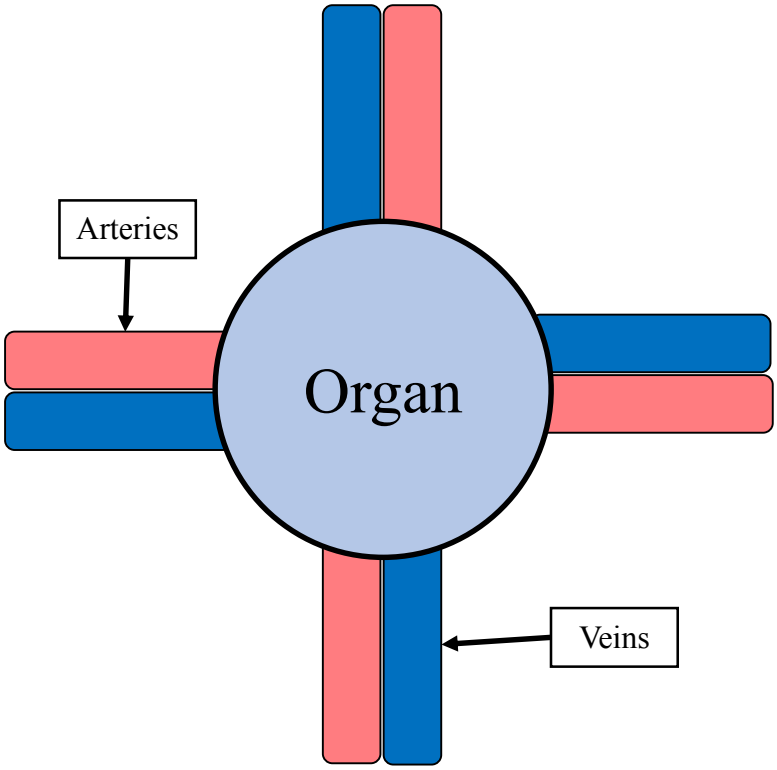

Figure 2: Model of Organ Connected to Arteries and Veins

The following sections will describe the components of tissue sealing, the work other researchers have done in the field of tissue fusion, and the components of arteries and how this will affect the current study.

1.1.1 Components of Tissue Seal

This work focuses on sealing arteries as these are sealed frequently in surgical procedures. A sealing device needs to apply both pressure and heat to both sides of the artery in order to form a seal. Important factors for artery sealing are the ratio of collagen to elastin in the artery, water content of the artery, apposition force, and temperature applied to the artery. First, the collagen-elastin ratio has a positive correlation with seal strength

[7]. Second, greater arterial water content resulted in greater seal strength [51]. Third, apposition force is necessary for artery sealing, but the seal does not hold at either very high or low apposition force [52]. Finally, temperature has a positive correlation with seal strength [53, 54].

1.1.2 Literature Review of Tissue Sealing

The Advanced Medical Technologies Laboratory (AMTL) in Boulder, CO has investigated the causes of tissue sealing. They have investigated the already mentioned water effect in sealing [51]. Additionally, they were able to measure the temperature of a tissue sealing medical device [55]. In an additional study, the ATML group varied the applied temperature to the tissue from 120ºC – 170ºC and the time from 300 – 3000ms at a constant temperature of 170ºC [54]. Similarly, Reyes, et al. varied temperature from 60 – 90ºC and found that burst pressure correlated positively with temperature and apposition force [53]. Also, Cezo, from the AMTL group, showed that ex vivo burst pressure is greater than in vivo burst pressure [56]. Finally, the AMTL group studied how apposition force affects the mechanical strength of arteries [52].

1.2 Tissue Vasculature Overview

Arteries are composed of three main components going from the innermost to the outermost: intima, media, and adventitia [57]. The intima, media, and adventitia are composed of cells such as endothelial and smooth muscle and an extracellular matrix (ECM) which contains important proteins such as collagen and elastin. Collagen and elastin provide most of the mechanical structure of an artery [58]. Carotid arteries, used in this study, are composed approximately of 22% collagen and 17% elastin within the media [59].

Type I collagen is the most abundant protein in the human body and makes up approximately 30% of total protein mass [60]. Additionally, the adventitia contains the largest amount of collagen [58]. Collagen and elastin content varies depending on artery movement. For example, abdominal arteries that move very little have large amounts of collagen whereas femoral arteries that have a large range of motion have large amounts of elastin [7]. Additionally, elastin is very prominent in arteries. The elastin content in carotid arteries changes depending on how close one is to the heart. Pearce and Thomsen

showed that elastin content is more dense in proximal than distal carotid arteries [61] shown in Figure 3.

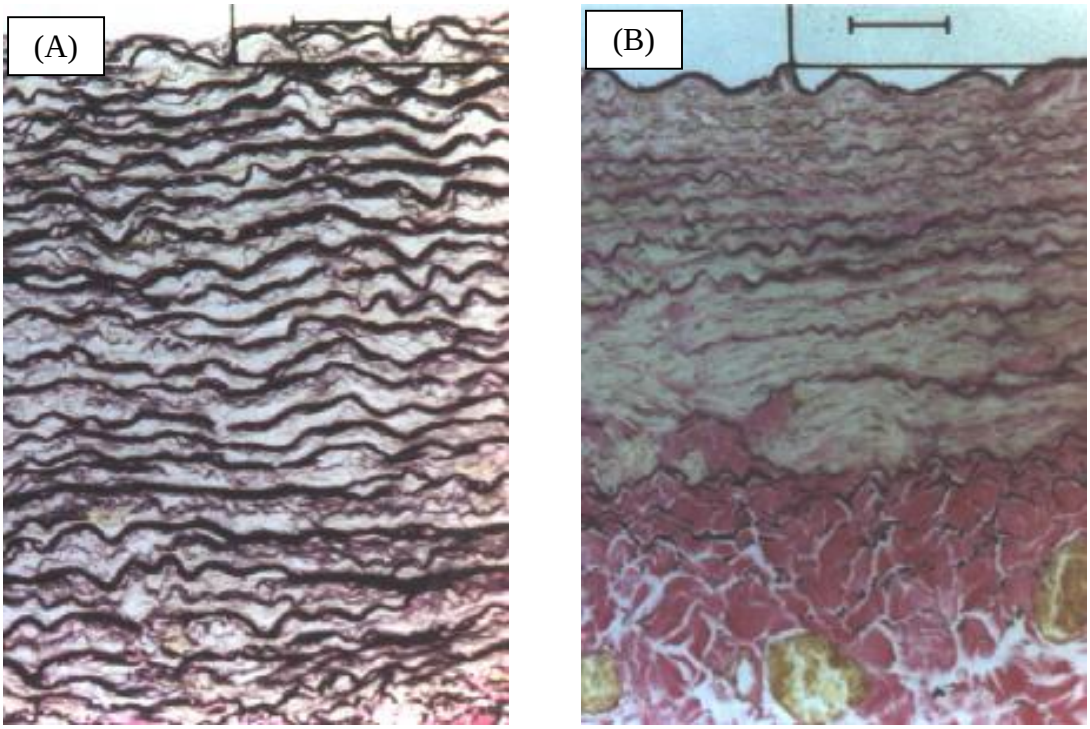

Figure 3: Histology of (A) proximal and (B) middle carotid arteries. Elastin is shown as black and collagen shows up as pink. Histology completed by Dr. Sharon Thomsen. The top of the picture is the intima of the artery.

Thus, it is imperative to understand how these proteins respond to temperature and pressure. This understanding will enable researchers to understand how different energy treatments affect arteries. This work will focus on collagen.

1.2.1 Collagen Response to Temperature

Collagen responds to heating by denaturing. Denaturation refers to the change from a soluble to insoluble state. A common example of protein denaturation is the thickening of egg whites due to heating [62, 63]. Collagen denaturation occurs around 60ºC whereas elastin denatures at higher temperatures in the range of 118 – 130ºC [64, 65]. In heat denaturation, Miles [66] used the method of differential scanning calorimetry to show that heat denaturation is irreversible with the model of rat tail tendon. Thus, once the protein has been denatured by heat, it is not possible to re-nature the protein.

1.2.2 Collagen Response to Osmotic Pressure

By using dehydration methods of freeze/thaw [67] and cross-linking with glutaraldehyde, hexamethylene diisocyanate (HMDC), and malondialdehyde (MDA) [68], the protein stabilizes which is indicated by the increased denaturation onset temperature. Osmotic pressure [67] with mannitol solutions causes the onset denaturation temperature also to increase. Work done here will show the stabilizing effect of mechanical pressure.

1.3 Relationship between Collagen Denaturation and Tissue Fusion

It is important to understand how collagen and elastin respond to temperature and pressure as these proteins make up a significant portion of the vasculature. Temperature and pressure are the primary variables involved in affecting the tissue during a sealing event. Commercial sealing devices apply temperature well above the needed threshold to denature collagen. Many papers denote the observation that protein denaturation is involved when making a seal [3, 17, 53, 69, 70].

1.4 Benefit of Below Work to Tissue Fusion Understanding

The AMTL group in Boulder, CO run by Dr. Mark Rentschler investigated the amount of temperature, pressure and time it takes to form a sufficient seal. An understanding how pressure and temperature affect the denaturation of collagen is lacking. This work will seek to fill this gap.

2. METHODS

This section will cover two parts. First, the methods used in sealing and testing the strength of those arteries will be presented. Second, the methods used in testing rat tail tendon and carotid arteries with FTIR will be presented.

2.1 ENSEAL Device

The ENSEAL device from Ethicon (Cincinnati, OH) is a bipolar electrocautery device for sealing tissue [71]. It is described as a bipolar device as it uses two electrodes through which electric current is passed in a controlled manner. Figure 4 shows the device used by Ethicon.

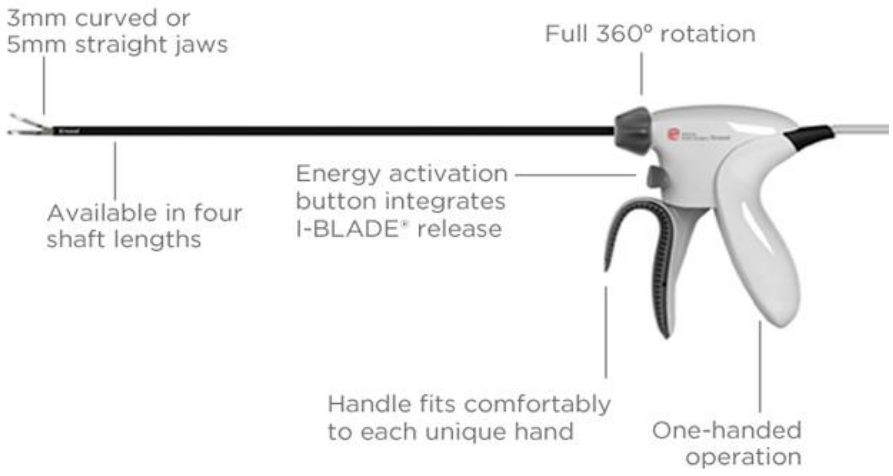

Figure 4: Ethicon ENSEAL Device[72]

When the product is activated, current flows between the upper and lower jaws of the device. The tissue acts as an electrical impedance and heats up through electrical resistance.

Figure 5 shows a zoomed-in view of the ENSEAL jaws.

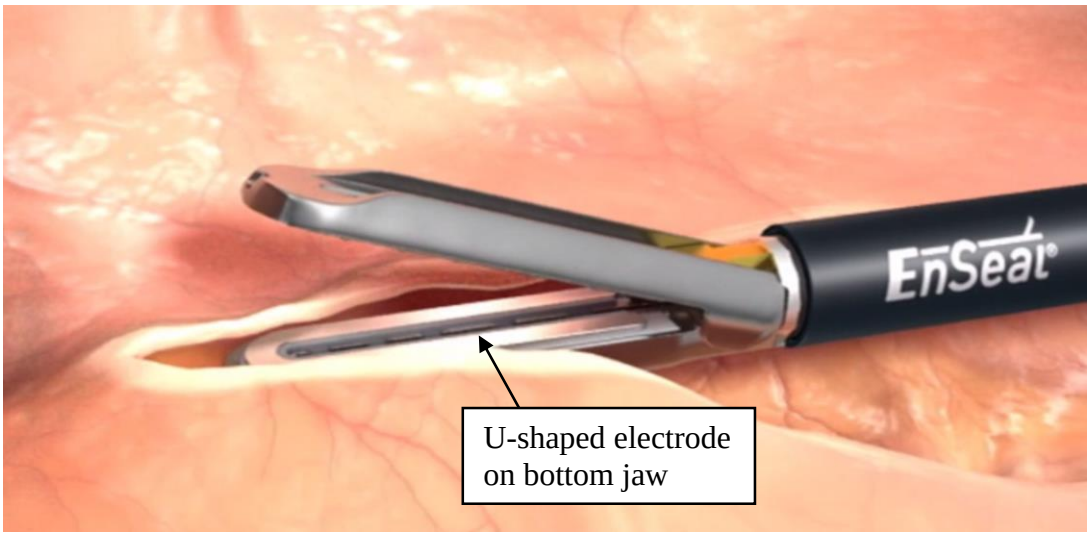

Figure 5: Zoomed-in image of ENSEAL jaws[73]

The heating component of the device takes place along the U-shaped portion of the jaws, and the tissue is cut by the "I-blade" which runs in the middle of the U-shaped electrode. Figure 6 shows the "I-blade" advancing through the ENSEAL device.

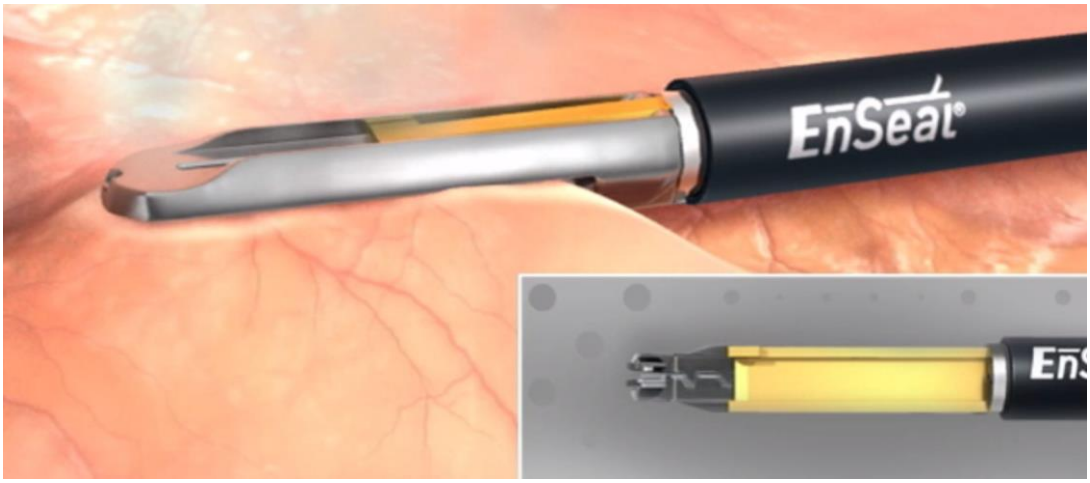

Figure 6: View of "I-blade" technology[73]

The electrode configuration is shown below in Figure 7. This offset electrode design is for the purpose of reducing thermal spread to adjacent vasculature. The ENSEAL device uses a generator to supply the electricity, and the temperature of the tissue is controlled through the Positive Temperature Control (PTC) component located in the upper jaw of the device in Figure 7. This PTC technology is designed to maintain the tissue temperature around 100ºC by reducing its electrical conductivity after exceeding 100ºC. This enables the device to maintain a uniform temperature across the affected tissue [73].

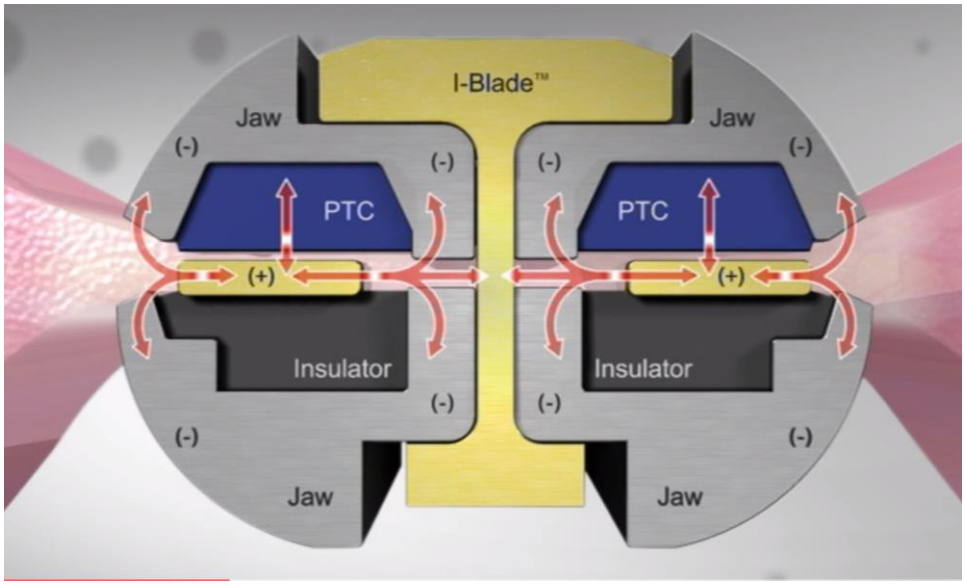

Figure 7: Electrode design of Ethicon ENSEAL which show the electrical current pathways [73]

The ENSEAL device works by closing the jaws of the device over the tissue. Once closed, the energy activation button needs to be pressed to activate the generator. De-pressing the button also allows the I-blade to move. The generator audibly announces to the user that the device is in use after depressing the button, and it continues to beep through the duration of the treatment. It signals the completion of the treatment by giving a distinct tone. While holding the power button, the user needs to advance the I-blade to cut the tissue. The total process should take approximately ten seconds.

2.2 Thermal Jig

The ENSEAL device is able to control the power applied to the tissue, but the ENSEAL device is not able to very precisely control the applied pressure and temperature. In order to circumvent this issue, a thermal jig was constructed to mimic the design of the ENSEAL and to control pressure, temperature, and time. For structure, the Thermal Jig can be divided into two main segments: electrical power and structural frame.

2.2.1 Electrical Power:

The Thermal Jig uses resistance heating to supply the energy for the tissue sealing process. The electrical components are described in Table 3 below.

Table 3: Electrical Components for the Thermal Jig

Description	**Distributor**	**Part No.**	**Quantity**
T-Type Thermocouple 0.076mm (0.003in.) diameter	OMEGA	5TC-TT-T-40-36	Two thermocouples
VT26 Fuzzy Enhanced Pid Controller	Accuthermo	VT4826-T-R-N-N-A	Two temperature controllers
Kapton Standard Heater	BIRK	BK3500-28.8-L12-06	Two kapton heaters
9.6”x10”x3.9” Aluminum Box	Mouser	546-1402K	One box
AC Receptacle	Digi-Key	Q212-ND	One receptacle
Fan AC 60x30mm 115V	Mouser	OA60AP-11-1WB	Two fans
AC/DC CONVERTER 12V 25W	Digi-Key	285-1884-ND	One AC/DC Converter
SPST, Off-On; 15 Amps, Solder Lug	McMaster	7343K711	One switch
Panel-Mount Thermocouple Connection Strip,	McMaster	3921K23	One panel mount with two connections

As explained in Table 3 above, the electrical components consist of two temperature controllers (Part No.: VT4826TRNNA; Distributor: Accuthermo; Freemont, CA). Additionally, two T-Type thermocouples (Model No.: 5TC-TT-T-40-36; Distributor: OMEGA; Distributor Location: Stamford, CT) were used in conjunction with the temperature controllers to control the temperature. The Accuthermo controller limited the temperature setting to 160ºC. In order to heat the sample, two kapton heaters (Model No.: BK3500-28.8-L12-06; Distributor: Birk Mfg. Distributor Location: East Lyme, CT); were used to heat through resistance heating. The housing for the electronics was a 9.6”x10”x3.9” Aluminum box (Part No.: 546-1402K; Distributor: Mouser; Mansfield, TX). AC power was routed through an AC receptacle (Part No.: Q212-ND; Distributor: Digi-Key; Thief River Falls, MN). The front view of the housing of the electrical components is show in Figure 8.

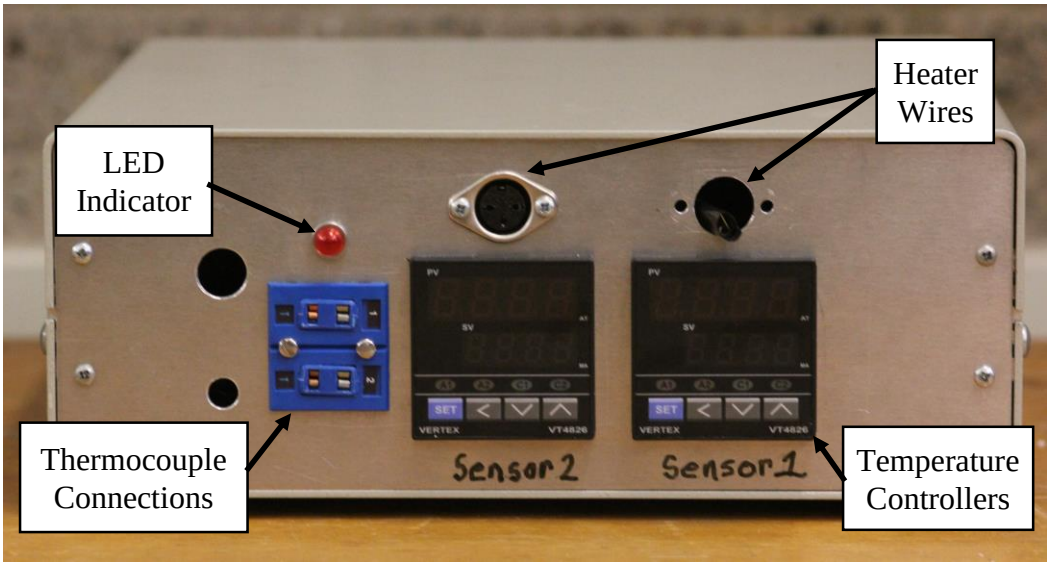

Figure 8: Front View of Electrical Housing

The temperature controller and the two cooling fans (Part No.: OA60AP-11-1WB; Distributer: Mouser, Mansfield, TX) were powered by 120 AC power while the LED indicator (Part No.: 2779K5; Distributor: McMaster-Carr; Elmhurst, Il) and the two kapton heaters were powered through 12V DC power. The AC power was converted to DC power through a AC-DC power supply (Part No.: 285-1884-ND; Distributor: Digi-Key;

Thief River Falls, MN). The inside of the electrical housing is shown below in Figure 9 which shows the internal wiring of the heater box.

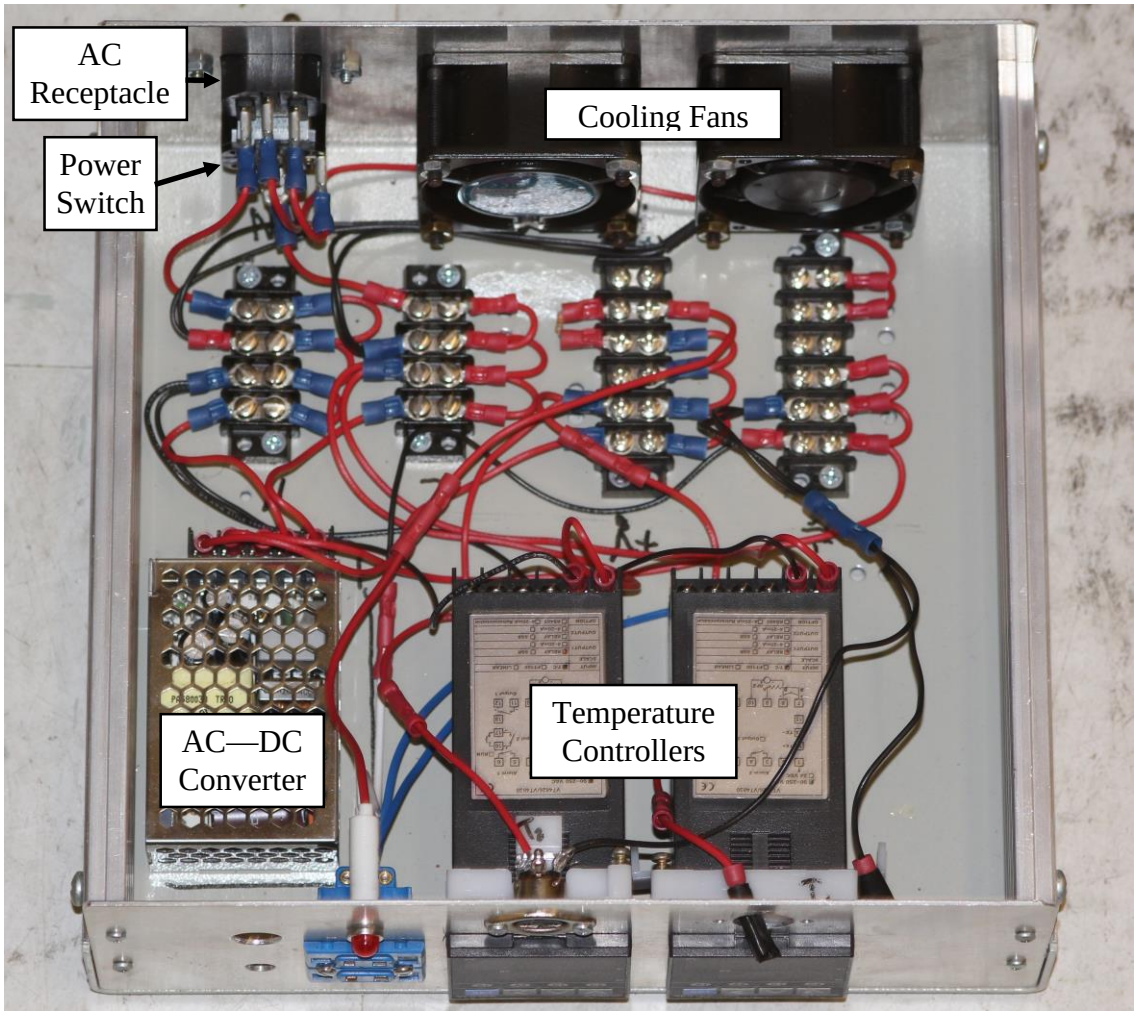

Figure 9: Internal Wiring of Electrical Heater Box

2.2.2 Mechanical Component

The mechanical components are summarized in Table 4 below.

Table 4: Mechanical Components of the Thermal Jig

Description	Distributor	Part No.	Quantity
PEEK – 0.5in. x 3in. x 12in.	McMaster	9089K128	One bar
Aluminum – 0.5in. x 3in. x 12in.	McMaster	8975K513	One bar
Steel Shafts – 0.25in Diameter x 6in.	McMaster	6061K11	Two shafts
Rulon J Bushings – 0.25in. shaft Diameter x 0.5in. length	McMaster	6377K12	Four bushings
Set screws – 8-32 x 0.5in.	McMaster	92158A205	One pack of 25 set screws
Thermal Conductive Epoxy	Mouser	517-TC-2810-37ML	One tube

The mechanical portion has two plates, a top and bottom plate. These are made of Polyether ether kertone (PEEK) (Model No.: 9089K128; Distributor: McMaster-Carr; Distributor Location: Elmhurst, Il). The bottom plate has two 8-32 x 0.5” set screws (Model No.: 94355A194; Distributor: McMaster-Carr; Distributor Location: Elmhurst, Il) which fixes two 0.25” x 6” 1566 steel shafts (Model No.: 6061K11; Distributor: McMaster-Carr; Distributor Location: Elmhurst, Il) which keeps the top plate in line with the bottom plate so the two heater components line up with each other. The top plate has Rulon J bushings (Model No.: 6377K12; Distributor: McMaster-Carr; Distributor Location: Elmhurst, Il) to enable smooth sliding of the top plate. Both the bottom and top plate have 0.25” protrusions of Peek on which the heater and aluminum (Model No.: 8975K513; Distributor: McMaster-Carr; Distributor Location: Elmhurst, Il) are placed and fixed with a 3M Thermally Conductive Adhesive (Model No.: TC-2810; Distributor: Mouser; Distributor Location: Mansfield, TX) below in Figure 10

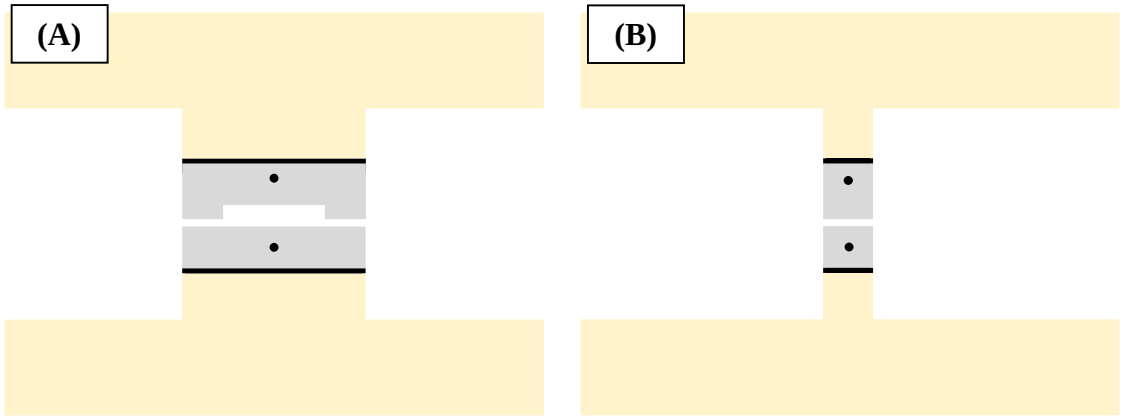

Figure 10: (A) Front view of Thermal Jig top and bottom plates; (B) Side View of Thermal Jig. Both views show the tan colored-PEEK baseplate with the black heater. Also, the grey is for the aluminum block with the black dots representing the embedded thermocouples.

Figure 11 below shows Top Plate of the Thermal Jig which contains the components described above in Table 4.

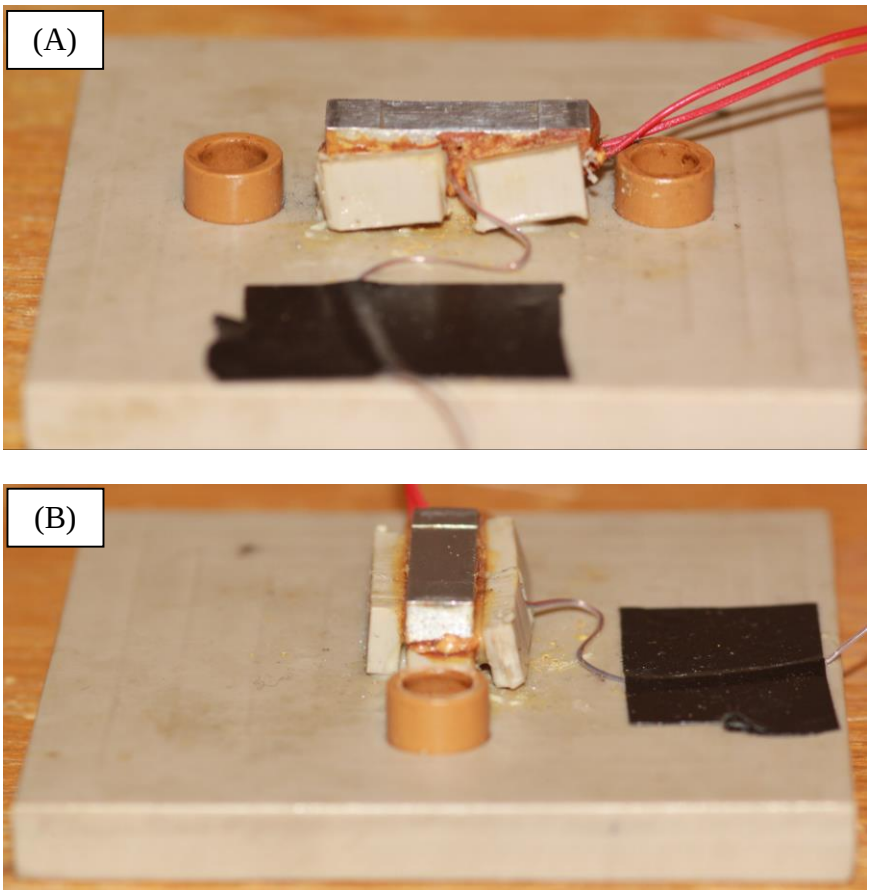

Figure 11: Top Plate of Thermal Jig with two views shown in Panel (A) and Panel (B)

Similarly, the bottom plate of the Thermal Jig is shown in Figure 12 with a nearly identical design with the exception of a flat aluminum surface as opposed to the top plate which has a 0.006in. milled step in its aluminum block.

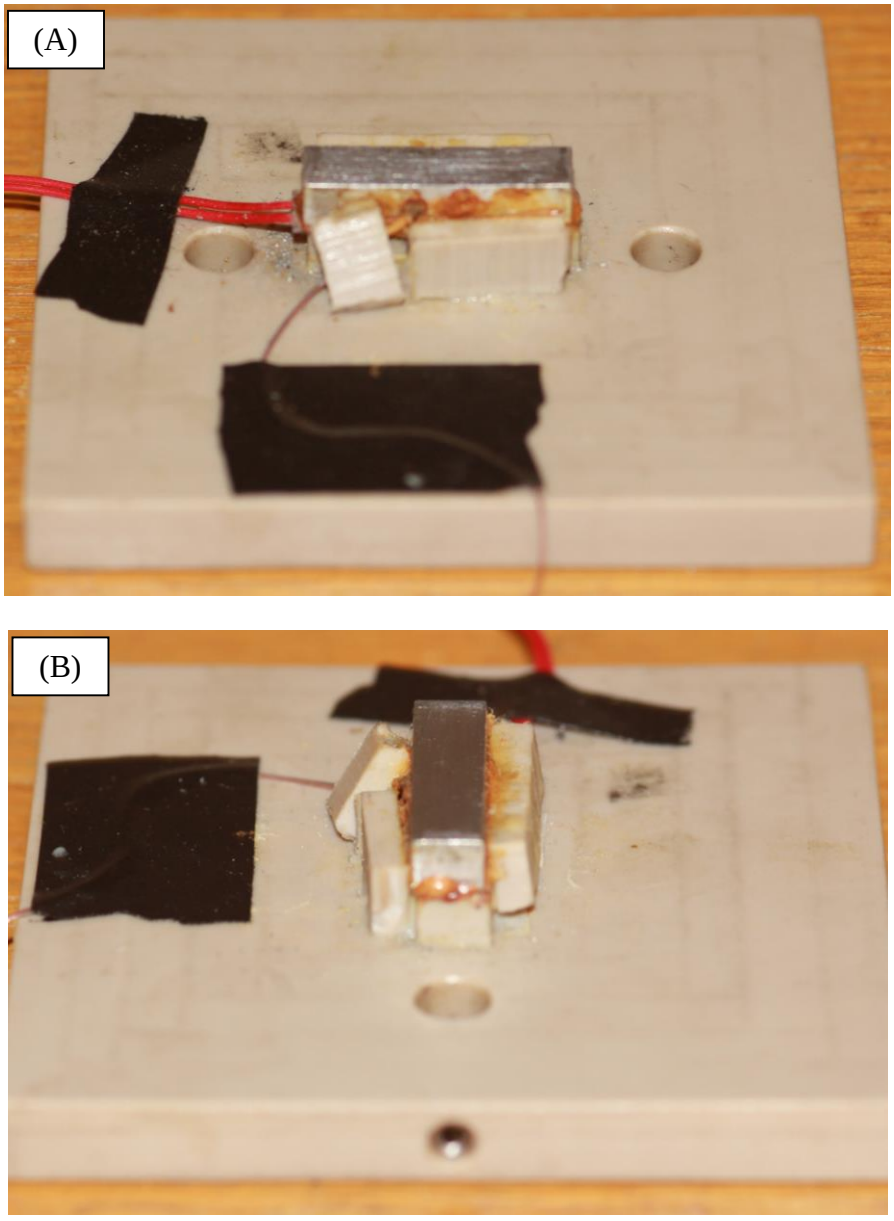

Figure 12: Bottom Plate of Thermal Jig with rotated views shown in Panels (A) and (B)

Connecting the steel shafts to the bottom plate and placing the top plate on the steel guides, Figure 13 shows the setup of the Thermal Jig with both the Mechanical and Electrical Components.

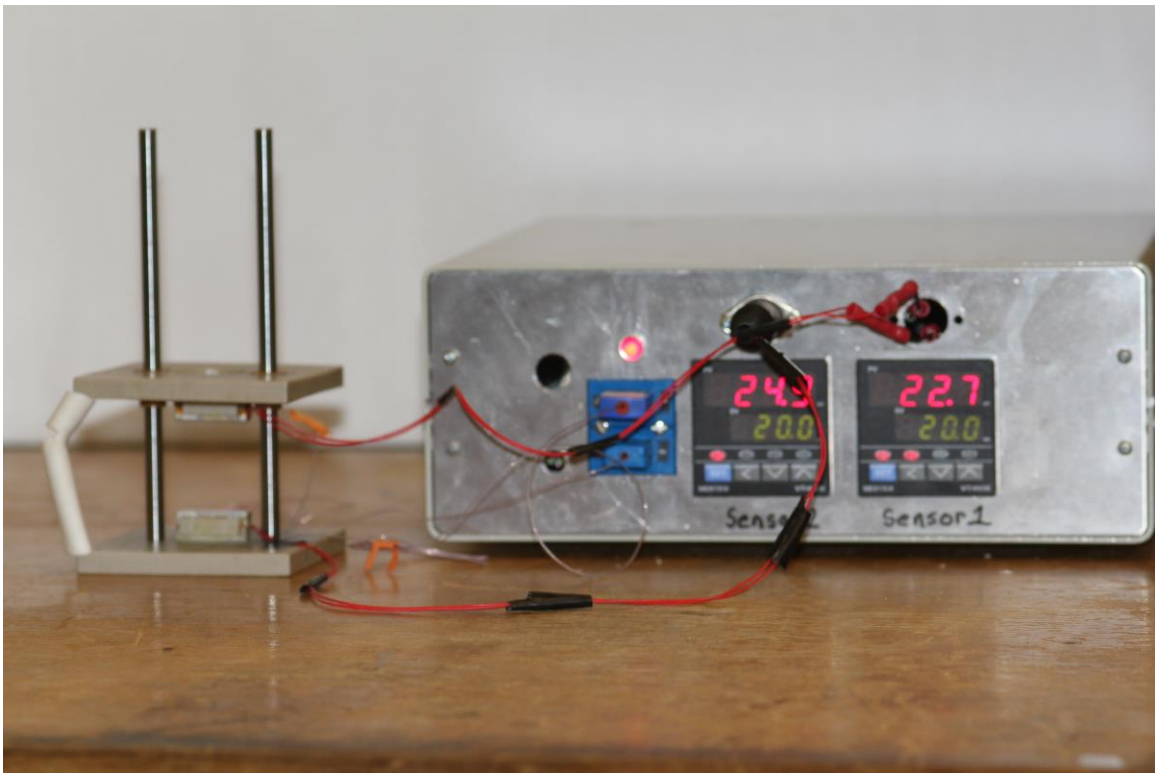

Figure 13: Thermal Jig Setup

The device had a gap of 0.006in. to mimic the gap in the ENSEAL device. This gap, however, made it difficult to determine the pressure applied to the tissue. Applied loads of 20lb and 50lb were used in the sealing process. With the .006 in. milled step in the top plate, the pressure was not well known. Pressure was determined in terms of minimum and maximum pressure from the loads that were used. See APPENDIX A for details on pressure calculations from load.

2.2.3 Sealing Procedure with Thermal Jig

The sealing procedure is governed by application of known pressure and temperature. Initially, the heaters were set from 0 – 20ºC above the set temperature. For example, the heaters were initially set to 150ºC in order to maintain a temperature at 140ºC. The artery was laid across the bottom heater once the target temperature was reached. Figure 14 shows a schematic of an artery placed within the Thermal Jig.

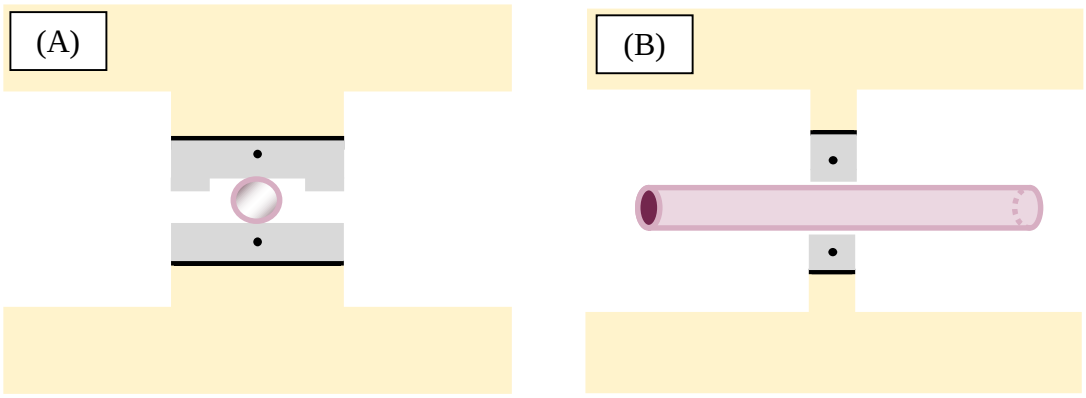

Figure 14: Artery placed in Thermal Jig before sealing. Panel (A) shows the Front View of the Thermal Jig. Panel (B) shows the side view of the Thermal Jig.

The thermal treatment of the arteries was 30 seconds. After this time, the top plate of the Thermal Jig was removed, and the sealed artery was extracted and placed into a 5mL vial filled with a saline solution and placed into a 4ºC fridge until the arteries were tested for burst and peel. The sealed artery was noticeably damaged at the spot of thermal treatment. Figure 15 shows this damage.

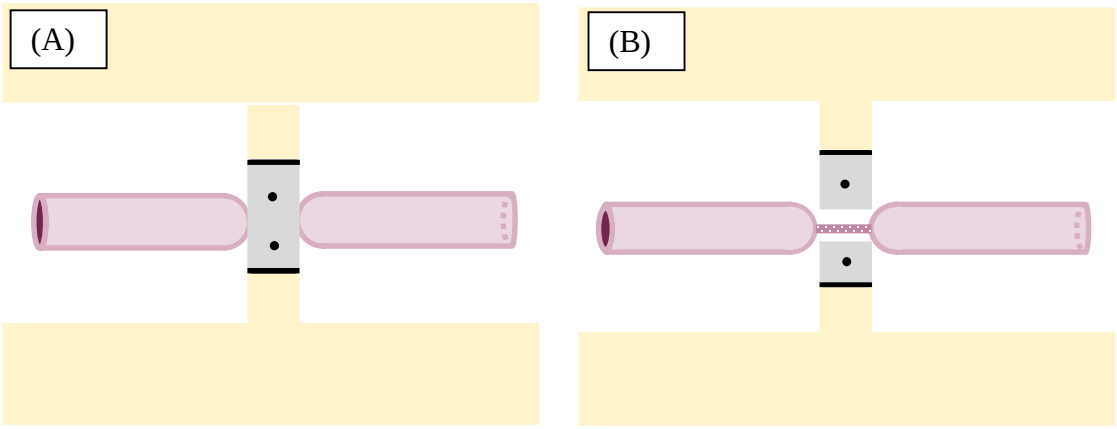

Figure 15: Panel (A) shows the artery during Thermal Jig sealing process. Panel (B) is a sealed artery that is irreversibly damaged.

An additional thermocouple was used in the Thermal Jig for sealing measurements initially (APPENDIX B). The final measurements did not use this extra thermocouple as it was likely to break.

2.2.4 Tissue Preparation for Sealing

On a given week, were harvested on Monday, and they arrived at UMN on ice by Wednesday afternoon. The middle of the common carotid arteries were chosen as they have a relatively constant diameter. These were transferred from saline-filled 2mm x 3mm plastic bags to 15mL marked conical tubes with approximately 5mL of saline in each. Sealing and burst testing were performed on Thursday. Majority of testing was performed with a different method of tissue preparation as explained in APPENDIX C.

2.3 Seal evaluation

For evaluating the strength of the seal, two methods burst and peel test were used The burst test is a very common way to determine the strength of sealed vessels and the peel test was performed to see if it provided any insight into the strength of the seal. A common minimum burst pressure threshold is 360mm Hg as it is approximately three times that of normal physiological burst pressure [21].

2.3.1 Burst device

The burst device provided by Ethicon was used to determine the burst strength of the artery. The burst pressure is recorded in millimeters of mercury (mm Hg) so as to correspond to a person's systolic blood pressure (~120mm Hg). After the application of treatment with the ENSEAL or the Thermal Jig, the sealed artery was cut into two pieces at the middle of the seal margin. Figure 16 below shows what happened to the arteries after being sealed by the Thermal Jig.

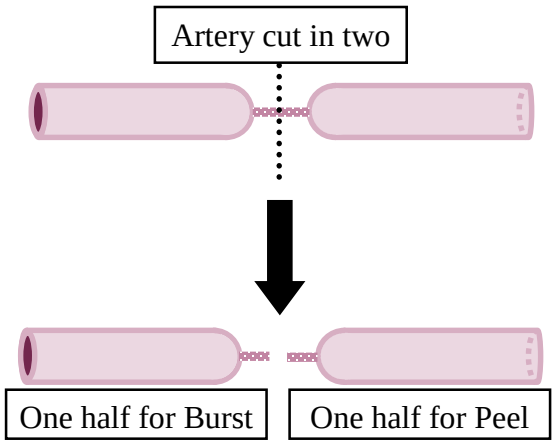

Figure 16: Artery process after sealing with Thermal Jig

One of the sealed artery halves were then placed in the burst system, shown in Figure 17, which was comprised of a syringe pump system (Harvard Apparatus PHD Ultra) and a housing for the artery bursting which consisted of a spring-loaded iris head (Edmund, Barrington, NJ, Model No. Model 53-910) with an orifice. The iris head clamped the un-sealed portion of the artery against the orifice.

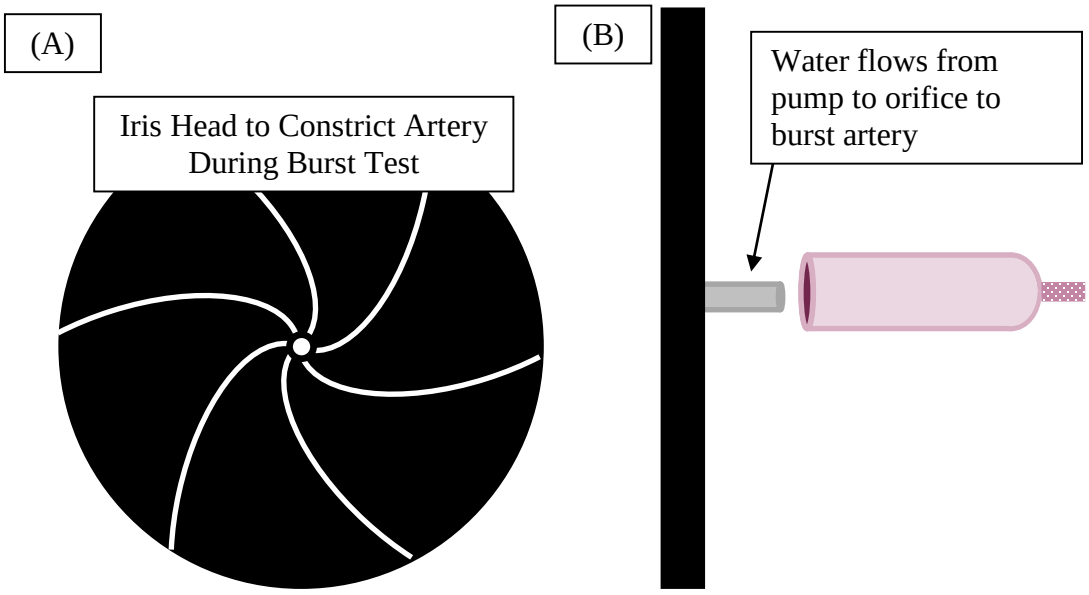

Figure 17: Iris Head Setup. Panel (A) shows the front view of the iris head which constricted the artery during the burst test. Panel (B) shows the side view of the iris head which shows the orifice on the iris head through which the water flows.

A block diagram of the burst system is shown below in Figure 18 where the iris head is a part of the "Burst Container" block.

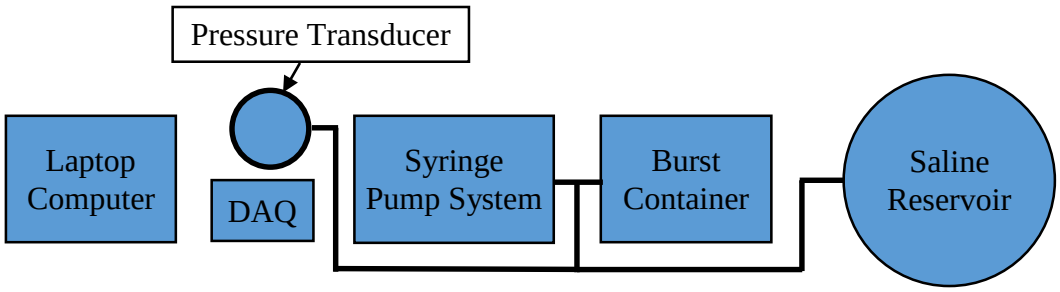

Figure 18: Burst Pressure System

A prepared saline solution was pumped at a rate of 47mL/min through an iris head that filled the artery until it burst. A pressure transducer (OMEGA, Stamford, CT, Model No: PX303-05065V) was connected in this process to record the pressure in real time as displayed by the LabView software which utilized a data acquisition module (National Instruments, Austin, TX, Model No: USB-6008) to record the data. The maximum pressure was recorded as the burst pressure.

2.3.2 Peel device

The peel device was another method of tracking the mechanical strength of the artery burst seal as the burst pressure test is the "gold standard" in determining the effectiveness of seal treatment. A little more preparation was required for the peel test as the sides of the arteries were removed to fold the artery in a way that one could pull the artery apart with only the seal holding the artery together. The unfolded artery prepared for sealing looked like the following in Figure 19.

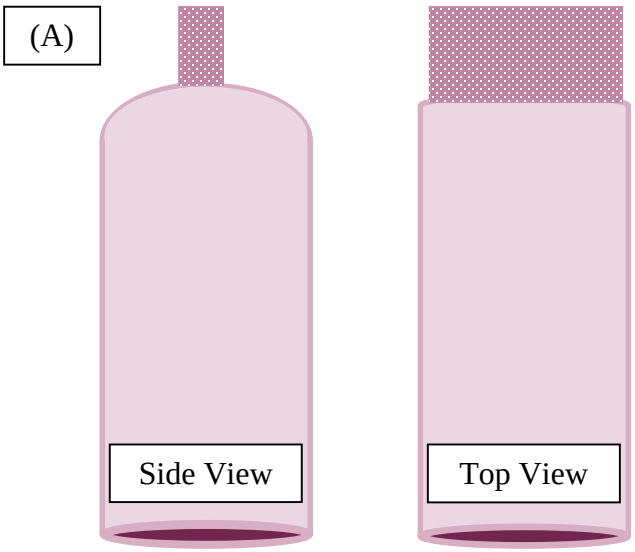

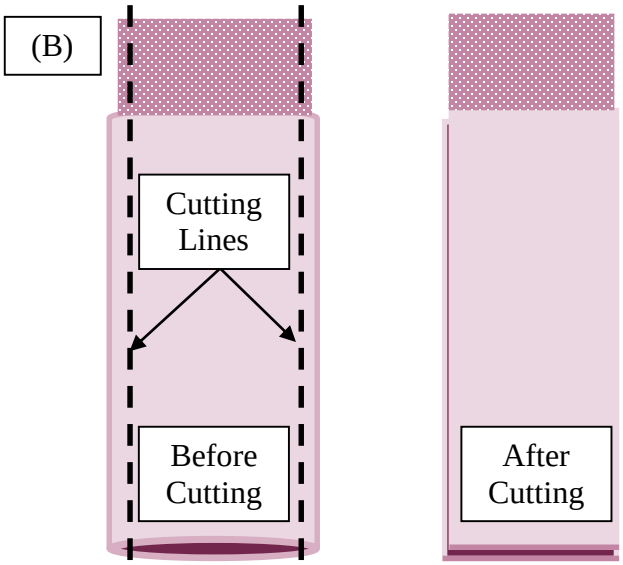

Figure 19: Artery Prepared for Peel Test. Panel (A) shows the side view and top view of the unprepared artery for the peel test. Panel (B) shows the process of cutting the artery so that the seal will bear the load when it is pulled apart.

A uniaxial tester (TestResources; Shakopee, MN) as shown below in Figure 20 was used to record the force necessary to pull apart the artery.

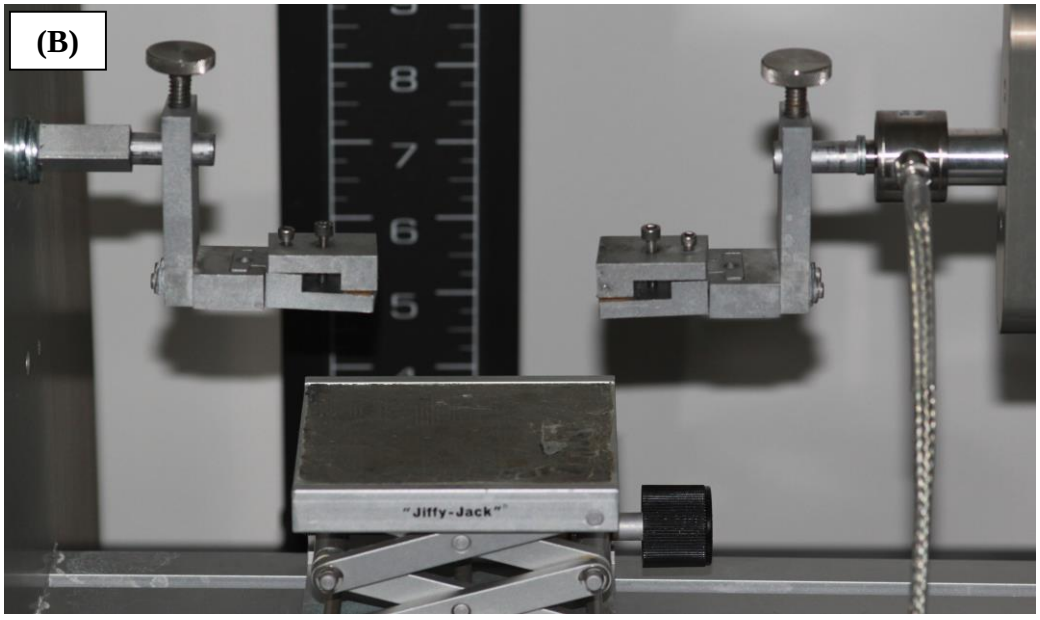

Figure 20: Panel (A) shows the overview of the peel device which uses a uniaxial tensile tester on its side. Panel (B) shows a zoomed-in view of the jaws that held the artery prepared for the peel test.

A uniaxial device pulled the artery apart at a rate of 2mm/s in a saline bath. The artery was speckled with graphite to have a better means of visually tracking the artery. Videos were taken of each run. Also, the uniaxial tester recorded details of the run which included the elapsed time, force in Newtons, and distance stretched. Figure 21 shows how the arteries were pulled apart.

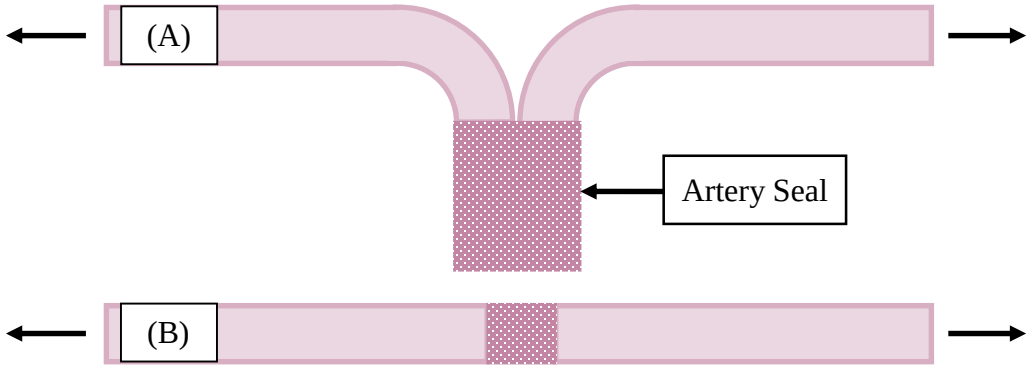

Figure 21: Peel Test Schematic. Panel (A) shows the Front View. Panel (B) shows the Top View.

The peel test was processed by taking the initial failure (i.e., the place with the initial reduction in force) and dividing it by the seal width. The initial failure was taken as it was

thought that the seal would be compromised at this point. An example of the initial failure is seen below in Figure 22. The seal width was calculated by taking pictures of the arteries with a scale bar and measuring the width with ImageJ software. These results were used to see how they compared with the burst pressure values since one side of the artery was tested with burst and the other side was tested with peel to see if peel strength was associated with burst pressure. Both of the artery sides were assumed to have similar mechanical strength properties.

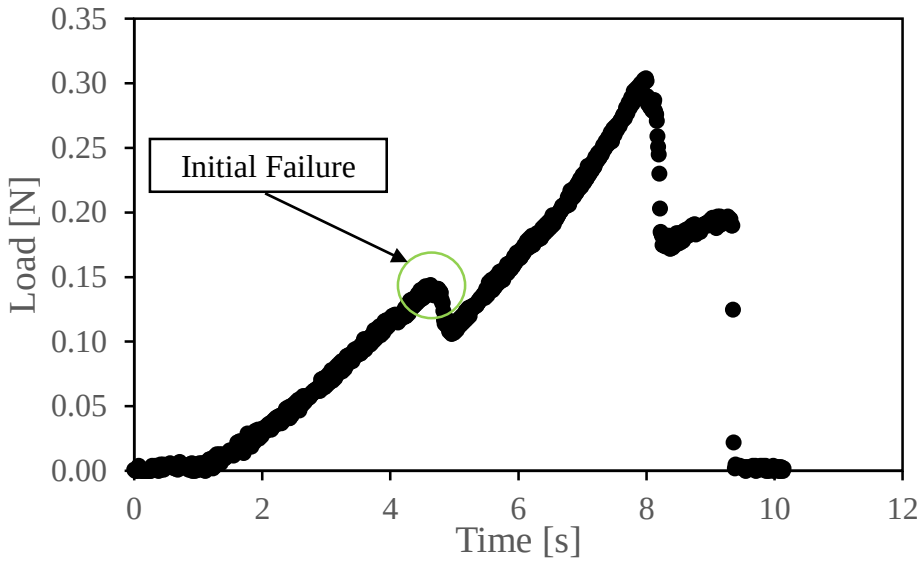

Figure 22: Depiction of initial failure calculation in peel test.

2.4 Fourier-Transform Infrared (FTIR)

Fourier-Transform infrared (FTIR) spectroscopy is a means of examining chemical changes in a sample. The infrared ng the absorbance of light from an infrared source to determine what components are in a particular sample.

2.4.1 Working Principles

The FTIR uses an infrared light source which is passed through a Michelson interferometer. The interferometer uses constructive and deconstructive interference to convert the single frequency signal into frequencies ranging from 4000 to 600 cm^{-1} (wavenumbers). The FTIR from the Characterization Facility at the University of Minnesota was used. It is a Nicolet iS50 FT-IR Spectrometer (Thermo Scientific), and it has a spectral range from 4000 – 600 cm^{-1}. It utilizes Windows-based OMNIC software for data analysis. It has a Potassium-Bromide (KBR) beamsplitter, and a liquid nitrogen cooled Mercury Cadmium Telluride/A (MCT)/A detector.

Figure 23: Nicolet iS50 FT-IR

2.4.2 Attenuated Total Reflectance (ATR) vs. Transmission Mode

Various ways of performing FTIR are available which include transmission and ATR mode. In transmission mode, infrared radiation, "I_0", is emitted and passes through the sample which attenuates to "I". In ATR mode, infrared light, I_0, is totally reflected at the interface between the crystal and the sample, but some radiation penetrates into the sample. This penetration is called an evanescent wave. The depth of penetration is determined by the indices of refraction of the crystal and the sample. See Figure 24 for a deptiction of transmission and ATR modes. The equation for the penetration depth is the following:

$$d_p = \frac{\lambda_c}{\{2\pi[sin^2\theta - (\eta_s/\eta_c)^2]\}^{1/2}} \quad (1)$$

where λ_c is the wavelength in the crystal (λ/η_c), θ is the angle of incidence, and η_s and η_c are the refractive indices for the sample and crystal, respectively. Transmission mode works well for gas and liquid sample, but it does not work as well for solid samples as the infrared light may be too scattered for an accurate measurement. For solid samples, ATR may prove useful as the infrared radiation only penetrates into a thin layer of the sample. ATR also may be used for liquids, powders, pastes, and others that can be pressed up to the surface of the crystal [74].

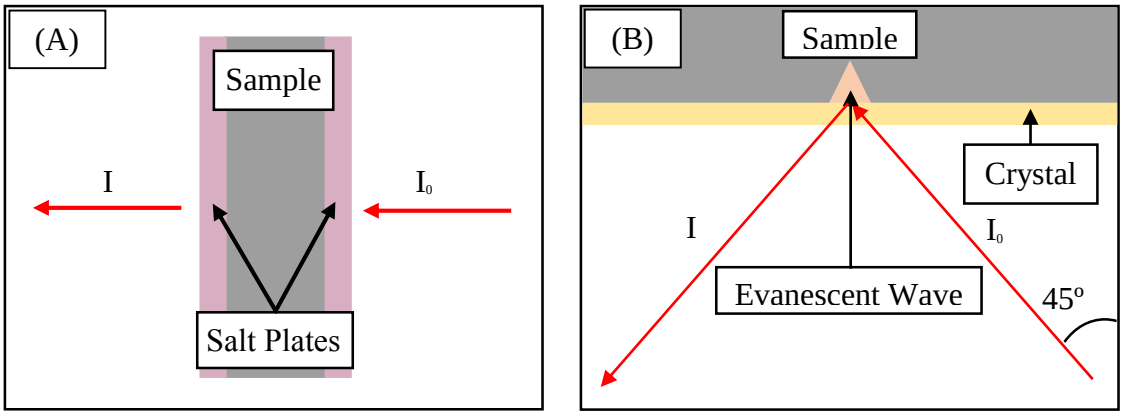

Figure 24: Panel (A) shows how transmission mode works as infrared radiation passes through the sample. Panel (B) shows how ATR mode uses internal reflectance to transmit an evanescent wave to be absorbed into the surface of the sample.

2.4.3 ATR Accessory: Temperature and Pressure Control

Additionally, the ATR accessory MVP-Pro (Harrick Scientific) with a diamond crystal was used to provide controlled temperature and pressure surface measurements of artery samples. The MVP-Pro is a single reflection with a 45º angle of incidence instrument. It is shown below in Figure 25.

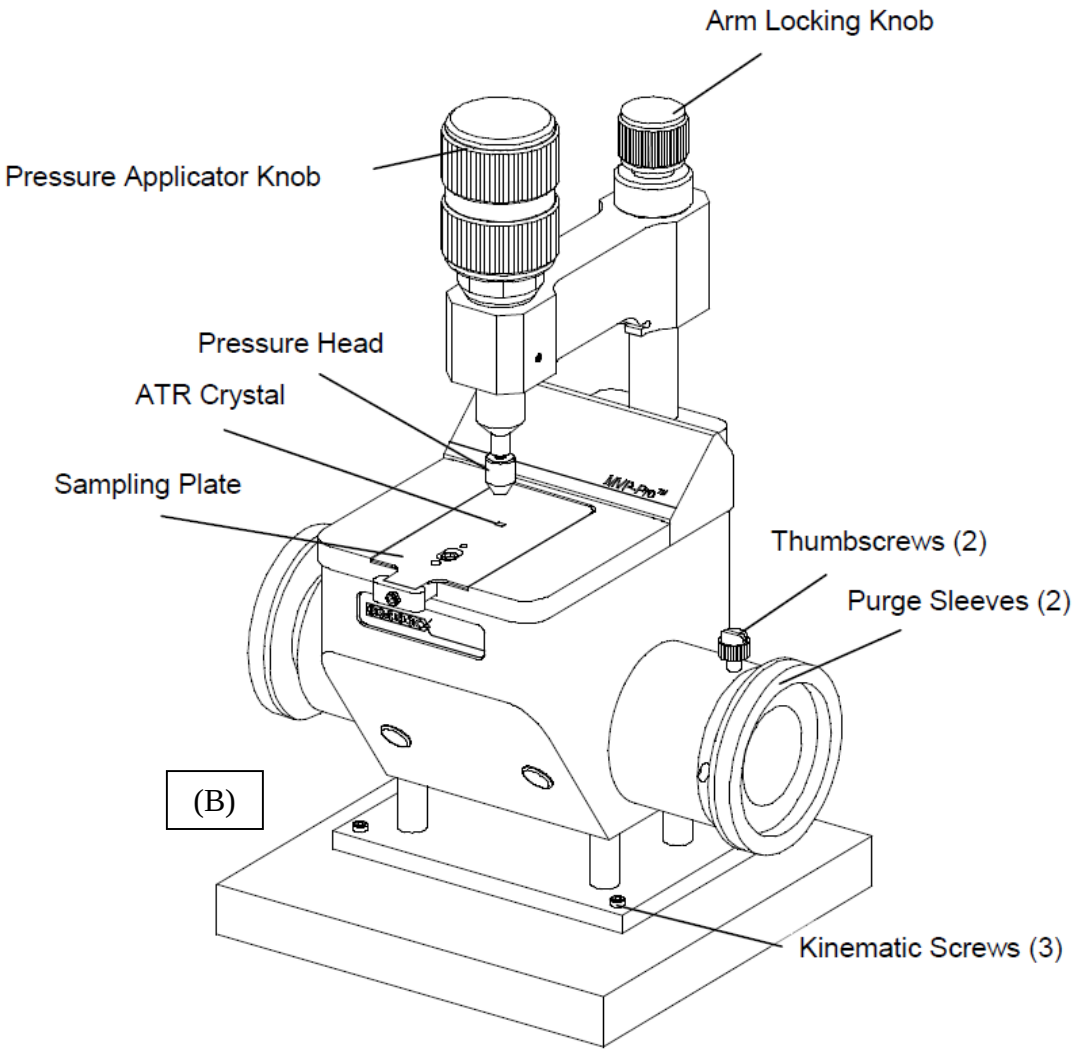

Figure 25: Panel (A) shows the MVP-Pro Schematic (taken from MVP-Pro User Manual).

Figure 26 shows the MVP-Pro in the Nicolet iS50.

Figure 26: MVP-Pro setup inside Nicolet iS50

The layout of the sampling plate of the ATR accessory has the heaters below the diamond crystal. Also, the crystal is between the heater thermocouple and the sample. This layout is seen in Figure 27 below.

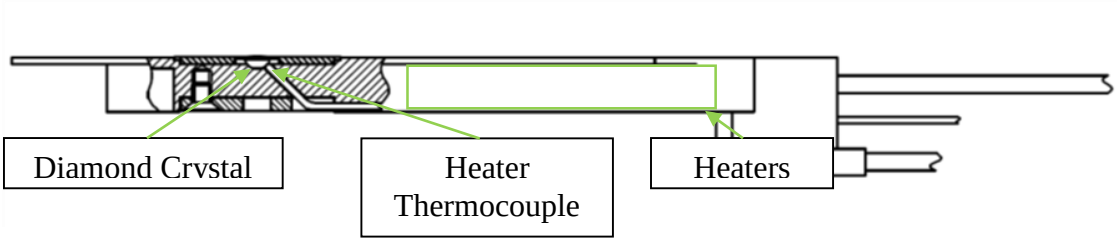

Figure 27: Zoomed-in View of ATR Sampling Plate

Characterization experiments were completed to investigate the thermal lag between the heater thermocouple and the sample placed on top of the crystal.

2.4.4 Sample Preparation

Both rat tail tendon and carotid artery were used in testing. Testing was done within three days of harvest. See APPENDIX D for details on how denaturation onset was affected

when testing was done on samples that were older than three days from harvest. For both samples, deuterium oxide (D_2O) (soaked for one hour based on reference to complete total deuteration[75] with 0.9% w/v NaCl was used for the purpose of looking at the Amide-I region. Normally, water (H_2O) conflicts with the Amide-I as the H_2O scissoring vibrational mode occurs in the same area [75, 76].

Carotid artery samples were taken from the Visible Heart Lab under the supervision of Dr. Paul Iaizzo. Additionally, carotid artery samples were also received from Ethicon. Arteries received from the Visible Heart Lab were fresh from harvest, but the arteries from Ethicon were received two days after harvest. Also, Ethicon cleaned and processed arteries while arteries from the Visible Heart Lab were not processed at all. Furthermore, no distinction to the location (i.e., distal or proximal) of the carotid artery was made for either of the sources.

2.4.5 Heating Rate (Denaturation) Measurements

The protocol for measuring denaturation of tissue was to prepare the samples as discussed above in Section 2.4.4. Once prepared, a sample was placed on top of the diamond crystal. Next, a Teflon-coated insulating cap that came with the ATR MVP-Pro was used to insulate the metal pressure head from the heated sampling plate. Silicon grease (Dow Corning; Midland, MI) was used to coat the area between the sampling plate and the insulating cap to avoid dehydration. Figure 28 shows how ATR measurements were setup.

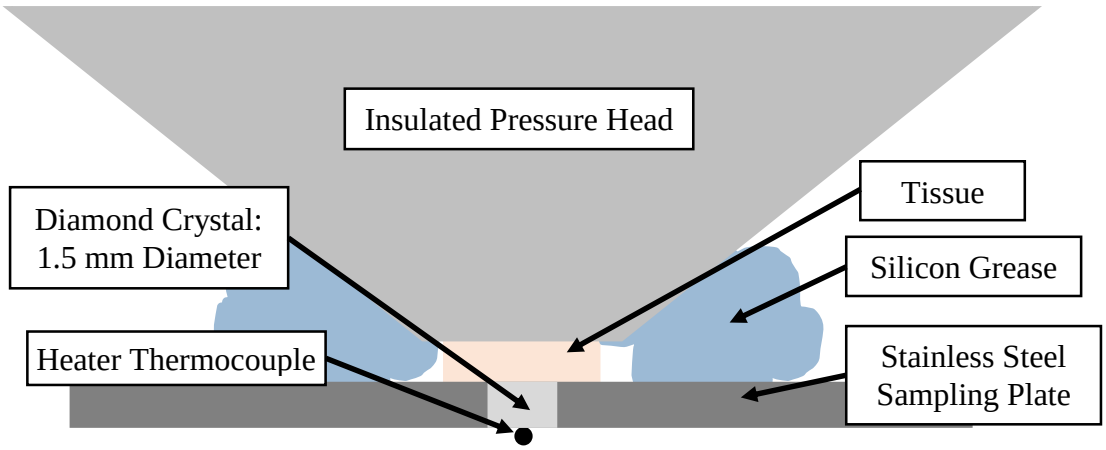

Figure 28: ATR Setup with Denaturation Measurements

The temperature range of the experiment was from 25 – 100ºC. Spectra were taken every 1ºC heater temperature change. 16 co-added scans at resolution of 4cm^{-1} were used when acquiring spectra. The time to collect a single spectrum was ten seconds. These data were saved in a .spa format which came from operating the OMNIC software, and the data was analyzed in MATLAB by converting the .spa files to .csv with the OMNIC software.

2.4.5.1 Extracting Denaturation

Denaturation is determined as the sharp increase in beta-sheets (a characterisitic band in the Amide I region of the FTIR spectra) with a simultaneous decrease of alpha-helices [67, 76, 77].. See APPENDIX E for a step-by-step description of determining the onset of denaturation. Also, APPENDIX F shows how to run the MATLAB code for calculating β-sheet formation.

2.4.5.2 Point Measurements

Measurements were taken with the sample at room temperature after Thermal Jig treatments. Carotid arteries soaked in D_2O solution with 0.9% NaCl and then treated with the Thermal Jig according to the following parameters in Table 5. The peak location of Amide-I was determined by finding the maximum value in the range between 1600 – 1700 cm^{-1}.

Table 5: Thermal Jig Parameters for Point Measurements

100ºC 20lb	100ºC 50lb
140ºC 20lb	140ºC 50lb

These point measurements were used to compare with sealing measurements made with the Thermal Jig to see if any spectroscopic difference could be seen from the different treatments and if the peak locations of the Amide I correlated with protein denaturation (Wim Wolkers – personal communication).

2.4.6 ATR Characterization

The performance of the MVP-Pro was characterized to see how the machine responded with respect to its temperature and pressure control. The main focus of the characterization was the temperature response of the heating rate and the thermal lag observed while taking measurements. Secondarily, the force gage was studied to see how it was affected by increasing temperature.

2.4.6.1 Heating Rate

The heating rate was characterized by using the setup described in Section 2.4.5 but with an added thermocouple to measure the sample temperature. A temperature lag between the heater thermocouple and the sample thermocouple will develop especially since the heating is done at a constant ramp rate. This can also be seen from the layout of the sampling plate which is shown in Figure 29.

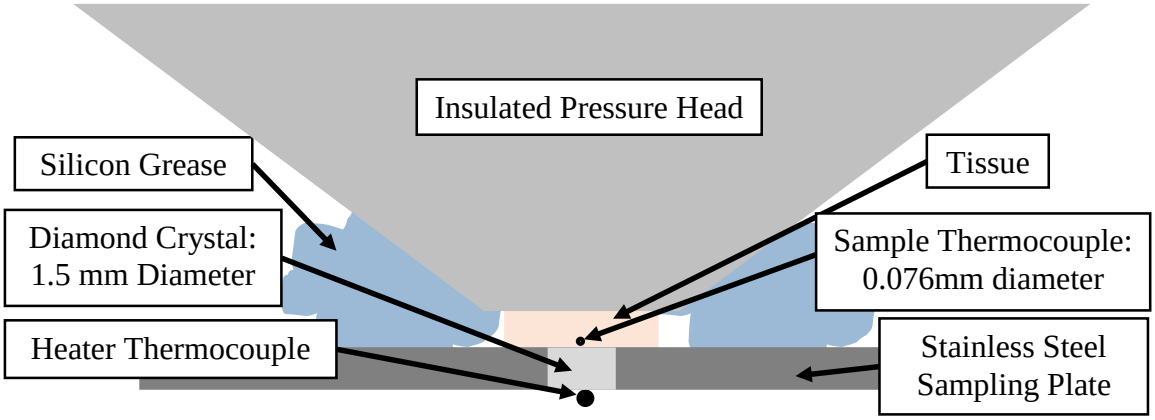

Figure 29: Description of ATR Characterization Setup

See APPENDIX G for a description of the all of the results of the characterization. See APPENDIX *H* for a description of how denaturation onset was affected by using the sample thermocouple.

2.4.6.2 Force Gage

The force gage was tested to see if it was reporting correct results by testing the load with a calibrated spring. See APPENDIX G for more details.

3 RESULTS

The results can be divided into two parts: FTIR and Tissue Sealing. FTIR measurements include both denaturation measurements and point measurements after Thermal Jig treatment. For tissue sealing, the initial measurements are included in addition to the final measurements made.

3.1 FTIR

For FTIR measurements, both heating rate measurements in order to calculate the onset of denaturation and room temperature point measurements were taken. Both will be described in the sections below.

3.1.1 Denaturation Measurements

Data is shown below from the following three methods: temperature only, pressure only, and both temperature and pressure.

3.1.1.1 Temperature Only

Heating rate measurements started with the model of Rat Tail Tendon since it is a well characterized system for collagen denaturation. Figure 30 shows my measurement of denaturation onset compared with that in the literature.

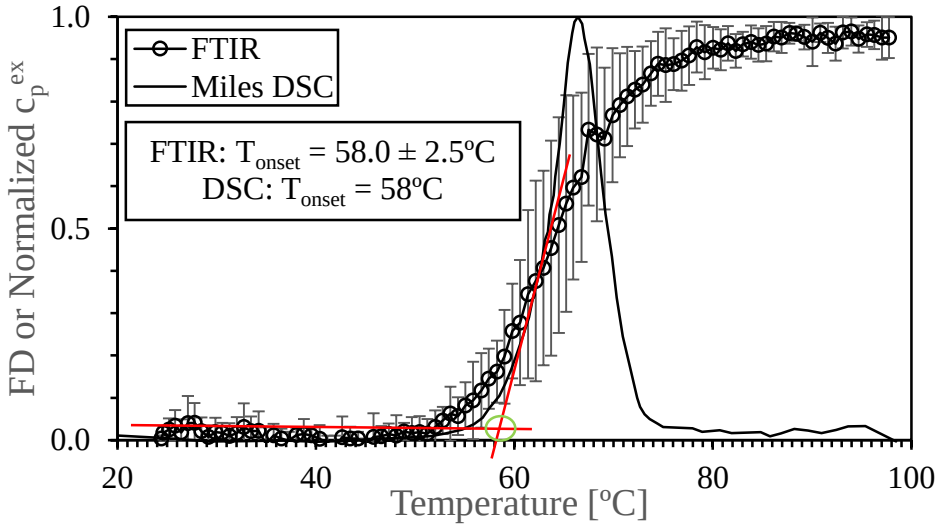

Figure 30: FTIR Rat Tail Tendon with denaturation onset of 58 ± 2.5ºC (results come from using the tangent line method described in APPENDIX I) at heating rate of 1.91ºC/min. Also Miles [66] Rat Tail Tendon with DSC at 2ºC/min with onset of ~58ºC using tangent line method on graph presumed to be used in [67, 75].

The above plot shows the experimental data with an onset of 58 ± 2.5ºC that overlaps with the calculated onset from Miles which has an onset of ~58ºC. This overlap of onset values validates later denaturation measurements. See APPENDIX I for a discussion on processing FTIR and DSC data in order to determine denaturation onset. Additionally, the denaturation onset of carotid artery was compared with previously published iliofemoral artery to see if comparable data could be gathered. Figure 31 shows the results.

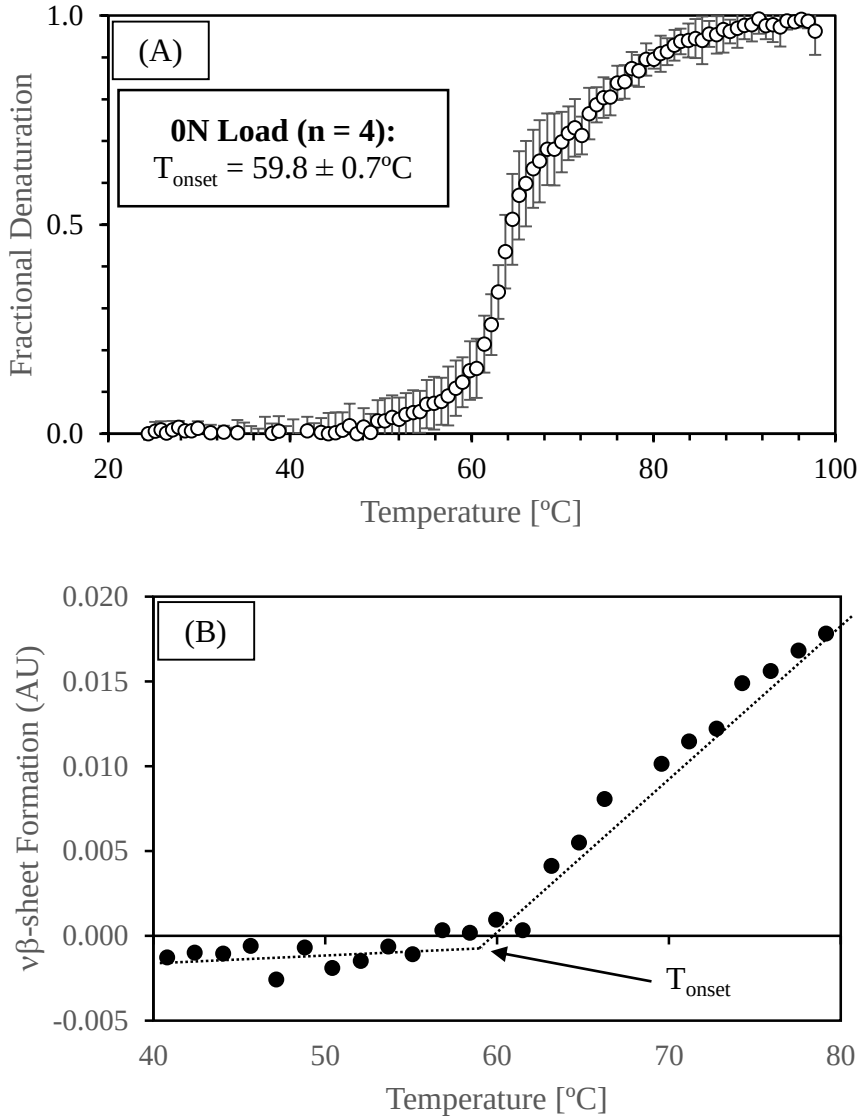

Figure 31: (A) Experimental carotid artery measurements with denaturation onset of 59.8 ± 0.7ºC. (B) Published control iliofemoral artery by Venkatasubramanian [67] with denaturation onset of 57.0 ± 3.0ºC

3.1.1.2 Pressure Only

Pressure only measurements were taken with carotid arteries with no heating but with applied loads of 0N, 10N, 20N, and 50N. This is shown below in Figure 32.

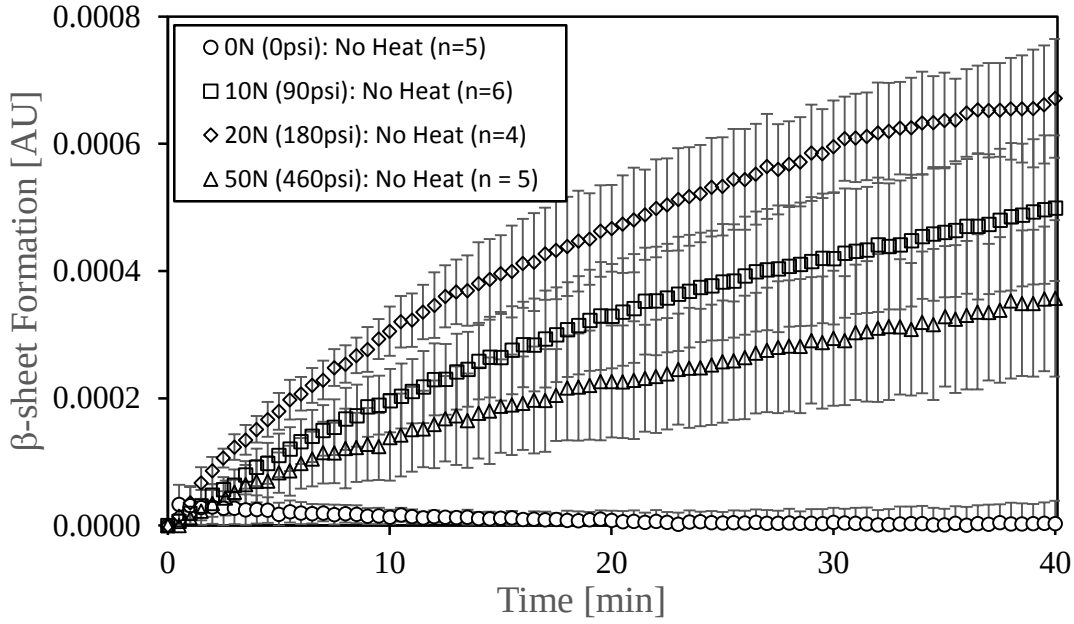

Figure 32: Pressure only measurements at various loading conditions

This loading essentially no beta-sheet formation with 0N load. The 50N load is next highest followed by 10N and 20N. In each of the loading cases of 10N, 20N, and 50N, the beta-sheet area increases with time until the experiment ends at 40min, this is the same time for a heating rate measurement. See APPENDIX J to see how pressure affects the inverted second derivative graphs.

3.1.1.3 Temperature and Pressure

Pressure and Temperature effects were seen with both rat tail tendon and carotid artery. For rat tail tendon, only load of 2N was used. For carotid artery, loads of 2N, 10N, 20N, and 50N were used. Figure 33 below shows results for both rat tail tendon and carotid artery under load.

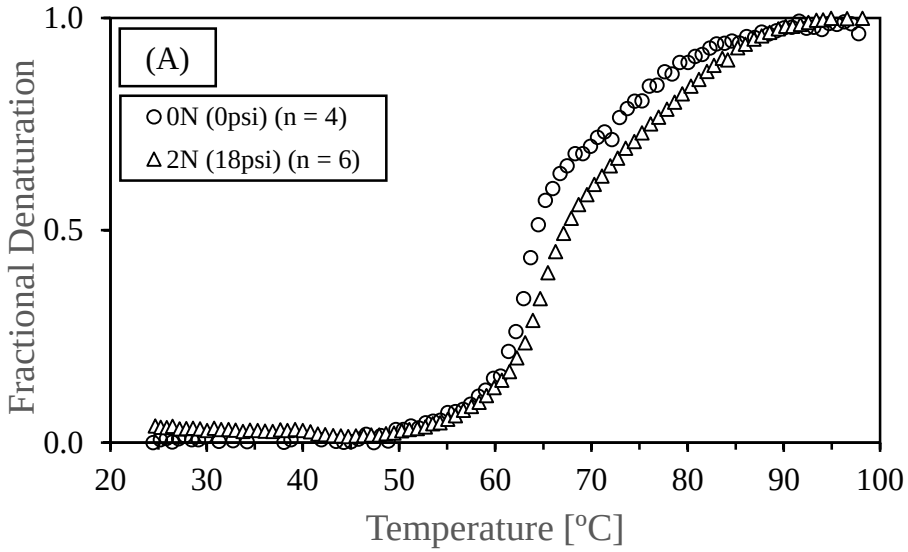
(A)
0N (0psi) (n = 4)
2N (18psi) (n = 6)
Fractional Denaturation
1.0
0.5
0.0
20
30
40
50
60
70
80
90
100
Temperature [ºC]

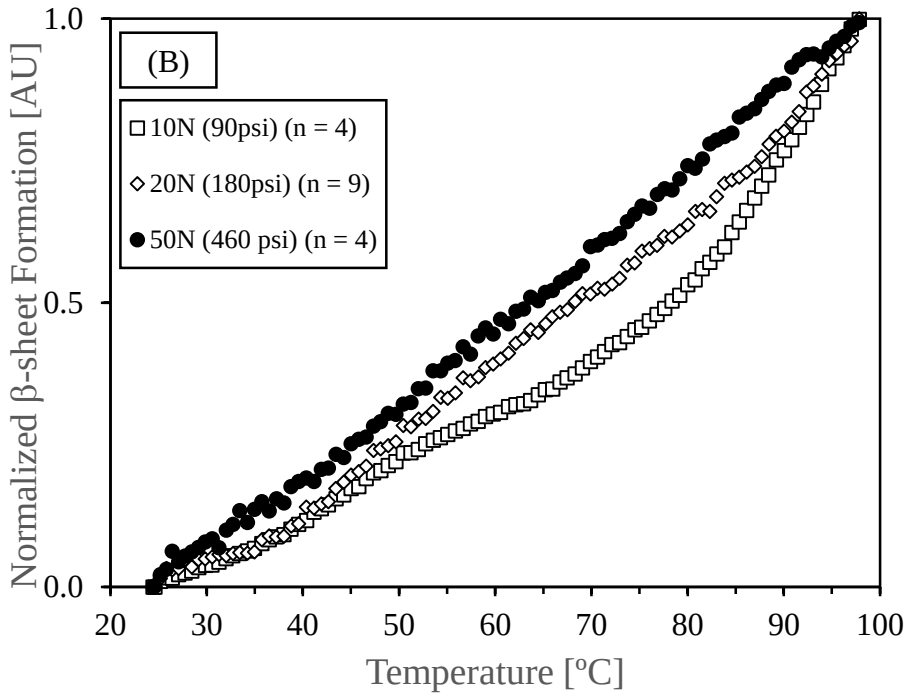
(B)
10N (90psi) (n = 4)
20N (180psi) (n = 9)
50N (460 psi) (n = 4)
Normalized β-sheet Formation [AU]
1.0
0.5
0.0
20
30
40
50
60
70
80
90
100
Temperature [ºC]

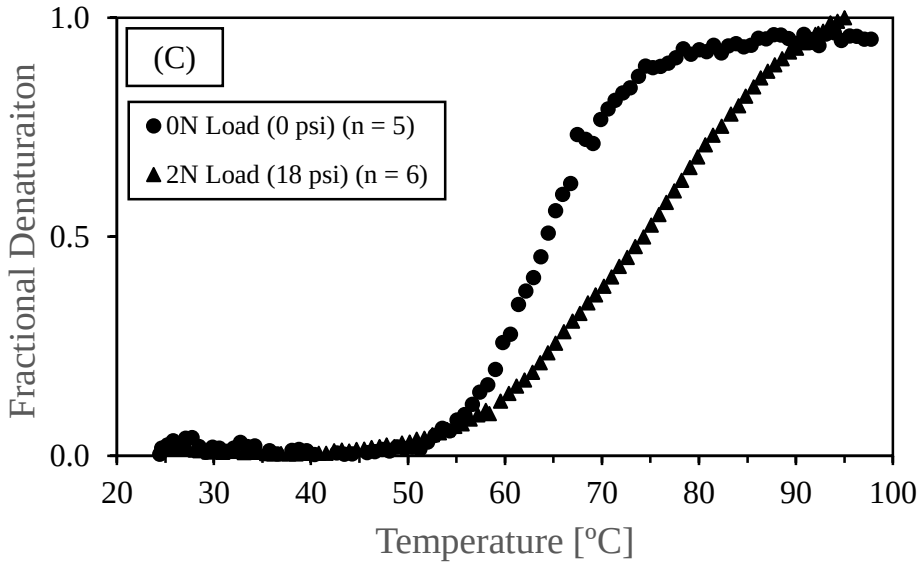

Figure 33: (A) Carotid artery measurements with loads of 0N and 2N which seem to show complete protein denaturation by 100ºC. (B) Carotid artery measurements with loads of 10N, 20N, and 50N which do not show complete protein denaturation. Samples need to be heated more to see if complete profile is observable. (C)Rat tail tendon measurements with loads of 0N and 2N. Error bars are removed from the plot in order to see the data more clearly. The error is approximately 15% of the maximum value.

With the rat tail tendon, the 0N load has a denaturation onset of 58.0 ± 2.5ºC, and the 2N load has an onset of 60.1 ± 4.9ºC. For the carotid artery, the denaturation onset for loads of 0N, 2N, and 10N are 59.8 ± 0.7ºC, 59.8 ± 1.9ºC, and 79.1 ± 4.3ºC, respectively. These loads were applied by the force applicator on the MVP-Pro with a diameter of 4.5mm. One simply divides the applied force by the circular area of the force applicator in order to calculate the applied stress. One may need to heat in excess of 150ºC in order to observe the full denaturation profile at loads of 10N, 20N, and 50N.

3.1.2 Point Measurements – Amide I peak shift

Point measurements were taken before and after applying thermal jig treatments to carotid arteries. These arteries were soaked in D_2O before any measurements were taken. Figure 34 shows an overview of the spectra taken for the point measurements.

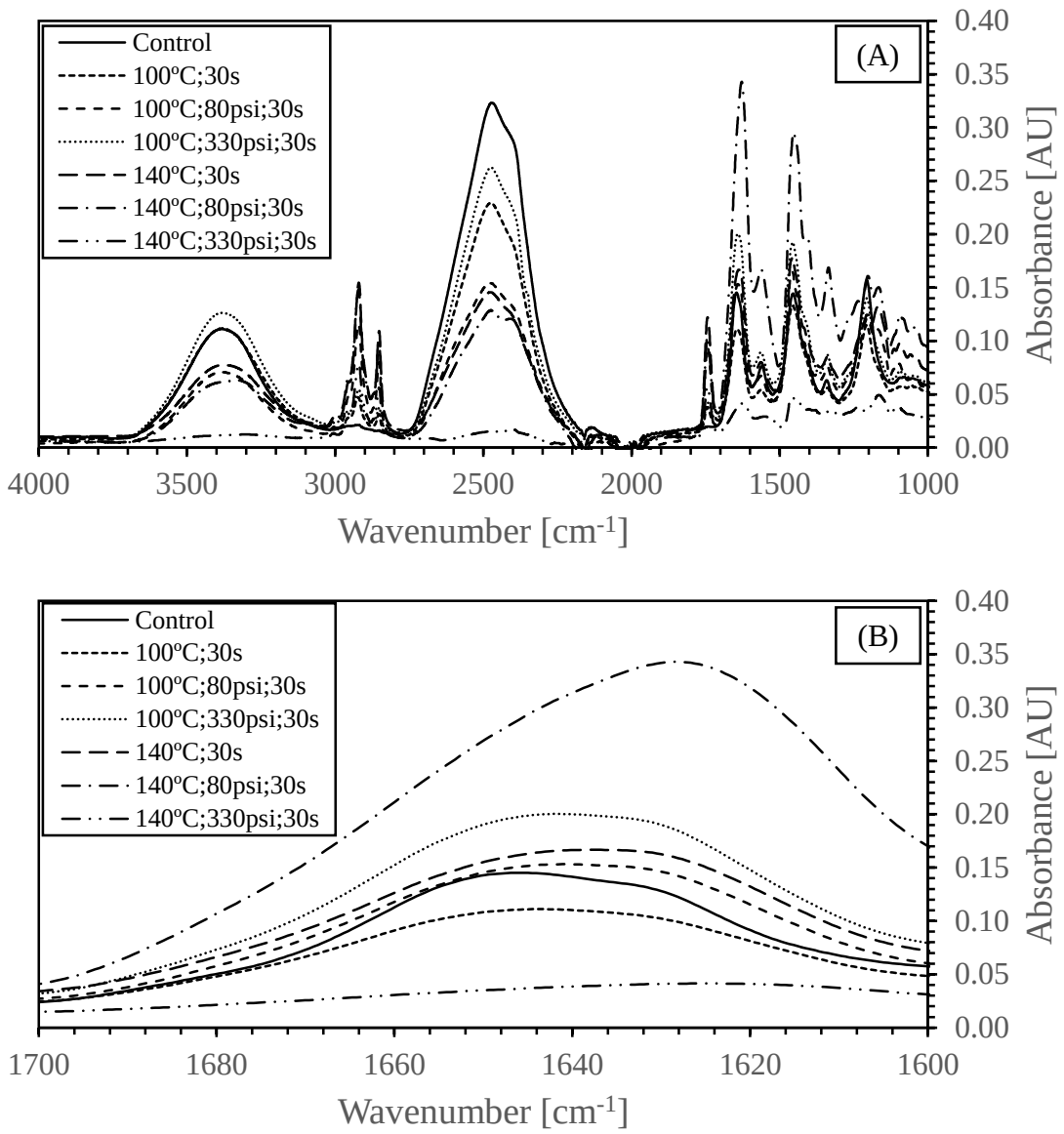

Figure 34: FTIR Overview of Point Measurements. Panel (A) shows a representative example of FTIR spectra for reach of the point measurement treatments. Panel (B) shows a zoomed-in view of the Amide I (1600 – 1700cm^{-1}).

Figure 35 shows how the Amide-I peak position changes with increasing temperature.

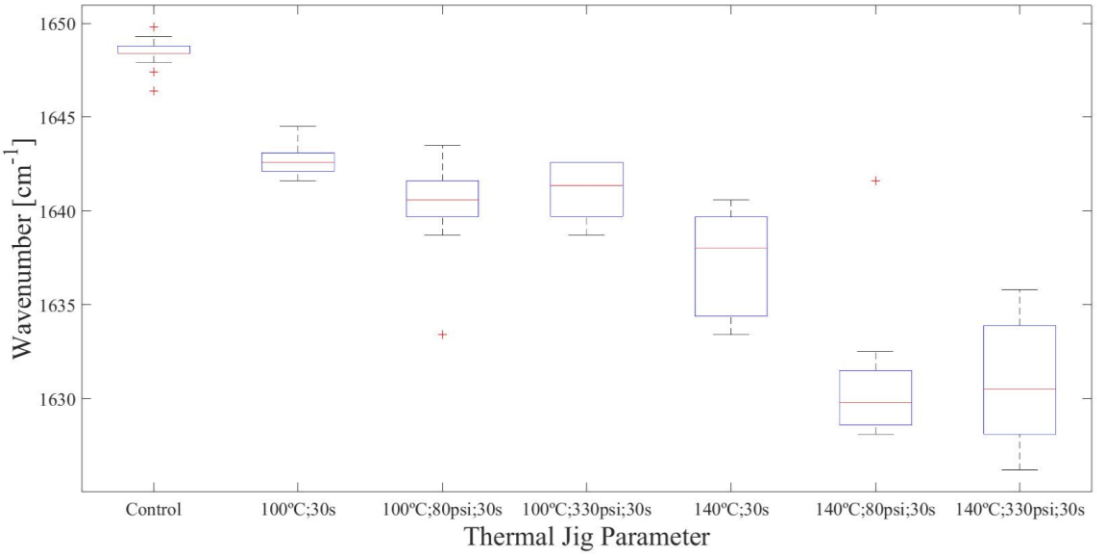

Figure 35: Amide-I peak position vs Thermal Jig treatments with a sample size of n = 60 for "Control" and a sample size of n = 10 for all of the remaining treatments.

Figure 35 shows that the Amide-I peak position shifts to a lower wavenumber as the temperature and pressure increases with Thermal Jig treatments. This lower wavenumber at a higher temperature corresponds to denaturation as the Amide-I peak has β-sheets centered at 1630cm^{-1} and α-helices centered at 1652cm^{-1} [78]. The shift of the Amide-I peak position indicates more denaturation which would correlate with a better seal. More details on point measurements can be found in APPENDIX K.

3.1.3 Point Measurements – Tissue Weight Data

The arteries that were used for the point measurements were blotted with tissues until no more water was easily removed. Next, the arteries were treated with the Thermal Jig according to the following settings: 100ºC;30s, 100ºC;20lb;30s, 100ºC;50lb;30s, 140ºC;30s, 140ºC;20lb;30s, and 140ºC;50lb;30s. Also, an oven was used to completely dry the tissue out to determine the water content. The amount of weight removed was calculated as follows:

$$Blotting = \frac{m_{wet} - m_{blotting}}{m_{wet}} \quad (1)$$

$$Sealing = \frac{m_{blotting} - m_{sealing}}{m_{wet}} \quad (2)$$

$$Drying = \frac{m_{wet} - m_{dry}}{m_{wet}} \quad (3)$$

where m_{wet} is the weight of the tissue when wet, $m_{blotting}$ is the weight of the tissue after blotting the artery with a tissue paper, $m_{sealing}$ is the weight of the tissue after applying the sealing treatment, and m_{dry} is the weight of the artery after being in the oven for approximately 48 hours at 60ºC. Figure 36 shows a summary of these measurements.

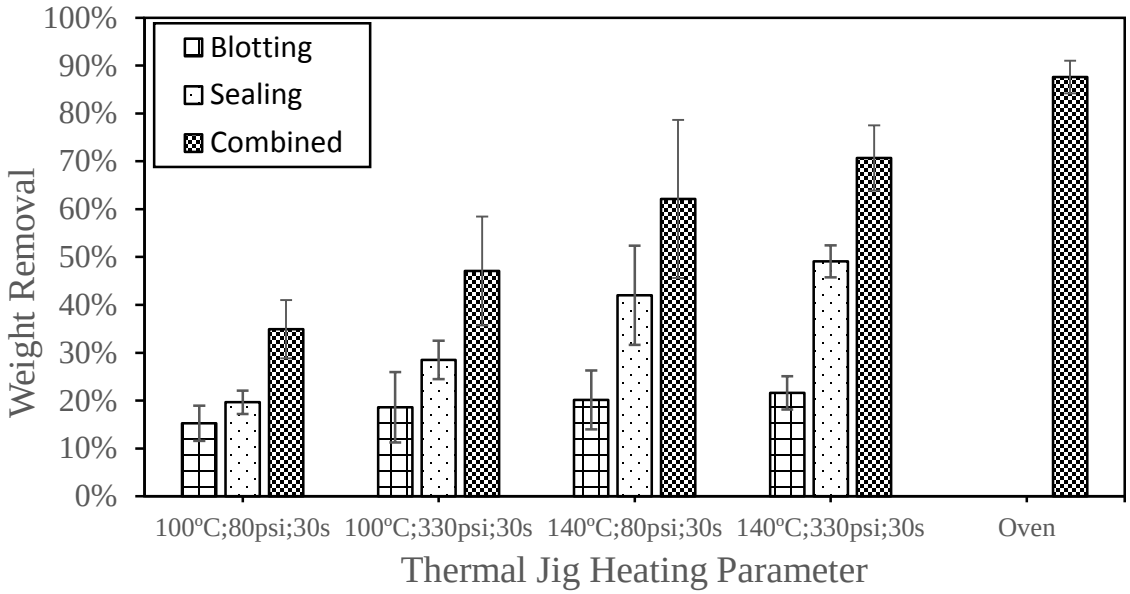

Figure 36: Tissue Weight data from blotting, sealing, and drying

With the above measurements, one must keep in mind that the treatment was only applied to artery rings that fit within the Thermal Jig jaws. Thus, the weight removed due to sealing in the above test may be overestimated to normal tissue sealing of the Thermal Jig since the artery is smaller in the above test than what it normally is during a sealing procedure.

3.2 Tissue Sealing

Tissue sealing was performed with both the Thermal Jig and Ethicon's ENSEAL device. The Thermal Jig was used exclusively at UMN whereas the ENSEAL was used by both Ethicon and UMN as Ethicon sent a generator and several ENSEAL devices to UMN for use. This section will describe initial artery measurements by Ethicon with the ENSEAL device. Next, sealing performed by the Thermal Jig will be presented.

3.2.1 Final Measurements from Thermal Jig compared with ENSEAL

Sealed arteries from Ethicon using their ENSEAL device were sent to UMN to be burst and peel tested in order to determine the strength of the vessels. The representative burst results are shown below in Figure 37. This testing was completed to see if the margin on the artery had any effect on the expected burst pressure. Regardless, the burst pressure achieved with the margin testing had a mean burst pressure of 876.7 ± 338.2 mm Hg. Ethicon described an acceptable seal as an artery which had a burst pressure threshold between 600 – 800 mm Hg. Figure 37 shows a box plot graph of the results achieved by the Thermal Jig.

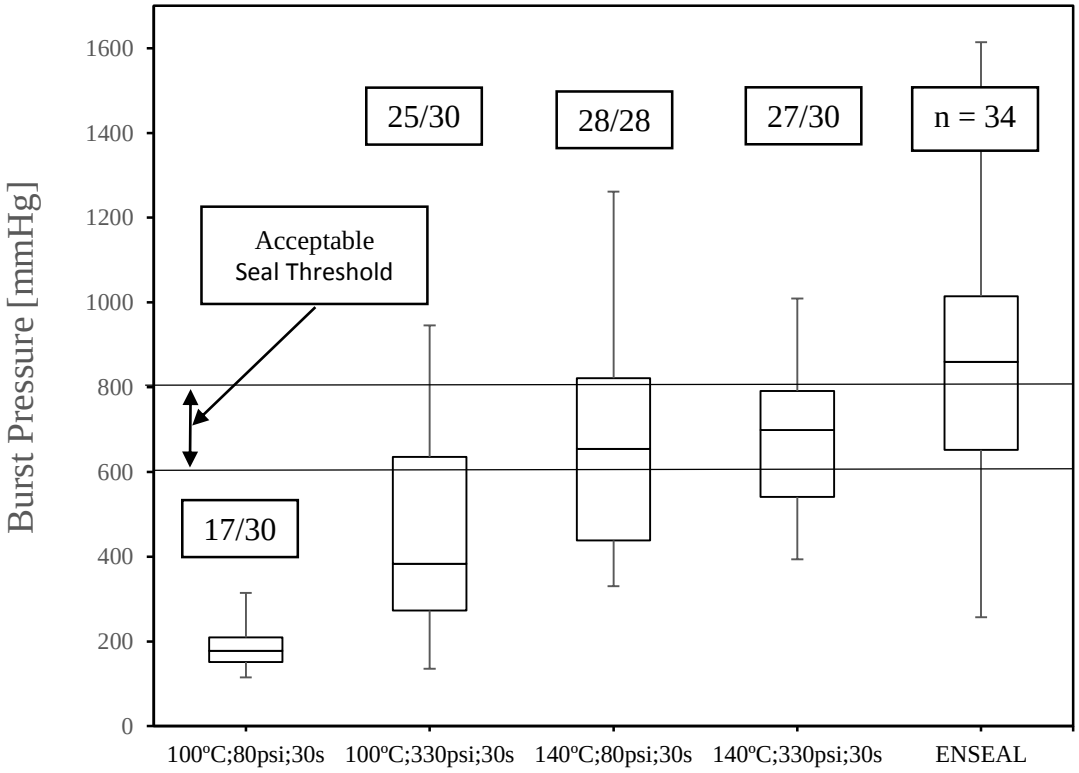

Figure 37: Thermal Jig Burst Pressure results at different treatments where the ENSEAL data came sealed from Ethicon, and Nathan Cal cut the tissue and performed burst tests

Thirty (n = 30) samples were sealed for each of the four Thermal Jig treatments. The graph only shows arteries that had successful burst pressure runs. A "successful" run was defined as the artery recording a burst pressure greater than 100 mmHg. thirteen (n = 13) samples failed immediately at the 100ºC and 20lb treatment. Only five (n = 5) samples

failed immediately increasing the weight from 20lb to 50lb and keeping the temperature constant. Two (n = 2) samples were removed at the treatment of 140ºC and 20lb because they did not conform to normality. Thus, these two data points at burst pressures of 1651.1 and 1719.5 mm Hg were removed. Finally, three (n = 3) samples that failed immediately at the treatment of 140ºC and 50lb. The average burst pressure and standard deviation of the 100ºC-20lb, 100ºC-50lb; 140ºC-20lb, and 140ºC-50lb were 188.4 ± 55.3 mm Hg, 439 ± 232.6 mm Hg, 647.3 ± 241.3 mm Hg, and 678.1 ± 153.7 mm Hg, respectively.

3.2.2 Visualization of sealed tissue

Unsealed carotid arteries look like the following in Figure 38.

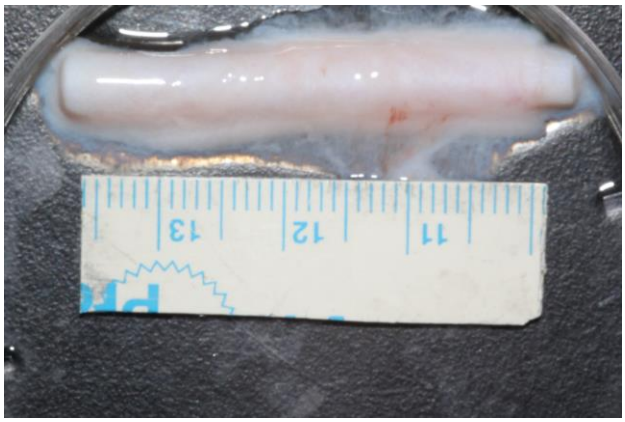

Figure 38: Unsealed carotid artery as received from Ethicon

Figure 39 shows a representative sealed artery at each of the Thermal Jig treatments of 100ºC-20lb, 100ºC-50lb, 140ºC-20lb, and 140ºC-50lb.

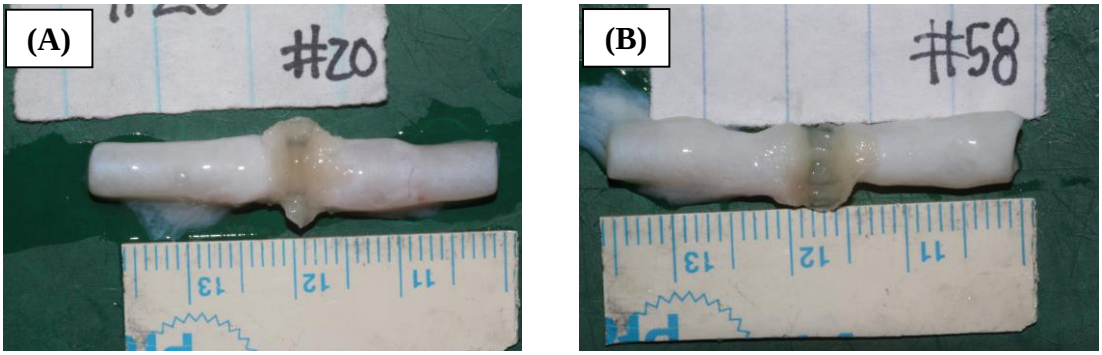

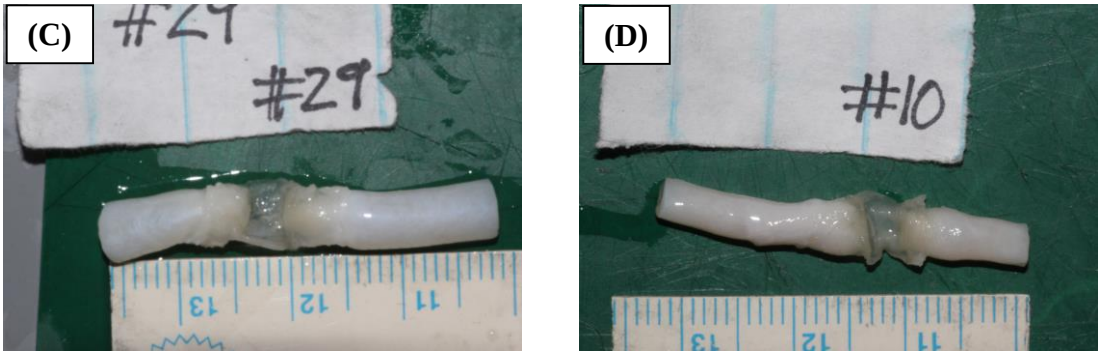

Figure 39: Arteries sealed at (A) 100ºC;80psi;30s, (B) 100ºC;330psi;30s, (C) 140ºC;80psi;30s, and (D) 140ºC;330psi;30s. These arteries show the variation in Ethicon's cleaning of the arteries.

Figure 39 shows how the 100ºC;80psi;30s treatment does not fully push away the intima. The intima is clearly pushed away in subsequent pictures of (B), (C), and (D), and a translucent seal margin is visible. This seal margin is quite wide in (C) and (D) with treatments at a temperature of 140ºC.

3.3 Summary

This section is a summary of the main results which includes the denaturation of collagen and the mechanical strength of the artery as pressure and temperature are varied.

3.3.1 Temperature denatures collagen at roughly 60°C by DSC or FTIR

Collagen has been shown in this study with models of carotid artery and rat tail tendon to denature with the aid of both FTIR and DSC. Experimental data of carotid artery and rat tail tendon is compared with published rat tail tendon by DSC.

3.3.2 Sealing was found to correlate strongly with both T and P

In Figure 37, the burst pressures are shown from sealing with the Thermal Jig. The burst pressure is significantly higher 50lb (330psi) compared with 20lb (80psi) at the same temperature of 100ºC. Also, the burst pressure is significantly higher when increasing the temperature from 100ºC to 140ºC at both loads of 20lb (80psi) and 50lb (330psi) . No significant difference was observed between the two load values of 20lb (80psi) and 50lb (330psi) at a constant temperature of 140ºC.

4 DISCUSSION

The discussion will cover the following topics: the effect of pressure and temperature on denaturation, water loss and its relationship to tissue sealing, and the effect of pressure and temperature on artery burst strength.

4.1 Effect of Temperature and Pressure on Denaturation

Heat denaturation occurs around 60ºC for both rat tail tendon and carotid artery. The denaturation of the carotid artery was delayed through increasing load. The denaturation experiment is unable to detect an onset for loads greater than 10N (90psi). The denaturation profile at loads of 10N, 20N, and 50N are incomplete. The samples at these temperatures need to be heated in excess of 150ºC to observe the complete protein denaturation profile. Thus, when one increases the pressure (through mechanical or osmotic means), the denaturation onset temperature is delayed. Pressure causes the delay in denaturation onset by forcing water out of the tissue. Miles hypothesized that dehydrating a tissue displaces the water that is held between collagen molecules. The loss of water in dehydration causes the shape of the collagen fiber to shrink which reduces the number of possible configurations it can be in which reduces the configurational entropy. This reduction in entropy, argued by Miles, is said to increase the temperature of denaturation [79] by increasing the proteins stability.

4.2 Water loss

Water loss occurs in arterial sealing with either the Thermal Jig or the ENSEAL device. Water loss was recorded for artery sealing measurements with the Thermal Jig, and the results showed that more water was lost at higher temperatures of 140ºC versus 100ºC. Burst pressure correlates positively with water loss and temperature.

Tissue sealing may be compared to the making of collagen glue. Glue has several steps which include: preparing stock or raw material, cooking stock with hot water, and chilling the glue liquor [80]. In the cooking step, the water is heated to 70 to 90ºC for 2 to 6 hours. This temperature does not reach the sealing temperatures of 140ºC, but the time for preparing collagen glue is much longer than artery sealing (~10 seconds) so water is removed faster in artery sealing than in making collagen glue. Also, the cooked glue is dried, and it is then stored at constant humidity and temperature so it does not soften or

crack. Both temperature and water loss are important factors that contribute to the strength of the glue.

4.3 Temperature and Pressure Effect on Seal Strength and Visualization

Figure 37 showed that burst pressure of the arteries increased dramatically with the temperature was increased from 100ºC to 140ºC. One hypothesis of this is that the arteries were more fully denatured at the higher temperatures. This can be seen from Figure 39 as the "sealed" portion of arteries sealed at 140ºC were more consistently translucent. From 100C and 20lb to 100C and 50lb showed a significant increase. This may be caused by the additional force caused the jaws of the thermal jig to be closed more quickly. Additionally, no significant difference is shown at the higher temperature of 140ºC at the two force values. Since the temperature is much higher, the tissue collapses more to the temperature (boiling, evaporation) than to the mechanical pressure.

5 CONCLUSION

5.1 Impact of Temperature and Pressure on Tissue

Heat, pressure, and time are important parameters when designing a high-energy medical device, specifically a tissue sealing device.

5.2 Denaturation Requirements

With no pressure, one only needs temperature greater than 60ºC to cause the onset of denaturation. With added pressure, the rate at which denaturation occurs seems to drop off. With increased pressure of 90 psi, the denaturation onset is significantly delayed. At 180 psi, the denaturation onset is not clearly defined, and it seems that denaturation does not occur at temperatures beneath 100ºC.

5.3 Seal Requirements

In order to seal reliably, it was shown through the experiments that temperature greater than 100ºC is needed. This was shown since the burst pressure at 100ºC did not meet the necessary burst pressure threshold of 600 – 800 mm Hg. In contrast to the poor sealing of the tissue at 100ºC, the tissues sealed at 140ºC provided a reliable seal with a median burst pressure in the acceptable range of 600 – 800 mm Hg. This increase of 40ºC in ad-

dition to the pressure is necessary to cause an artery to be sufficiently sealed. The pressure although necessary to force the tissue together is unclear how much it helps after a certain amount.

5.4 Future Work

Limitations of this work are related to both the tissue sealing and protein denaturation work. For tissue fusion, not much tissue was sealed with the UMN Thermal Jig after the extra cleaning process was determined and stopped. Thus, it would be interesting to fuse more tissue with the Thermal Jig at various time increments and various temperature thresholds. The time for sealing was held at a constant of 30 seconds. Proposed values for future tissue sealing would be from 5 – 30sec as commercial sealing devices operate closer to 10 seconds. Proposed temperature values for tissue sealing would be between 100 and 140ºC.

For tissue denaturation, it would be interesting to run the heating experiment in excess of 140ºC since that is where the Thermal Jig produced the best seals and to see if complete protein denaturation profiles can be achieved. The protein denaturation profiles were not complete at loads of 10N, 20N, and 50N. Finally, it may be interesting to test the reversibility of protein denaturation with and without pressure as it may give some insight to the use of pressure in sealing tissue.

BIBLIOGRAPHY

[1] Hon, L.-Q., Ganeshan, A., Thomas, S. M., Warakaulle, D., Jagdish, J., and Uberoi, R., 2009, "Vascular Closure Devices: A Comparative Overview," Curr Probl Diagn Radiol, **38**(1), pp. 33-43.

[2] Harold, K. L., Pollinger, H., Matthews, B. D., Kercher, K. W., Sing, R. F., and Heniford, B. T., 2003, "Comparison of Ultrasonic Energy, Bipolar Thermal Energy, and Vascular Clips for the Hemostasis of Small-, Medium-, and Large-Sized Arteries," Surg Endosc, **17**(8), pp. 1228-1230.

[3] Kennedy, J. S., Stranahan, P. L., Taylor, K. D., and Chandler, J. G., 1998, "High-Burst-Strength, Feedback-Controlled Bipolar Vessel Sealing," Surg Endosc, **12**(6), pp. 876-878.

[4] Nelson, M. T., Nakashima, M., and Mulvihill, S. J., 1992, "How Secure Are Laparoscopically Placed Clips? An in vitro and in vivo Study," Arch Surg, **127**(6), pp. 718-720.

[5] Romano, F., Caprotti, R., Franciosi, C., De Fina, S., Colombo, G., and Uggeri, F., 2002, "Laparoseopic Splenectomy Using Ligasure," Surg Endosc, **16**(11), pp. 1608-1611.

[6] Schuchert, M. J., Abbas, G., Landreneau, J. P., Luketich, J. D., and Landreneau, R. J., 2012, "Use of Energy-Based Coagulative Fusion Technology and Lung Sealants During Anatomic Lung Resection," J Thorac Cardiovasc Surg, **144**(3), pp. S48-S51.

[7] Sindram, D., Martin, K., Meadows, J. P., Prabhu, A. S., Heath, J. J., McKillop, I. H., and Iannitti, D. A., 2011, "Collagen-Elastin Ratio Predicts Burst Pressure of Arterial Seals Created Using a Bipolar Vessel Sealing Device in a Porcine Model," Surg Endosc, **25**(8), pp. 2604-2612.

[8] Bulsara, K. R., Sukhla, S., and Nimjee, S. M., 2006, "History of Bipolar Coagulation," Neurosurg Rev, **29**(2), pp. 93-96.

[9] Tucker, R., and Voyles, C. R., 1995, "Laparoscopic Electrosurgical Complications and Their Prevention," AORN Journal, **62**(1), pp. 49-71.

[10] Sileshi, B., Achneck, H., Ma, L., and Lawson, J. H., 2010, "Application of Energy-Based Technologies and Topical Hemostatic Agents in the Management of Surgical Hemostasis," Vascular, **18**(4), pp. 197-204.

[11] Tomita, Y., Koike, H., Takahashi, K., Tamaki, M., and Morishita, H., 1998, "Use of the Harmonic Scalpel for Nephron Sparing Surgery in Renal Cell Carcinoma," J Urol, **159**(6), pp. 2063-2064.

[12] Jackman, S. V., Cadeddu, J. A., Chen, R. N., Micali, S., Bishoff, J. T., Lee, B. R., Moore, R. G., and Kavoussi, L. R., 1998, "Utility of the Harmonic Scalpel for Laparoscopic Partial Nephrectomy," J Endourol, **12**(5), pp. 441-444.

[13] Phillips, C. K., Hruby, G. W., Duvak, E., Lehman, D. S., Humphrey, P. A., Mansukhani, M. M., and Landman, J., 2008, "Tissue Response to Surgical Energy Devices," Urology, **71**(4), pp. 744-748.

[14] Landman, J., Kerbl, K., Rehman, J., Andreoni, C., Humphrey, P. A., Collyer, W., Olweny, E., Sundaram, C., and Clayman, R. V., 2003, "Evaluation of a Vessel Sealing System, Bipolar Electrosurgery, Harmonic Scalpel, Titanium Clips, Endoscopic Gastrointestinal Anastomosis Vascular Staples and Sutures for Arterial and Venous Ligation in a Porcine Model," J Urol, **169**(2), pp. 697-700.

[15] Hruby, G. W., Marruffo, F. C., Durak, E., Collins, S. M., Pierorazio, P., Humphrey, P. A., Mansukhani, M. M., and Landman, J., 2007, "Evaluation of Surgical Eenergy Devices for Vessel Sealing and Peripheral Energy Spread in a Porcine Model," J Urol, **178**(6), pp. 2689-2693.

[16] Lamberton, G. R., Hsi, R. S., Jin, D. H., Lindler, T. U., Jellison, F. C., and Baldwin, D. D., 2008, "Prospective Comparison of Four Laparoscopic Vessel Ligation Devices," J Endourol, **22**(10), pp. 2307-2312.

[17] Newcomb, W. L., Hope, W. W., Schmelzer, T. M., Heath, J. J., Norton, H. J., Lincourt, A., Heniford, B. T., and Iannitti, D. A., 2009, "Comparison of Blood Vessel Sealing Among New Electrosurgical and Ultrasonic Devices," Surg Endosc, **23**(1), pp. 90-96.

[18] Person, B., Vivas, D. A., Ruiz, D., Talcott, M., Coad, J. E., and Wexner, S. D., 2008, "Comparison of Four Energy-Based Vascular Sealing and Cutting Instruments: A Porcine Model," Surg Endosc, **22**(2), pp. 534-538.

[19] Box, G. N., Lee, H. J., Abraham, J. B., Deane, L. A., Elchico, E. R., Abdelshehid, C. A., Alipanah, R., Taylor, M. B., Andrade, L., Edwards, R. A., Borin, J. F., McDougall, E. M., and Clayman, R. V., 2009, "Comparative Study of in vivo Lymphatic Sealing Capability of the Porcine Thoracic Duct Using Laparoscopic Dissection Devices," J Urol, **181**(1), pp. 387-391.

[20] Carbonell, A. M., Joels, C. S., Kercher, K. W., Matthews, B. D., Sing, R. F., and Heniford, B. T., 2003, "A Comparison of Laparoscopic Bipolar Vessel Sealing Devices in the Hemostasis of Small-, Medium-, and Large-Sized Arteries," J Laparoendosc Adv Surg Tech A, **13**(6), pp. 377-380.

[21] Kennedy, J. S., Buysse, S. P., Lawes, K. R., and Ryan, T. P., 1999, "Recent Innovations in Bipolar Electrosurgery," Minim Invasive Ther Allied Technol, **8**(2), pp. 95-99.

[22] Shigemura, N., Akashi, A., and Nakagiri, T., 2002, "New Operative Method for a Giant Bulla: Sutureless and Stapleless Thoracoscopic Surgery Using the Ligasure System," Eur J Cardiothorac Surg, **22**(4), pp. 646-648.

[23] Shigemura, N., Akashi, A., Nakagiri, T., Ohta, M., and Matsuda, H., 2004, "A New Tissue-Sealing Technique Using the LigaSure System for Nonanatomical Pulmonary Resection: Preliminary Results of Sutureless and Stapleless Thoracoscopic Surgery," Ann Thorac Surg, **77**(4), pp. 1415-1418.

[24] Abdallah, E., Ellatif, M. A., El Awady, S., Magdy, A., Youssef, M., Thabet, W., Lotfy, A., Elshobaky, A., and Morshed, M., 2015, "Is LigaSure a Safe Cystic Duct Sealer? An ex vivo Study," Asian J Surg, **38**(4), pp. 187-190.

[25] Bessa, S. S., Al-Fayoumi, T. A., Katri, K. M., and Awad, A. T., 2008, "Clipless Laparoscopic Cholecystectomy by Ultrasonic Dissection," J Laparoendosc Adv Surg Tech A, **18**(4), pp. 593-598.

[26] El-Geidie, A. A. R., 2012, "Single-Incision Laparoscopic Cholecystectomy (SILC) Using Harmonic Scalpel," J Surg Res, **176**(1), pp. 50-54.

[27] Kwak, H. Y., Chae, B. J., Park, Y. G., Kim, S. H., Chang, E. Y., Kim, E. J., Song, B. J., Jung, S. S., and Bae, J. S., 2014, "Comparison of Surgical Outcomes Between Papillary Thyroid Cancer Patients Treated with the Harmonic ACE Scalpel and LigaSure Precise Instrument During Conventional Thyroidectomy: A Single-Blind Prospective Randomized Controlled Trial," J Surg Res, **187**(2), pp. 484-489.

[28] Markogiannakis, H., Kekis, P. B., Memos, N., Alevizos, L., Tsamis, D., Michalopoulos, N. V., Lagoudianakis, E. E., Toutouzas, K. G., and Manouras, A., 2011, "Thyroid Surgery with the New Harmonic Scalpel: A Prospective Randomized Study," Surgery, **149**(3), pp. 411-415.

[29] Tsamis, D., Natoudi, M., Arapaki, A., Flessas, I., Papailiou, I., Bramis, K., Zografos, G., Leandros, E., and Albanopoulos, K., 2015, "Using Ligasure or Harmonic Ace in Laparoscopic Sleeve Gastrectomies? A Prospective Randomized Study," Obes Surg, **25**(8), pp. 1454-1457.

[30] Pastore, A. L., Palleschi, G., Silvestri, L., Leto, A., Sacchi, K., Pacini, L., Petrozza, V., and Carbone, A., 2013, "Prospective Randomized Study of Radiofrequency Versus Ultrasound Scalpels on Functional Outcomes of Laparoscopic Radical Prostatectomy," J Endourol, **27**(8), pp. 989-993.

[31] Palazzo, F. F., Francis, D. L., and Clifton, M. A., 2002, "Randomized Clinical Trial of Ligasure Versus Open Haemorrhoidectomy," Br J Surg, **89**(2), pp. 154-157.

[32] Heniford, B. T., Matthews, B. D., Sing, R. F., Backus, C., Pratt, B., and Greene, F. L., 2001, "Initial Results with an Electrothermal Bipolar Vessel Sealer," Surg Endosc, **15**(8), pp. 799-801.

[33] Sengupta, S., and Webb, D. R., 2001, "Use of a Computer-Controlled Bipolar Diathermy System in Radical Prostatectomies and Other Open Urological Surgery," ANZ J Surg, **71**(9), pp. 538-540.

[34] Matthews, B. D., Pratt, B. L., Backus, C. L., Kercher, K. W., Mostafa, G., Lentzner, A., Lipford, E. H., Sing, R. F., and Heniford, B. T., 2001, "Effectiveness of the Ultrasonic Coagulating Shears, LigaSure Vessel Sealer, and Surgical Clip Application in Biliary Surgery: A Comparative Analysis," Am Surg, **67**(9), pp. 901-906.

[35] Schulze, S., Damgaard, B., Jorgensen, L. N., Larsen, S. S., and Kristiansen, V. B., 2010, "Cystic Duct Closure by Sealing With Bipolar Electrocoagulation," JSLS, **14**(1), pp. 20-22.

[36] Levy, B., and Emery, L., 2003, "Randomized Trial of Suture Versus Electrosurgical Bipolar Vessel Sealing in Vaginal Hysterectomy," Obstet Gynecol, **102**(1), pp. 147-151.

[37] Dubuc-Lissoir, J., 2003, "Use of a New Energy-Based Vessel Ligation Device During Laparoscopic Gynecologic Oncologic Surgery," Surg Endosc, **17**(3), pp. 466-468.

[38] Romano, F., Caprotti, R., Franciosi, C., De Fina, S., Colombo, G., Sartori, P., and Uggeri, F., 2003, "The Use of LigaSure During Pediatric Laparoscopic Splenectomy: A Preliminary Report," Pediatr Surg Int, **19**(11), pp. 721-724.

[39] Slakey, D. P., 2008, "Laparoscopic Liver Resection Using a Bipolar Vessel-Sealing Device: LigaSure," HPB, **10**(4), pp. 253-255.

[40] Strasberg, S. M., Drebin, J. A., and Linehan, D., 2002, "Use of a Bipolar Vessel-Sealing Device for Parenchymal Transection During Liver Surgery," J Gastrointest Surg, **6**(4), pp. 569-574.

[41] Samulak, D., Wilczak, M., Michalska, M. M., and Pieta, B., 2011, "Vaginal Hysterectomy with Bipolar Coagulation Forceps (BiClamp) as an Alternative to the Conventional Technique," Arch Gynecol Obstet, **284**(1), pp. 145-149.

[42] Chia, K. V., Tandon, S., and Moukarram, H., 2007, "Vaginal Hysterectomy is Made Easier with ERBE Biclamp Forceps," J Obstet Gynaecol, **27**(7), pp. 723-725.

[43] Pniak, T., Formanek, M., Matousek, P., Zelenik, K., and Kominek, P., 2014, "Bipolar Thermofusion BiClamp 150 in Thyroidectomy: A Review of 1156 Operations," Biomed Res Int, pp. 1-4.

[44] Sakuragi, T., Okazaki, Y., Mitsuoka, M., Yamasaki, F., Masuda, M., Mori, D., Satoh, T., and Itoh, T., 2008, "The Utility of a Reusable Bipolar Sealing Instrument, BiClamp, for Pulmonary Resection," Eur J Cardiothorac Surg, **34**(3), pp. 505-509.

[45] Lee, S. W., Jeon, S. S., Lee, J. D., Lee, J. Y., Kim, S. C., and Koh, Y. W., 2008, "A Comparison of Postoperative Pain and Complications in Tonsillectomy Using BiClamp Forceps and Electrocautery Tonsillectomy," Otolaryngol Head Neck Surg, **139**(2), pp. 228-234.

[46] McVay, D., Nelson, D., Porta, C. R., Blair, K., and Martin, M., 2013, "Optimum Cystic Duct Closure: A Comparative Study Using Metallic Clips, ENSEAL, and ENDOLOOP in Swine," Am J Surg, **205**(5), pp. 547-550.

[47] Dunay, M. P., Nemeth, T., Makra, Z., Izing, S., and Bodo, G., 2012, "Laparoscopic Cryptorchidectomy and Ovariectomy in Standing Horses Using the EnSeal Tissue-Sealing Device," Acta Vet Hung, **60**(1), pp. 41-53.

[48] Smaldone, M. C., Gibbons, E. P., and Jackman, S. V., 2008, "Laparoscopic Nephrectomy Using the EnSeal Tissue Seating and Hemostasis System: Successful Therapeutic Application of Nanotechnology," JSLS, **12**(2), pp. 213-216.

[49] Rothmund, R., Kraemer, B., Brucker, S., Taran, F.-A., Wallwiener, M., Zubke, A., Wallwiener, D., and Zubke, W., 2013, "Laparoscopic Supracervical Hysterectomy Using EnSeal vs Standard Bipolar Coagulation Technique: Randomized Controlled Trial," J Minim Invasive Gynecol, **20**(5), pp. 661-666.

[50] Takemasa, I., Sekimoto, M., Ikeda, M., Mizushima, T., Yamamoto, H., Doki, Y., and Mori, M., 2010, "Transumbilical Single-Incision Laparoscopic Surgery for Sigmoid Colon Cancer," Surg Endosc, **24**(9), p. 2321.

[51] Cezo, J., Kramer, E., Taylor, K., Ferguson, V., and Rentschler, M., 2013, "Tissue Fusion Bursting Pressure and the Role of Tissue Water Content," Proc. Energy-Based Treatment of Tissue and Assessment VII, **8584**, p. 85840M.

[52] Anderson, N., Kramer, E., Cezo, J., Ferguson, V., and Rentschler, M. E., 2015, "Bond Strength of Thermally Fused Vascular Tissue Varies with Apposition Force," J Biomech Eng, **137**(12), pp. 1-6.

[53] Reyes, D. A. G., Brown, S. I., Cochrane, L., Motta, L. S., and Cuschieri, A., 2012, "Thermal Fusion: Effects and Interactions of Temperature, Compression, and Duration Variables," Surg Endosc, **26**(12), pp. 3626-3633.

[54] Cezo, J. D., Passernig, A. C., Ferguson, V. L., Taylor, K. D., and Rentschler, M. E., 2014, "Evaluating Temperature and Duration in Arterial Tissue Fusion to Maximize Bond Strength," J Mech Behav Biomed Mater, **30**, pp. 41-49.

[55] Cezo, J. D., Kramer, E., Taylor, K. D., Ferguson, V., and Rentschler, M. E., 2013, "Temperature Measurement Methods During Direct Heat Arterial Tissue Fusion," IEEE Trans Biomed Eng, **60**(9), pp. 2552-2558.

[56] Cezo, J. D., Kramer, E. A., Schoen, J. A., Ferguson, V. L., Taylor, K. D., and Rentschler, M. E., 2015, "Tissue Storage ex vivo Significantly Increases Vascular Fusion Bursting Pressure," Surg Endosc, **29**(7), pp. 1999-2005.

[57] Patel, A., Fine, B., Sandig, M., and Mequanint, K., 2006, "Elastin Biosynthesis: The Missing Link in Tissue-Engineered Blood Vessels," Cardiovasc Res, **71**(1), pp. 40-49.

[58] Wagenseil, J. E., and Mecham, R. P., 2009, "Vascular Extracellular Matrix and Arterial Mechanics," Physiol Rev, **89**(3), pp. 957-989.

[59] Dinardo, C. L., Venturini, G., Zhou, E. H., Watanabe, I. S., Campos, L. C. G., Dariolli, R., da Motta-Leal-Filho, J. M., Carvalho, V. M., Cardozo, K. H. M., Krieger, J. E., Alencar, A. M., and Pereira, A. C., 2014, "Variation of Mechanical Properties and Quantitative Proteomics of VSMC Along the Arterial Tree," Am J Physiol Heart Circ Physiol, **306**(4), pp. H505-H516.

[60] Hynes, R. O., and Yamada, K. M., 2012, *Extracellular Matrix Biology*, Cold Spring Harbor Laboratory Press, Cold Spring Harbor, NY.

[61] Pearce, J., 2015, "Numerical Model Study of Radio Frequency Vessel Sealing Thermodynamics," Proc. Energy-Based Treatment of Tissue and Assessment VIII, **9326**, p. 93260A.

[62] Bischof, J. C., and He, X. M., 2005, "Thermal Stability of Proteins," Ann NY Acad Sci, **1066**, pp. 12-33.

[63] Johnson, F. H., Eyring, H., and Stover, B. J., 1974, *The Theory of Rate Processes in Biology and Medicine*, Wiley, New York, NY.

[64] Kakivaya, S. R., and Hoeve, C. A. J., 1975, "The Glass Point of Elastin," Proc Natl Acad Sci USA, **72**(9), pp. 3505-3507.

[65] Thomsen, S., 1991, "Pathologic Analysis of Photothermal and Photomechanical effects of Laser-Tissue Interactions," Photochem Photobiol, **53**(6), pp. 825-835.

[66] Miles, C. A., Burjanadze, T. V., and Bailey, A. J., 1995, "The Kinetics of the Thermal Denaturation of Collagen in Unrestrained Rat Tail Tendon Determined by Differential Scanning Calorimetry," J Mol Biol, **245**(4), pp. 437-446.

[67] Venkatasubramanian, R. T., Wolkers, W. F., Shenoi, M. M., Barocas, V. H., Lafontaine, D., Soule, C. L., Iaizzo, P. A., and Bischof, J. C., 2010, "Freeze-Thaw Induced Biomechanical Changes in Arteries: Role of Collagen Matrix and Smooth Muscle Cells," Ann Biomed Eng, **38**(3), pp. 694-706.

[68] Miles, C. A., Avery, N. C., Rodin, V. V., and Bailey, A. J., 2005, "The Increase in Denaturation Temperature Following Cross-Linking of Collagen is Caused by Dehydration of the Fibres," J Mol Biol, **346**(2), pp. 551-556.

[69] Sutton, C., 1995, "Power Sources in Endoscopic Surgery," Curr Opin Obstet Gyn, **7**(4), pp. 248-256.

[70] Foschi, D., Cellerino, P., Corsi, F., Previde, P., Allevi, R., and Trabucchi, E., 2009, "Closure of the Cystic Duct by Ultrasonic Energy An Electron-Microscopic and Biomechanical Study in Man," Surg Laparosc Endosc Percutan Tech, **19**(1), pp. 34-38.

[71] Dunay, M. P., Jakab, C., and Nemeth, T., 2012, "Evaluation of EnSeal, an Adaptive Bipolar Electrosurgical Tissue-Sealing Device," Acta Vet Hung, **60**(1), pp. 27-40.

[72] ETHICON, 2016, "ENSEAL® G2 Curved and Straight Tissue ", from http://www.ethicon.com/sites/default/files/products/energy/ENSEAL-G2-Device-popup-641x403.png.

[73] ETHICON, 2016, "ENSEAL® G2 Curved and Straight Tissue Sealers," from http://www.ethicon.com/healthcare-professionals/products/advanced-energy/enseal/enseal-g2-tissue-sealers#!science-and-technology.

[74] Ingle, J. D., and Crouch, S. R., 1988, *Spectrochemical Analysis*, Prentice Hall, Englewood Cliffs, NJ.

[75] Wang, S. P., Oldenhof, H., Dai, X. L., Haverich, A., Hilfiker, A., Harder, M., and Wolkers, W. F., 2014, "Protein Stability in Stored Decellularized Heart Valve Scaffolds and Diffusion Kinetics of Protective Molecules," Biochim Biophys Acta, **1844**(2), pp. 430-438.

[76] Wolkers, W. F., and Oldenhof, H., 2010, "In situ FTIR Studies on Mammalian Cells," Spectroscopy, **24**(5), pp. 525-534.

[77] He, X. M., Wolkers, W. F., Crowe, J. H., Swanlund, D. J., and Bischof, J. C., 2004, "In situ Thermal Denaturation of Proteins in Dunning AT-1 Prostate Cancer Cells: Implication for Hyperthermic Cell Injury," Ann Biomed Eng, **32**(10), pp. 1384-1398.

[78] Barth, A., 2007, "Infrared Spectroscopy of Proteins," Biochim Biophys Acta, **1767**(9), pp. 1073-1101.

[79] Miles, C. A., and Ghelashvili, M., 1999, "Polymer-in-a-Box Mechanism for the Thermal Stabilization of Collagen Molecules in Fibers," Biophys J, **76**(6), pp. 3243-3252.

[80] Alexander, J., 1923, *Glue and Gelatin*, The Chemical Catalog Company, Inc., New York, NY.

[81] Haris, P. I., and Severcan, F., 1999, "FTIR Spectroscopic Characterization of Protein Structure in Aqueous and Non-Aqueous Media," J Mol Catal B-Enzym, **7**(1–4), pp. 207-221.

[82] Savitzky, A., and Golay, M. J. E., 1964, "Smoothing and Differentiation of Data by Simplified Least Squares Procedures," Anal Chem, **36**(8), pp. 1627-1639.

[83] Qin, Z., Balasubramanian, S. K., Wolkers, W. F., Pearce, J. A., and Bischof, J. C., 2014, "Correlated Parameter Fit of Arrhenius Model for Thermal Denaturation of Proteins and Cells," Ann Biomed Eng, **42**(12), pp. 2392-2404.

APPENDIX TABLE OF CONTENTS

LIST OF APPENDIX TABLES

LIST OF APPENDIX FIGURES

APPENDIX A: Determination of Pressure Based on Load from Thermal Jig

Background: The thermal jig was built in order to control temperature and pressure applied to arteries.

Purpose: This appendix will clarify what pressure resulted from the load placed on the thermal jig to seal arteries.

Content: An artery was placed between the top and bottom plates of the thermal jig for a tissue sealing experiment. The weight was then placed on top of the top plate to squeeze the arteries together. The minimum and maximum pressures were estimated in the following way.

Minimum Pressure: The minimum pressure would correspond to the smallest load over the largest artery area. The lowest load used was 20lb. The largest area for the artery was estimated to be the 1.0 in wide plate. This would happen if the load was distributed equally across the length of the jaws. See highlighted area in Appendix Figure 1.

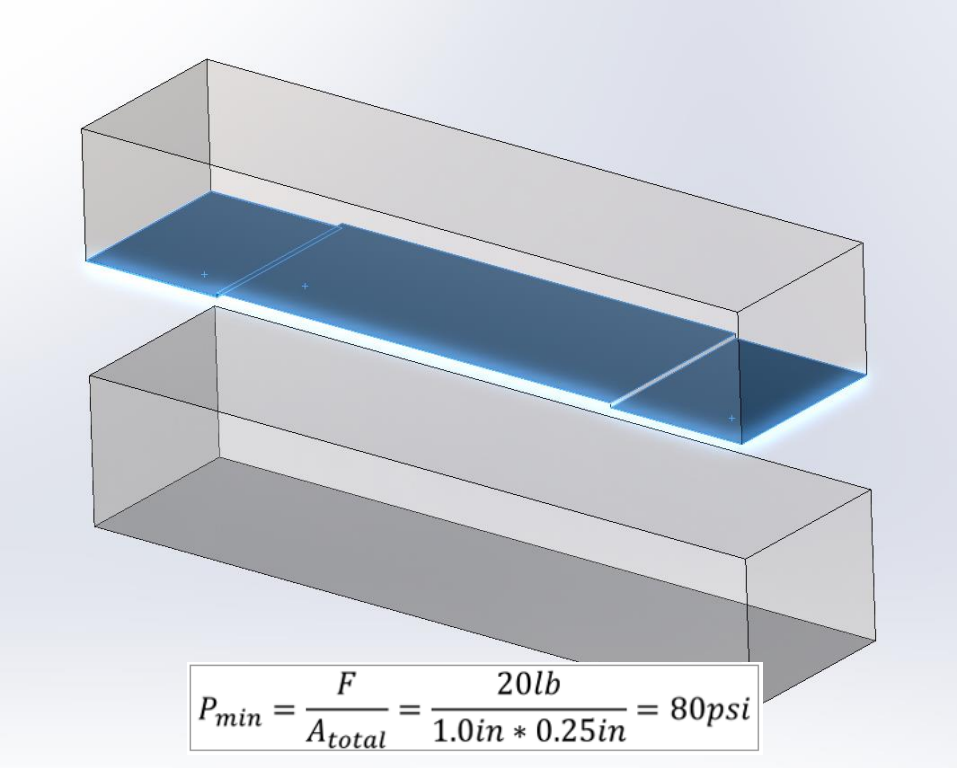

Appendix Figure 1: Highlighted region shows largest area interaction with artery

The area highlighted in the above figure may be on the high side as a typical seal width was ~8mm which is much smaller than 1.0in (25mm). Also, it would be highly unlikely for the load to be equally distributed along the whole jaws.

Maximum Pressure: The maximum pressure was determined by using the largest load (50lb) and dividing by a smaller artery area. This area is that corresponding to the .006 in milled step. It has a .6 in length. See **Appendix Figure 2** below.

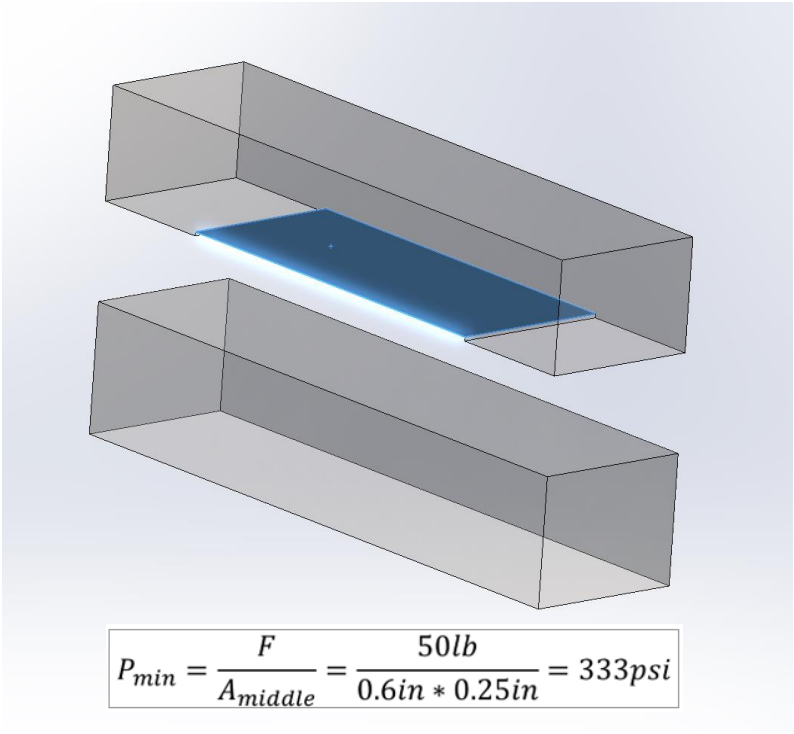

Appendix Figure 2: Area that artery bears under maximum pressure

This maximum pressure may be a little on the low side since a sealed artery may have a seal width of ~8mm and probably will not fill up the entire .6 in (15mm) milled step length.

Conclusion: This appendix was to show how pressure was calculated from the thermal jig design. The calculated pressures may be a little on the low side.

APPENDIX B: Timeline of Burst Measurements

Background: Ethicon provided the arteries for testing. Testing was done to determine the best temperature and pressure for sealing arteries.

Timeline: Initial Testing was done in the Fall of 2014 which proved the viability of performing controlled temperature and pressure sealing of arteries. During the Spring of 2015, more testing was completed in order to understand how the burst pressure was correlated with changing temperature and pressure.

1. Thermal Jig Proof of Concept (Fall 2014):

During Fall 2014, temperature measurements made corresponded to the highlighted boxes in **Appendix Table 1**.

Appendix Table 1: Fall 2014 Sealing Parameters

120ºC 20lb	120ºC 35lb	120ºC 50lb
140ºC 20lb	140ºC 35lb	140ºC 50lb

1.1 Initial Results: OCT 3 – 4 , 2014

Goal: The goal is to seal five (n = 5) samples at two different parameters. These samples will be given to Nathan for further testing.

Protocol: First the heaters were preheated to 120ºC. Next, tissue was placed on the heater. Next, the weight was placed on the thermal jig. Next, the timer was started. Once the timer had reached 30s or 120s for the run, the timer was stopped.

Sealing Summary: Sample temperature only reached 100 – 115ºC at the end of a given run. Because of reaching a low temperature of 100ºC initially, the heaters were increased to 125ºC and 134ºC, respectively. See Joel's Lab Notebook I pages 49 – 51.

Burst Summary: Sealing was performed by Nathan Cal. Only results from time interval 120s were recorded as none of the vessels treated at 30s were sealed. More information can be found in Nathan's Lab Notebook on page 52. See Appendix Figure 3 below for review of data at 120ºC and 50lb.

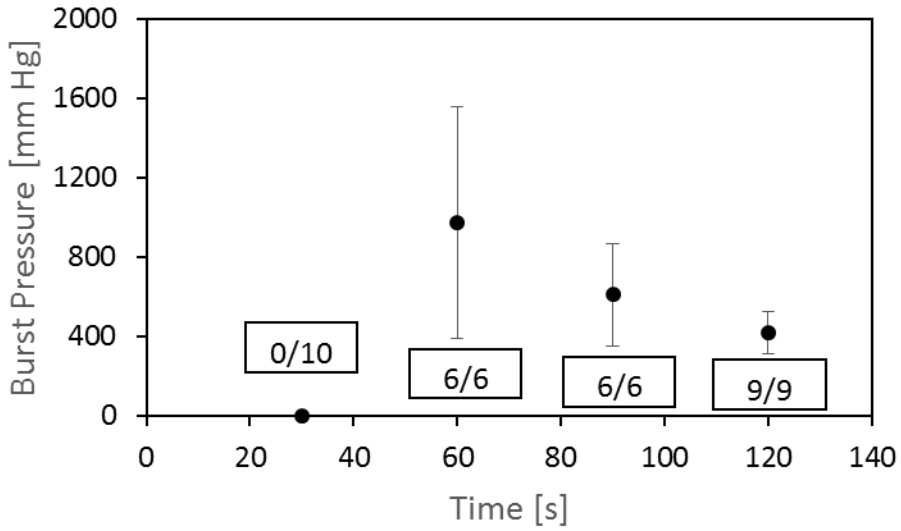

Appendix Figure 3: Summary of Burst measurements at 120ºC; 50lb

2 Thermal Jig Sealing Measurements (Spring 2015)

After the measurements in Fall 2014, Ethicon agreed to do more testing by varying the temperature and pressure of the Thermal Jig. The time interval was held essentially constant at 30s. This is longer than a conventional energy-based sealing device, but it was a time interval at which a seal would be confidently made. During the Spring of 2015, the measurements made corresponds to the highlighted boxes in Appendix Table 2.

Appendix Table 2: Measurements Made in Spring 2015

80ºC 20lb	80ºC 35lb	80ºC 50lb
100ºC 20lb	100ºC 35lb	100ºC 50lb
120ºC 20lb	120ºC 35lb	120ºC 50lb
140ºC 20lb	140ºC 35lb	140ºC 50lb
$160ºC_{set}$ 20lb	$160ºC_{set}$ 35lb	$160ºC_{set}$ 50lb

2.1 Intial Testing: JAN - APR 1 – 3, 2015 – ENSEAL and Thermal Jig

Testing from January to April yielded the following results in Appendix Figure 4.

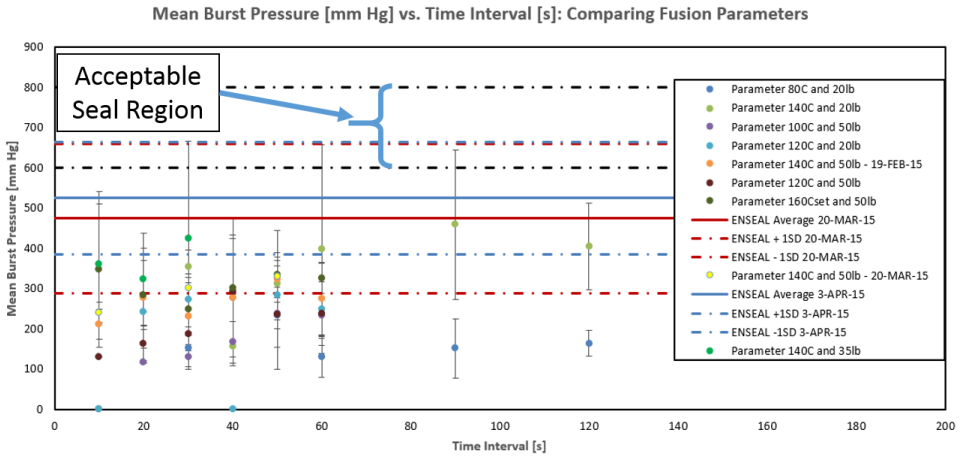

Appendix Figure 4: Initial Burst Results from January to April of 2015

The above burst results were below the expected values of burst pressure and did not reach the acceptable burst values between 600 – 800 mm Hg. Investigation was done to determine the cause of the low burst pressure with both the Thermal Jig and ENSEAL at UMN.

Ethicon did testing by varying the time from harvest, and changing how they prepare tissue. The results are shown below in Appendix Figure 5.

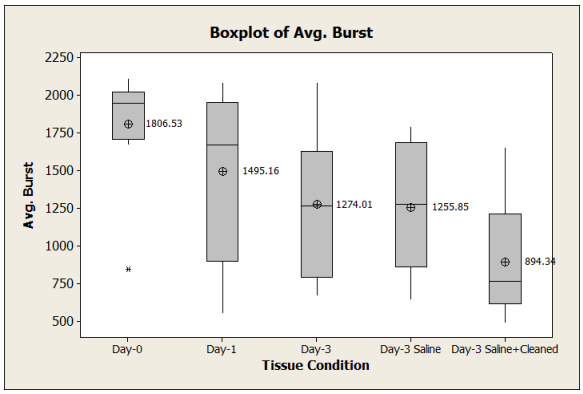

Appendix Figure 5: Ethicon testing results by varying sealing time and tissue preparation. The average burst pressure decreases with time from harvest. Additionally, the burst pressure decreases within Day-3 groups when the tissues were cleaned as seen in group "Day-3 Saline+Cleaned". The drop in burst pressure may be affected by the cleaning procedure done by UMN.

Conclusions:

The burst pressure at 140ºC and 35lbs still had means around 300mm Hg. The ENSEAL device sealed faster by blotting the tissue, and the mode seal time of 10s is close to historical ENSEAL sealing times which is approximately 8s. The time interval of 30s at 140ºC and 35lb is comparable to the ENSEAL data that UMN tested. Next round of UMN tissue

testing will test tissue with and without removing the outer layer of tissue that has been exclusively used at UMN up to this point.

2.2 Testing Date: APR 15 – 17, 2015 – ENSEAL and 140ºC & 35lb

Purpose: This testing will use ENSEAL device along with thermal jig parameters 140ºC and 35lb to determine if the tissue preparation (i.e., the removal of the "excessive tissue") is causing a reduction in burst pressure values. Also, the testing will be a day earlier as well.

Protocol: The Thermal Jig will be used to test sixteen arteries according to the following requirements. Eight arteries will be tested with tissue removed, and eight will be tested without tissue removed.

Sealing Summary:

Tissue was harvested on Apr 13th, 2015 and arrived on Apr 15th, 2015. Sealing was done on Apr 15th – 17th.

Heaters were set to 150ºC. Tissue temperature was initially at 143ºC, and it settled to approximately 140 ± 3ºC for the remainder of the run. Details on sealing can be found in Joel's Notebook III on pages 22 – 27 and 31 – 33.

For ENSEAL measurements, the sealing time was 9 ± 1s. Blotting the tissue and using the procedure outlined by Mark who said to "I typically start energy delivery, wait 1-2 seconds for the tissue effects to start, and then begin to move the I-Blade prior to hearing the change in pitch." The same generator and device were used as in Mar 18 – 20.

Burst and Peel Summary:

Sealed tissue was tested for burst and peel on Apr 3rd. Testing was done by Joel Scheumann, and the results can be found in Joel's Notebook III on pages 28 – 30 and 34. The results of burst pressure and burst vs. peel can be found in Appendix Figure 6 below.

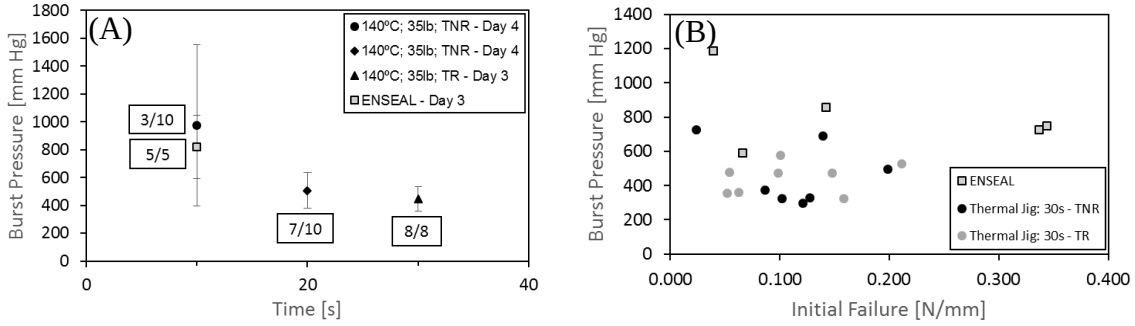

Appendix Figure 6: Panel (A) shows burst results from April 17th testing. Panel (B) shows the burst value plotted against initial peel value from the same artery again from the April 17th testing.

Conclusions:

This testing shows most pointedly that the data from the ENSEAL has a mean within of approximately 800mm Hg which is comparable to what commercial energy devices get. This is encouraging that the ENSEAL device at UMN is operating similar to how other

ENSEAL devices act in clinical applications. Future work was decided to do more testing on 100ºC and 140ºC to discern if this difference in burst pressure with the ENSEAL is observed with the Thermal Jig. Peel tests were suspended as they had not yielded a correlation between burst and took quite a bit of time to do.

2.3 Testing Date: APR 22 – 23, 2015 – 100ºC; 50lb and 140ºC; 50lb

Purpose: The purpose of this testing is to see if one can distinguish between the thermal jig parameters of 140ºC; 50lb; 30s and 100ºC; 50lb; 30s.

Protocol: Fifteen arteries will be used for each. With each artery being cut in half and tested, thirty samples will be available for each method. During sealing, seal the tissue as received by Ethicon. Store the sealed tissue in the polybags sent by Ethicon. Blot tissue before sealing.

Sealing Summary:

Tissue was harvested on Apr 20th, 2015 and arrived on Apr 22nd, 2015. Sealing was done on Apr 23rd.

For parameter 140ºC, heaters were set to 150ºC. Tissue temperature was initially at 143ºC, and it settled to approximately 140 ± 3ºC for the remainder of the run. For the 100ºC parameter, the heaters were set to 100ºC. Tissue temperature was within the range of 100 ± 5ºC for the whole run. Details on sealing can be found in Joel's Notebook III on pages 36 – 40.

Burst Summary:

Sealed tissue was tested for burst and peel on Apr 23rd. Testing was done by Joel Scheumann, and the results can be found in Joel's Notebook III on pages 41 – 42. The results of burst pressure and burst vs. peel can be found in Appendix Figure 7 below.

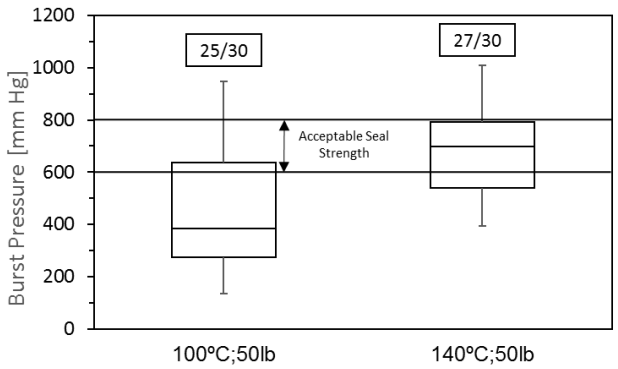

Appendix Figure 7: Boxplot of burst pressure for Thermal Jig with parameters of 100ºC; 50lb and 140ºC; 50lb for the time interval of 30s. The boxes above both of the boxplots indicate the number of successfully sealed arteries that recorded a burst pressure instead of leaking immediately.

Conclusions:

The measurements show that increasing the temperature from 100ºC to 140ºC, the burst pressure significantly increases. The increase of burst pressure of the 140ºC; 50lb parameter has its median in the range of 600 – 800mm Hg which is considered an acceptable seal strength according to Ethicon. The burst pressure at 140ºC; 50lb; 30s is much greater from previous testing from March 18th – 20th and February 18th – 20th. More work of testing 100ºC; 20lb; 30s and 140ºC; 20lb; 30s.

2.4 Testing Date: MAY 6 – 7, 2015 – 100ºC; 20lb and 140ºC; 20lb

Purpose: The purpose of this testing is to see if one can distinguish between the thermal jig parameters of 140ºC; 20lb; 30s and 100ºC; 20lb; 30s.

Protocol: Fifteen arteries will be used for each. With each artery being cut in half and tested, thirty samples will be available for each method. During sealing, seal the tissue as received by Ethicon. Store the sealed tissue in the polybags sent by Ethicon. Blot tissue before sealing. Additionally, the arteries were weighed at three times: before blotting, after blotting, and after sealing.

Sealing Summary:

Tissue was harvested on May 4th, 2015 and arrived on May 6th, 2015. Sealing was done on May 7th.

For parameter 140ºC, heaters were set to 150ºC. Tissue temperature was initially at 143ºC, and it settled to approximately 140 ± 3ºC for the remainder of the run. For the 100ºC parameter, the heaters were set to 100ºC. Tissue temperature was initially at 93ºC. After 10s, the temperature was within the range of 100 ± 5ºC for the remainder of the run. Details on sealing can be found in Joel's Notebook III on pages 44 – 49.

Burst Summary:

Sealed tissue was tested for burst and peel on May 7th. Testing was done by Joel Scheumann, and the results can be found in Joel's Notebook III on pages 50 – 51. The results of burst pressure and burst vs. peel can be found in Appendix Figure 8 below.

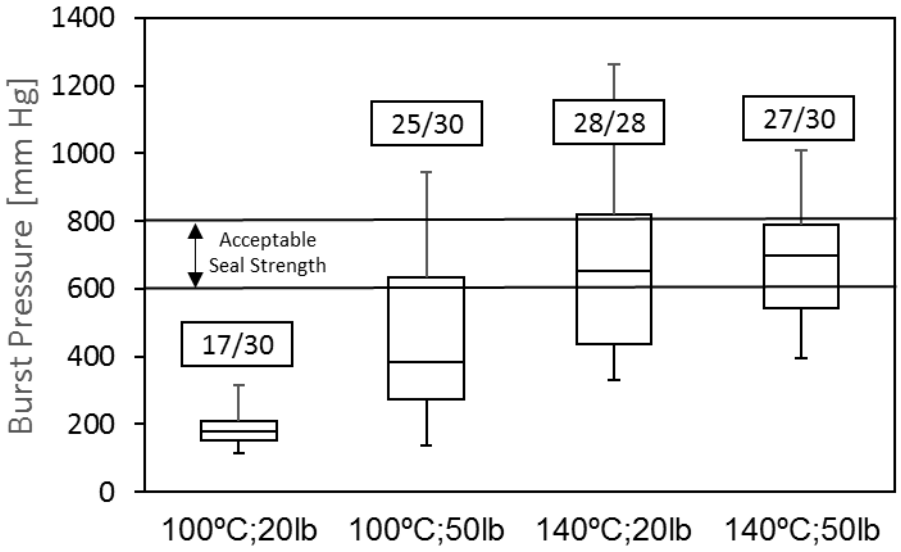

Appendix Figure 8: Burst pressure summary of 140ºC;50lb, 140ºC;20lb, 100ºC;50lb, and 100ºC;20lb at time interval of 30 seconds. The number in the boxes indicate the number of samples that recorded an appreciable burst pressure instead of leaking immediately. For 140ºC;20lb, two samples had abnormally high burst values of 1651 and 1719mm Hg which made the sample size not conform to normality. After removing them, the group met normality requirements.

Conclusions:

The latest data shows that a significant different arises from sealing the tissue as received from Ethicon. Also, it gives data that is comparable to what energy sealers output. With the significant difference in sealing by not removing the tissue, the previous data for both burst and peel seems to be invalidated. With the lack of correlation between burst and peel in the initial testing, it seems possible though still unlikely that performing measurements on burst and peel as received from Ethicon will yield a correlation.

APPENDIX C: Tissue Preparation Discovery

Purpose: This appendix will describe how the tissue preparation changed with recommendations from Ethicon.

Introduction:
The burst pressure values received when testing with the Thermal Jig and the ENSEAL device were much below the expected value of 600 – 800 mm Hg. The graph of the low burst values is shown below in Appendix Figure 9.

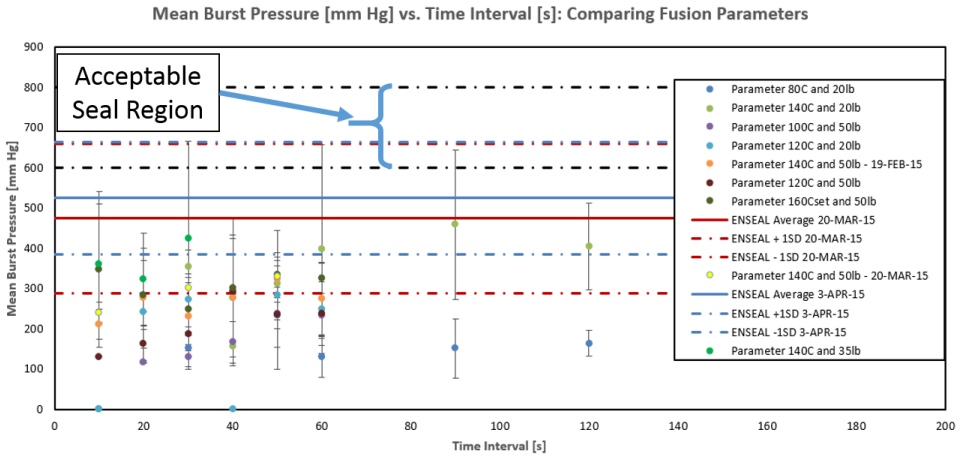

Appendix Figure 9: Initial Burst Values

In order to investigate why the burst values were so low, several processes were examined which included the time from harvest to burst testing, performance of the pressure transducer, and the preparation of the arteries themselves.

Methods:
Burst Time:
According to communication with UMN, Ethicon did some testing based on the timeline of when tissue was received from a slaughterhouse. The timeline for normal week was the following:

- **Monday:** Tissue was harvested by slaughterhouse and sent overnight to Ethicon
- **Tuesday:** Tissue received by Ethicon, cleaned and sent overnight to UMN
- **Wednesday:** Tissue received by UMN and performed sealing procedure
- **Thursday:** Tissue burst tested by UMN

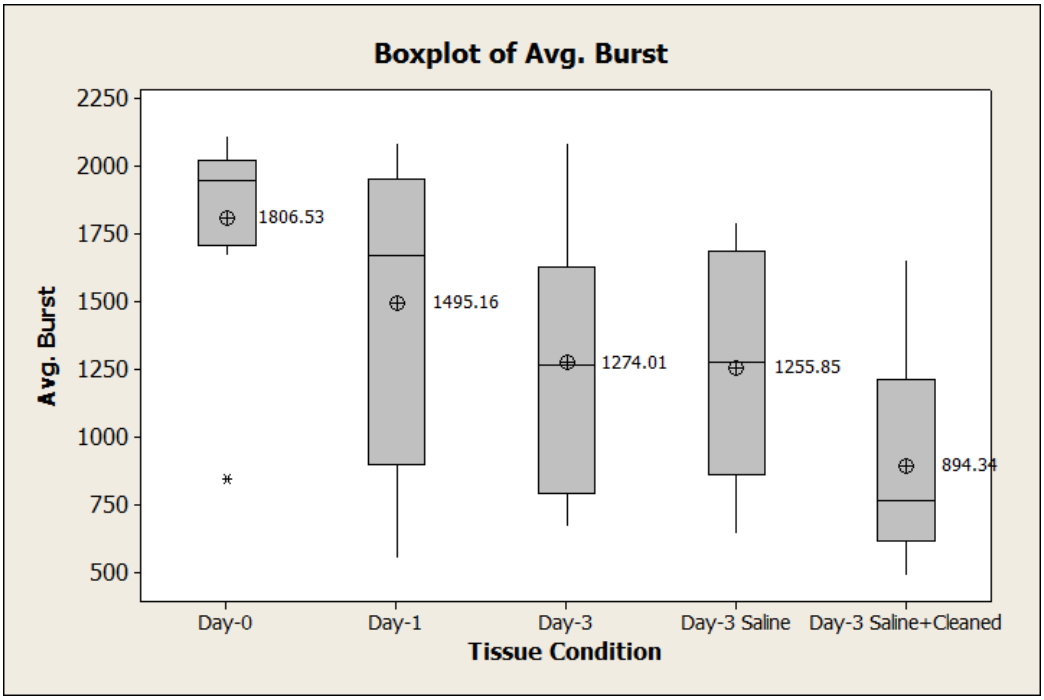

Appendix Figure 10: Ethicon Testing for Time and Preparation

Day-0 = Freshly harvested Carotids sealed on the day of delivery (Tuesday 4/7). No treatment besides standard Ethicon preparation protocol (which was done on all specimens).

Day-1 = Carotids sealed on the day after delivery (Wednesday 4/8). No treatment except refrigerated overnight. Observed lower mean and more variation in burst data.

Day-3 = Carotids sealed 3 days after delivery (Friday 4/10). No treatment except refrigerated for 3 days. Drop in burst mean but about the same variation as Day-1.

Day-3 Saline = Carotids sealed 3 days after delivery (Friday 4/10). Saline was added to the individual polybags and refrigerated for 3 days. The addition of saline is how I deliver to you. Burst mean and variation are the same as Day-3 data (no saline).

Day-3 Saline+Cleaned = Carotids sealed 3 days after delivery (Friday 4/10). These specimens were cleaned of excess tissue per your procedure. I did not take photos but am confident that they are similar in appearance to the images you provided. They were then placed back in the individual polybags, saline was added, and they were refrigerated for 3 days. Substantial drop in burst mean.

Pressure Transducer:
The pressure transducer was tested to determine if it was giving systematically low values. This was tested by hooking up a syringe to the transducer and compressing the syringe by 50%. This compression should result in a reading of 760mm Hg which is approximately 1 atmosphere. This follows from the assumption of ideal gas law relation that $P_1V_1 = P_2V_2$. By decreasing the volume by a factor of two, the pressure should increase by a factor of two (the reading will only show one atmosphere because of one atmosphere already being in the syringe at the beginning.

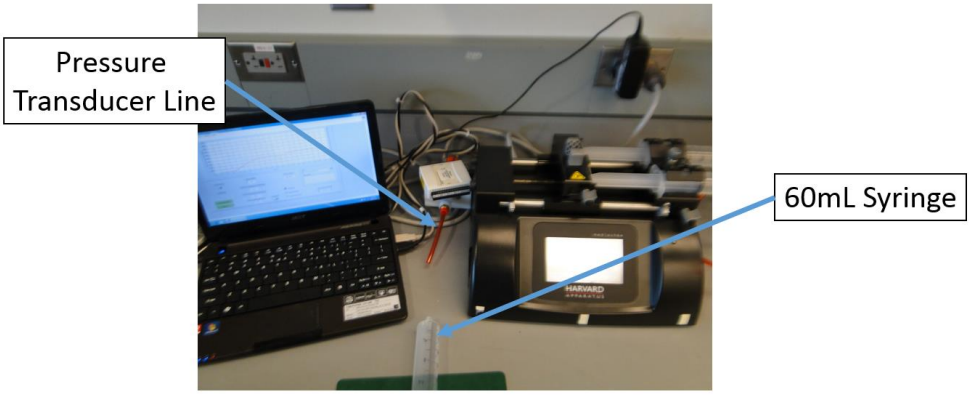

Appendix Figure 11: Testing Pressure Transducer

The results of the experiment are shown in Appendix Figure 12. Not only was the syringe compressed by 50% but also in 10mL increments from 50mL to 15mL.

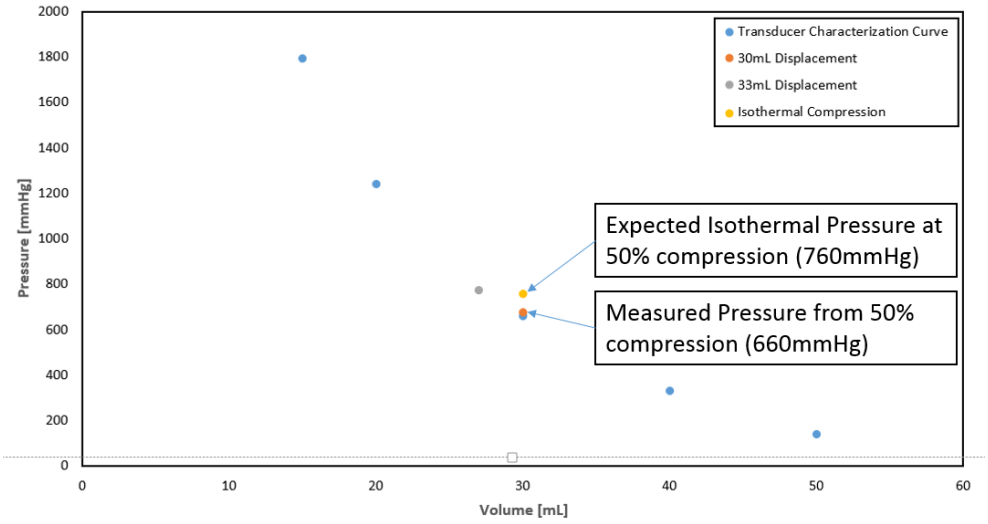

Appendix Figure 12: Pressure Transducer Results

From Appendix Figure 12, the pressure transducer was only off by 100mm Hg. This pressure difference is not enough to warrant a hypothesis that claims that the pressure transducer is responsible for the low burst pressure values.

Artery Preparation:
UMN Tissue preparation included further cleaning of the arteries that were sent by Ethicon. The arteries before and after cleaning are shown in Appendix Figure 13.

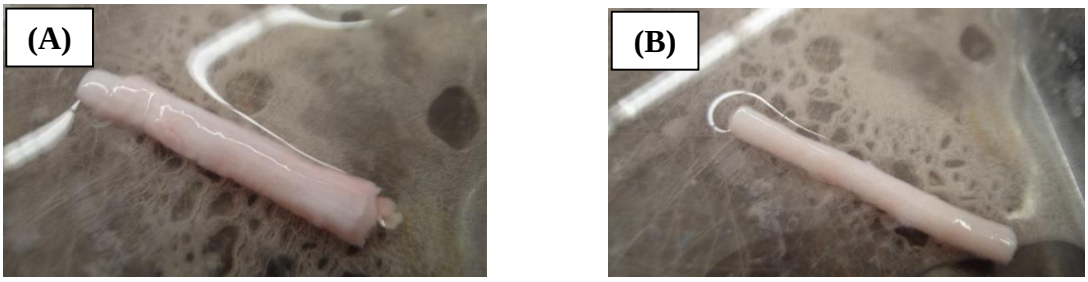

Appendix Figure 13: (A) Pre-Cleaning; (B) Post-Cleaning

This process was not encouraged by Ethicon, and they recommended to stop it and test the arteries as they were received as they perform the cleaning that they deem necessary.

Results:

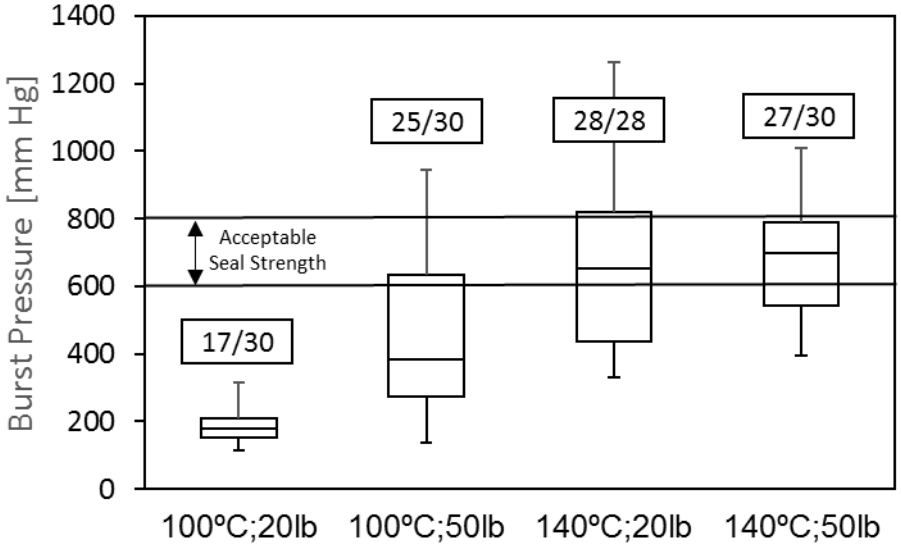

Appendix Figure 14: Thermal Jig sealing results by not performing the extra cleaning

Conclusion:
With the more reproducible results coming from the higher temperatures of 140ºC, it seems that the main cause was testing the arteries as received from Ethicon and not performing additional cleaning. The tissue removed was a part of the adventitia layer of the artery and probably high in collagen. One hypothesis why removing the adventitia decreased the burst pressure is that this extra cleaning process was removing large amounts of collagen which is a major contributor in sealing the artery. By removing this layer, the artery did not have enough material to provide an effective seal.

APPENDIX D: Denaturation Onset of Old Tissue

Background:

Denaturation onset measurements were completed on carotid arteries and rat tail tendons. Careful attention to the storage time of tissue was not kept track.

Purpose:

Demonstrate how the denaturation onset varied with time from harvest in both carotid arteries and rat tail tendon.

Protocol:

Initial denaturation measurements did not monitor closely the length of time between tissue harvest and testing performed. Thus, time from harvest to testing was as long as seventeen days from harvest to test. As the protocol for making denaturation measurements was finalized and tissue procurement was regular, time from harvest to test was reduced to a maximum of three days.

Results:

The difference in denaturation offset for carotid artery is shown below in Appendix Figure 15.

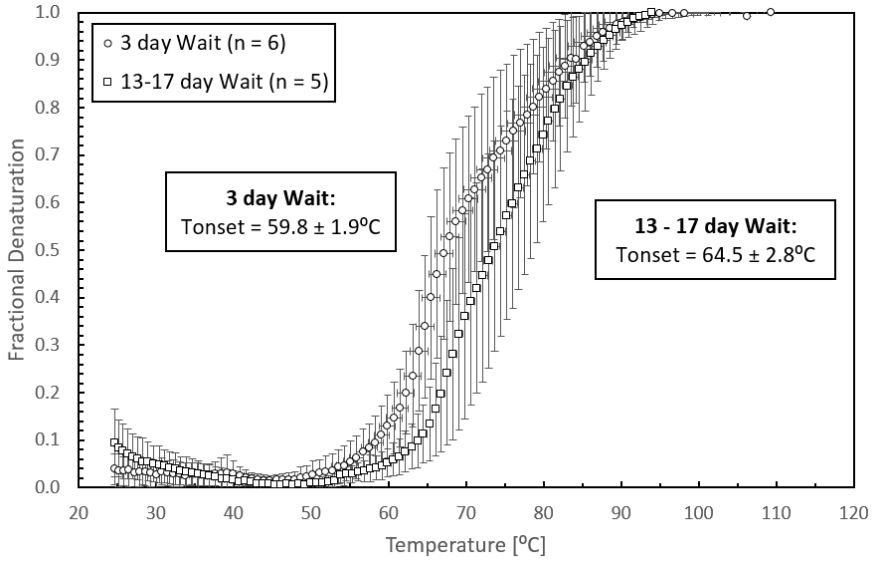

Appendix Figure 15: Denaturation for carotid artery with 3 day wait and 13-17 day wait

Also, the variation in denaturation onset can be seen for rat tail tendon in Appendix Figure 16.

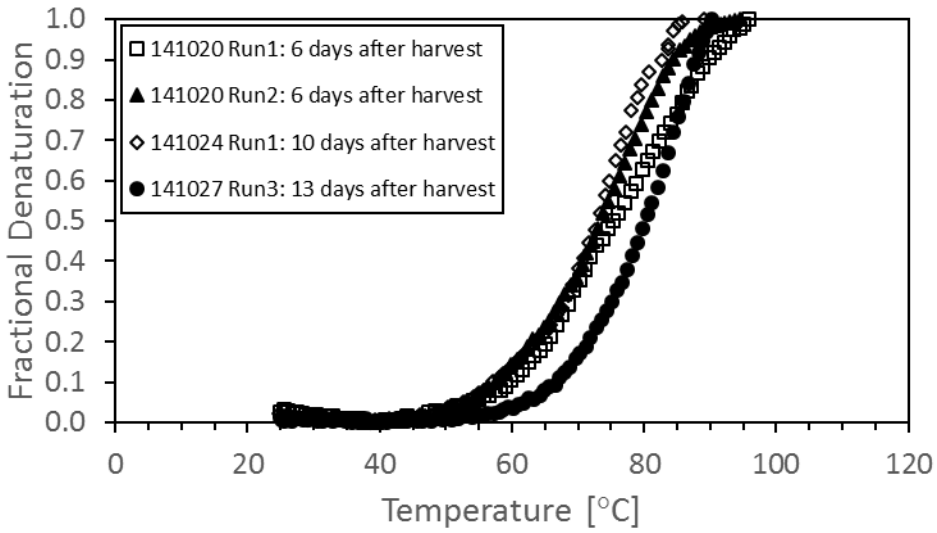

Appendix Figure 16: Denaturation for carotid artery with various lengths of time between harvest and test

Conclusion:

For the carotid artery testing, a significant difference is present between "3 day Wait" and "13 – 17 day Wait" ($p = 0.016$) using a two-tailed, unequal variance t-test. For the rat tail tendon, the denaturation onset at 13 days on October 27th is much larger than the earlier testing. More data would have to be taken to determine a significant difference in waiting with rat tail tendon. In summary, care should be taken in the time between harvest and test with denaturation measurements. In Wang, S. the denaturation onset did not change significantly for DSC when waiting 0 days, 9 days, and 34 days from harvest to test [75].

APPENDIX E: Calculation of Denaturation Onset

Purpose: This will describe the raw spectra was processed in order to calculate denaturation onset for a particular tissue specimen.

Starting Out: Raw Spectra:
An initial spectra of carotid artery soaked in a 0.9% w/v D_2O solution looks like the following in Appendix Figure 17. Also, it contains the characteristic bands from literature [75, 78, 81].

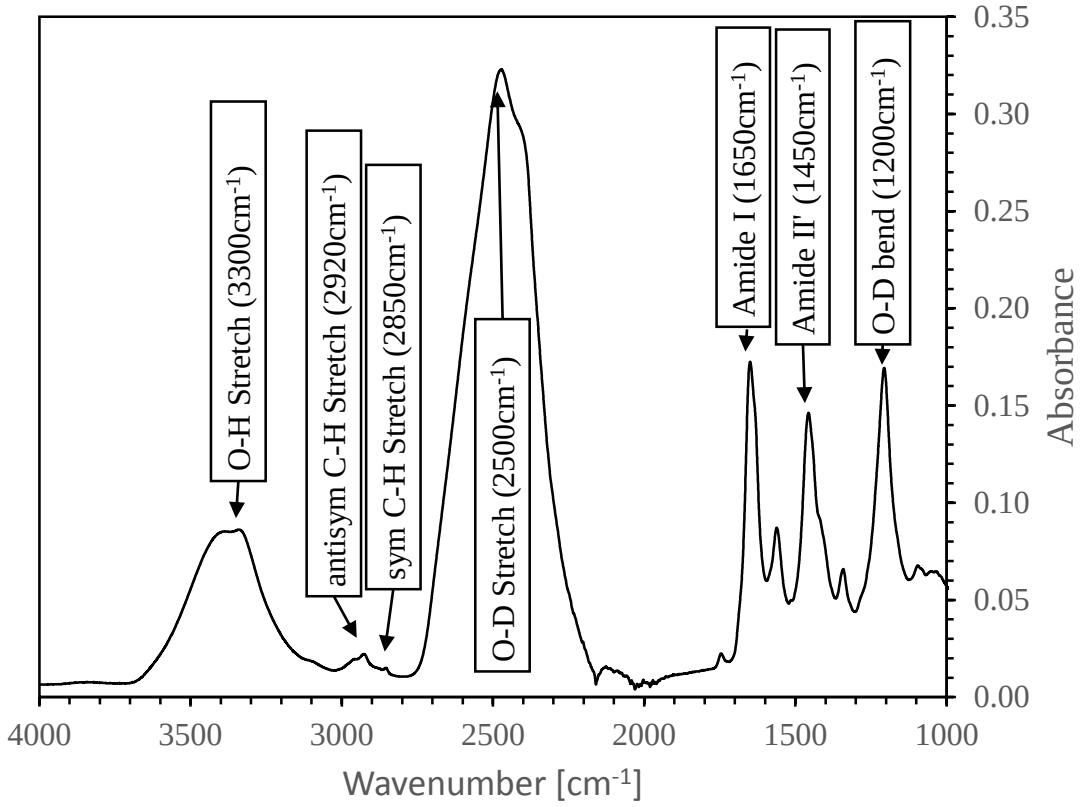

Appendix Figure 17: Representative FTIR Spectra of Sample Carotid Artery

Methods of Recording Spectra:
The heater was set to 2.5ºC/min, and the heating range was from 25ºC – 120ºC. Due to the heating lag between the heater and the sample (See Appendix B), the sample temperature heating range was from 25ºC to ~100ºC.

After starting the heating rate, spectra were recorded every 1ºC change in the heater temperature. To determine the sample temperature, an additional thermocouple was placed between the diamond crystal and the sample tissue as shown in Appendix Figure 18 below.

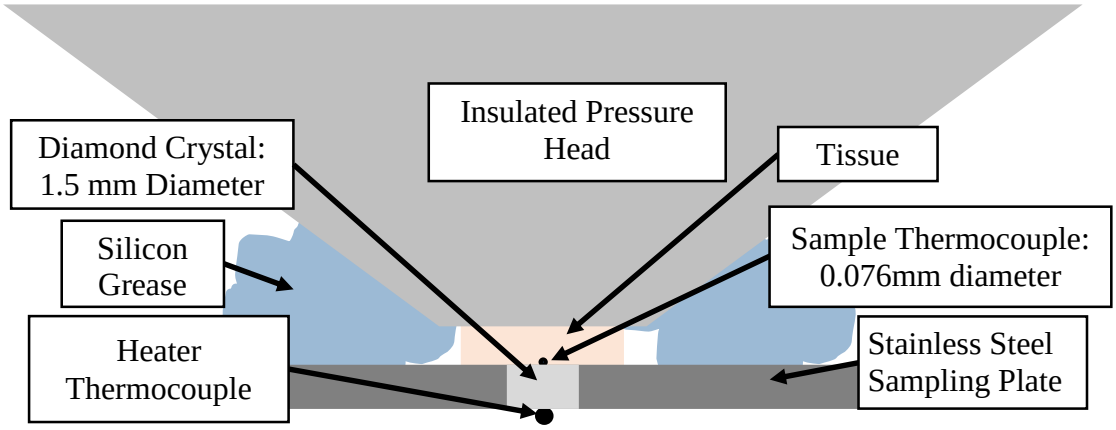

Appendix Figure 18: ATR Sample Plate Setup

Once all of the spectra have been recorded, the spectra files which have a .spa file extension are saved so as to have a .csv file extension so that they can be processed with a MATLAB script.

Processing Spectra with MATLAB Script

The MATLAB script processes the spectra in the following ways. First, the script takes the difference between each spectra and the initial spectra at 25ºC. Second, the script calculates the second derivative of the difference spectra using a 13-point smoothing factor from Savitzky and Golay [82]. Third, second derivative is inverted by multiplying by negative one. Fourth, the user is prompted to pick two points between which an are is calculated. The points taken are usually between 1608 and 1630cm^{-1}, become the baseline of the beta-sheet peak, and are subsequently used to calculate the area beneath each spectra and the baseline. Fifth, the program records the beta-sheet formation (area under the curve) for each spectra in a saved file. This process is described below with steps shown with manual Excel manipulation of spectra to show what happens with the MATLAB code.

Excel Explanation of Spectra Manipulation

The final picture of the spectra looks like the following in Appendix Figure 19 with only representative spectra shown every 8ºC.

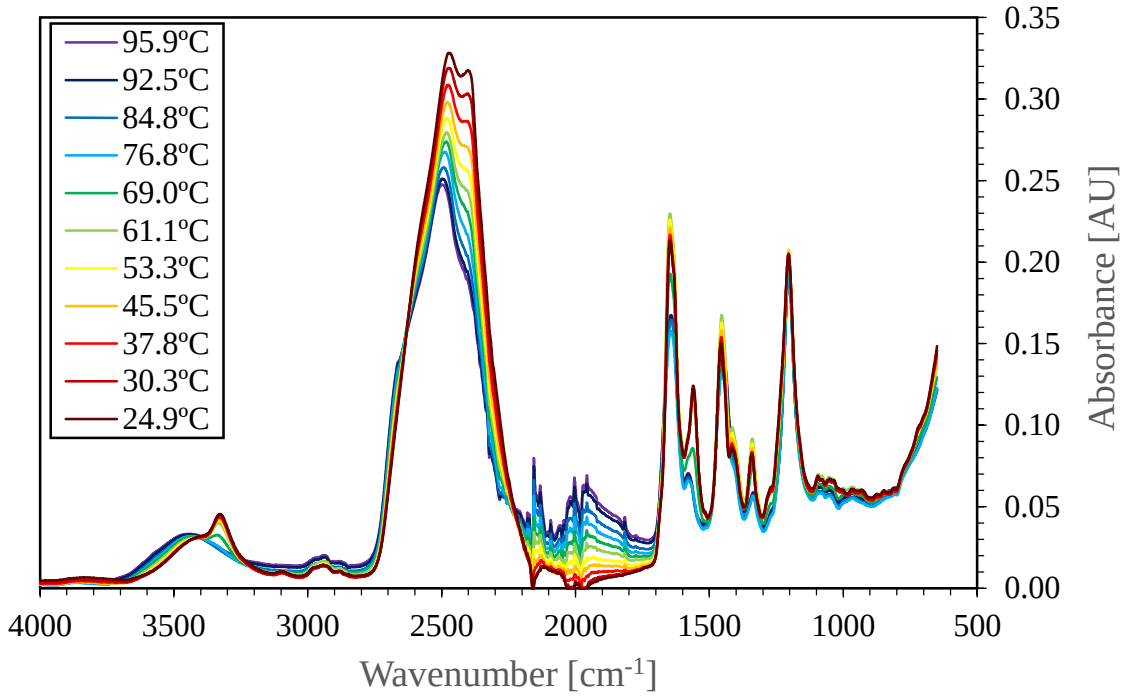

Appendix Figure 19: Sample Spectra Recorded During Denaturation Run

Since we are looking at the Amide-I region for analyzing the protein denaturation by using the beta-sheet as a marker, the sample spectra zoomed-in at the Amide-I position from 1600 – 1700cm^{-1} is shown in Appendix Figure 20.

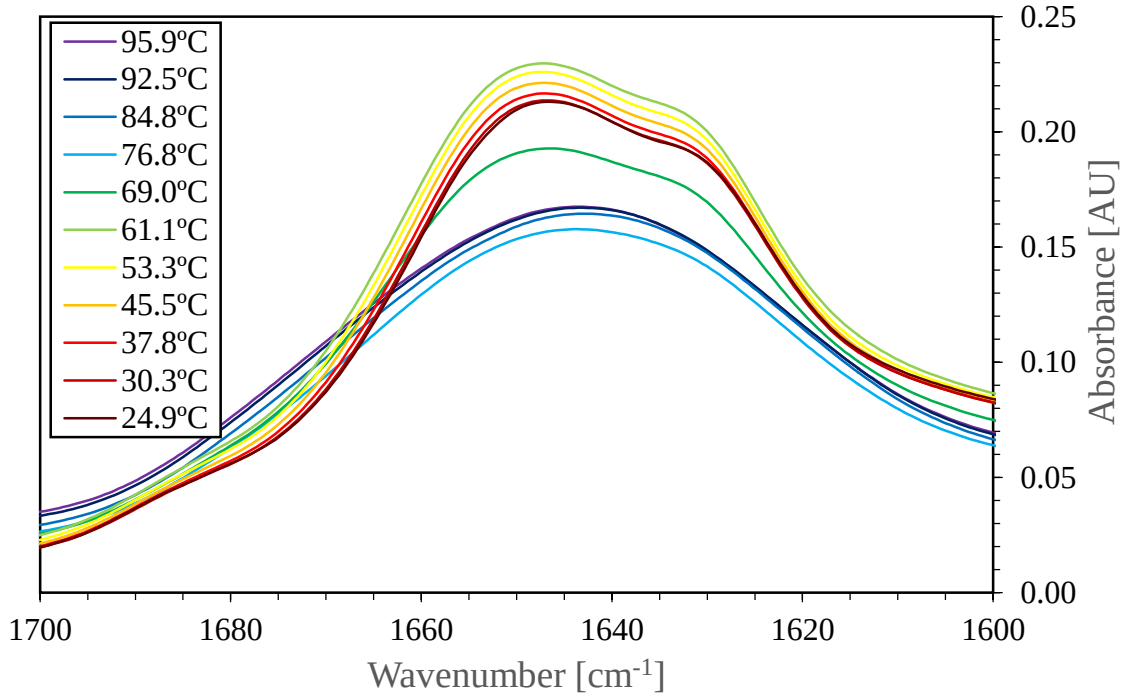

Appendix Figure 20: Sample spectra in Amide-I region

After the sample spectra are taken, difference spectra are recorded by subtracting the initial spectra at 25ºC from the subsequent spectra. The final result is shown below in Appendix Figure 21.

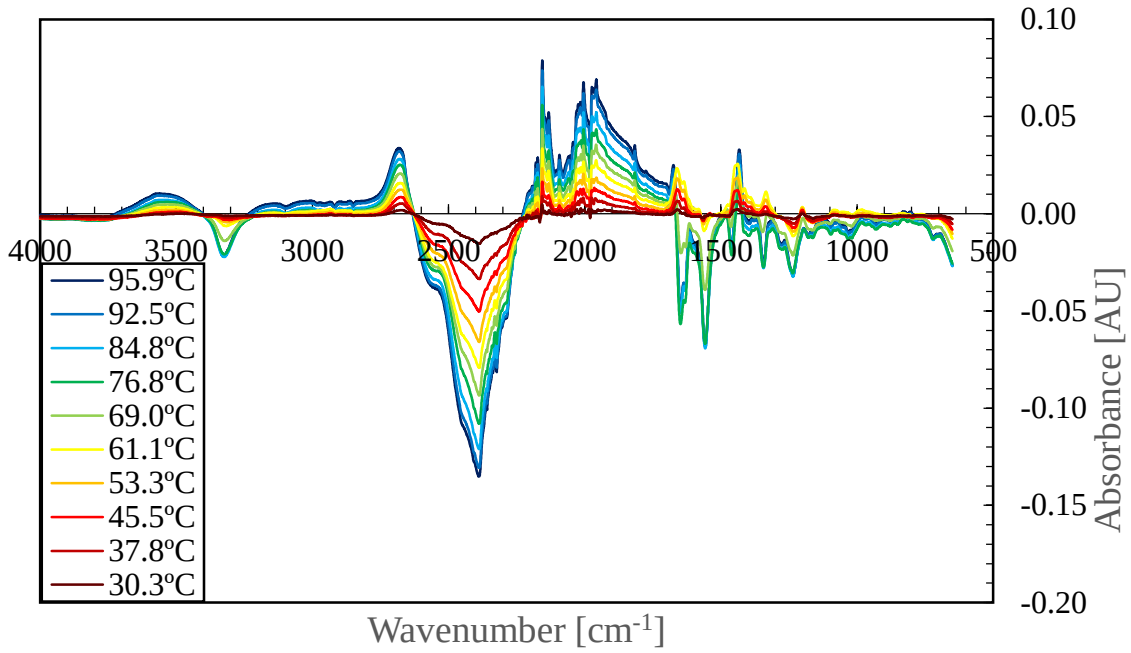

Appendix Figure 21: Difference Spectra

Additionally, the more useful portion of the graph is the Amide-I region. This is shown below in Appendix Figure 22.

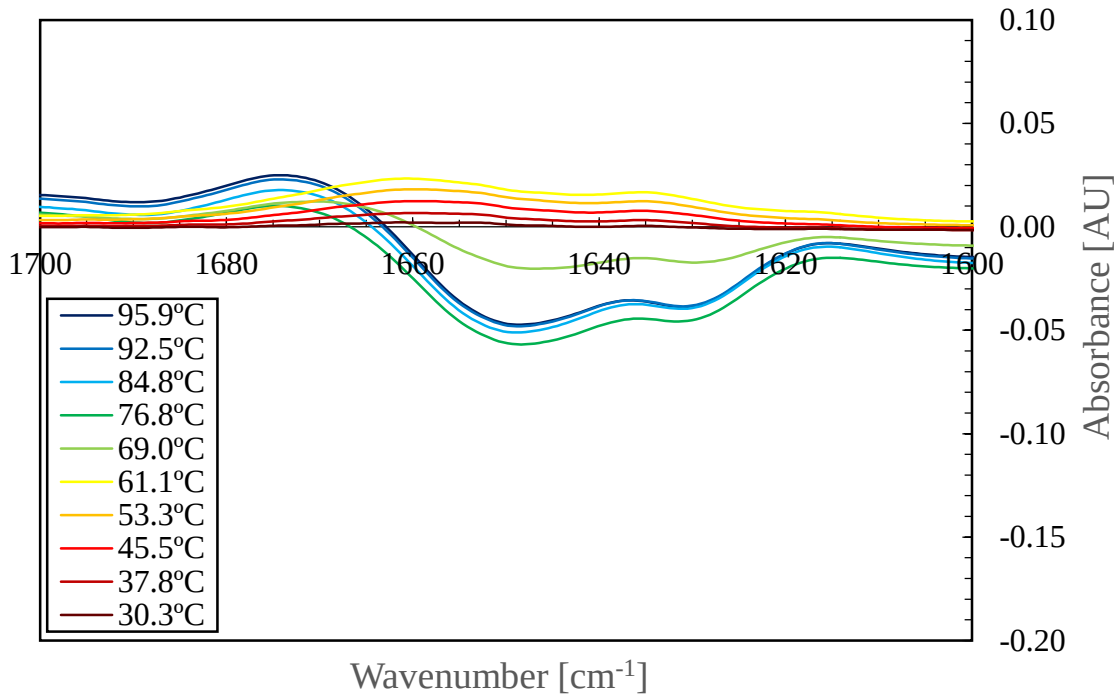

Appendix Figure 22: Difference Spectra in Amide – I Region

After calculating the difference spectra, a 13-point smoothing factor was used to calculate the second derivative from Savitzky [82]. Additionally, the second derivative was multiplied by a factor of -1 in order to get positive area from the peaks. The graph showing the inverted second derivative of the difference spectra is shown below in Appendix Figure 23.

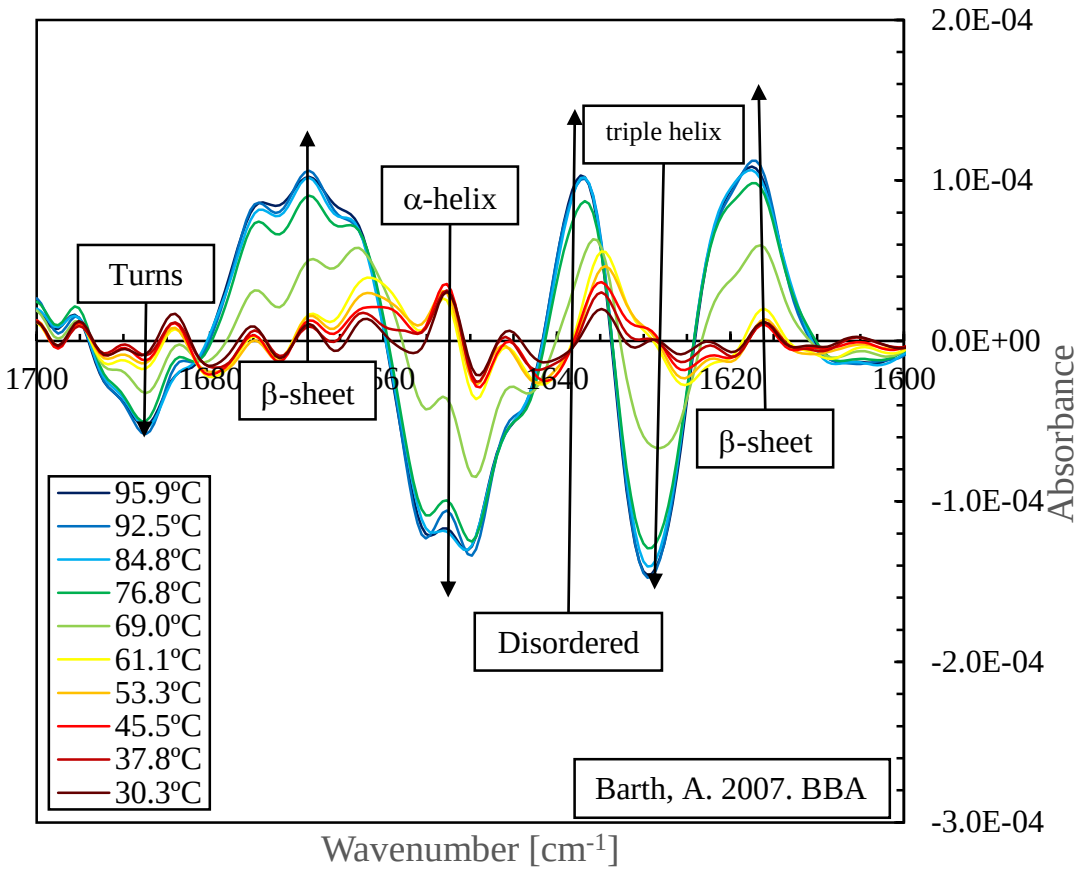

Appendix Figure 23: Inverted Second Derivative

After the calculation of the inverted second derivative, the area is calculated by first selecting a linear baseline calculated by the selection of two points and by second calculating the area between the spectra and the baseline. A sample baseline and the area of interest is shown below in Appendix Figure 24.

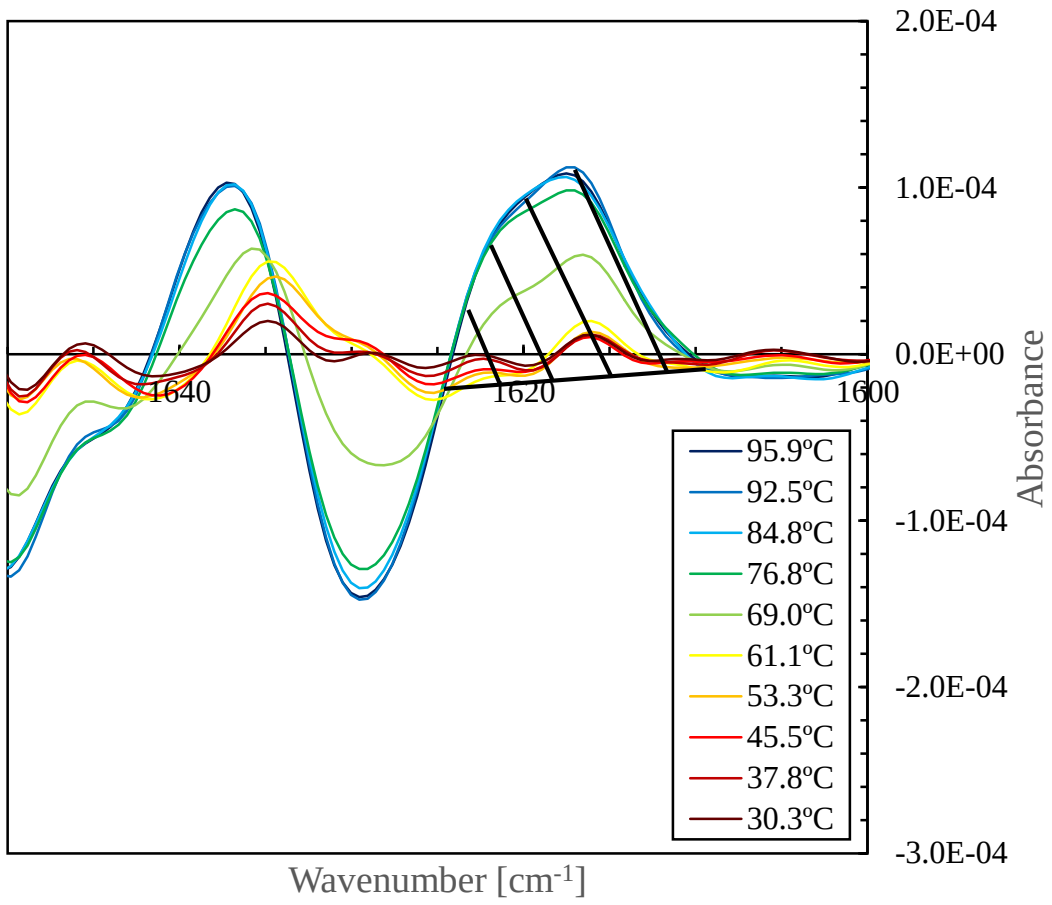

Appendix Figure 24: Baseline and Area Calculation

These areas for each spectra which correspond to a particular temperature are plotted to determine the onset of denaturation. The onset of denaturation is defined as a sharp increase in beta-sheets. One method of quantifying the denaturation is do draw tangent lines along the initial increase in beta-sheet formation and along the part of the curve before the beta-sheet starts to increase. An example of this process is shown below in Appendix Figure 25.

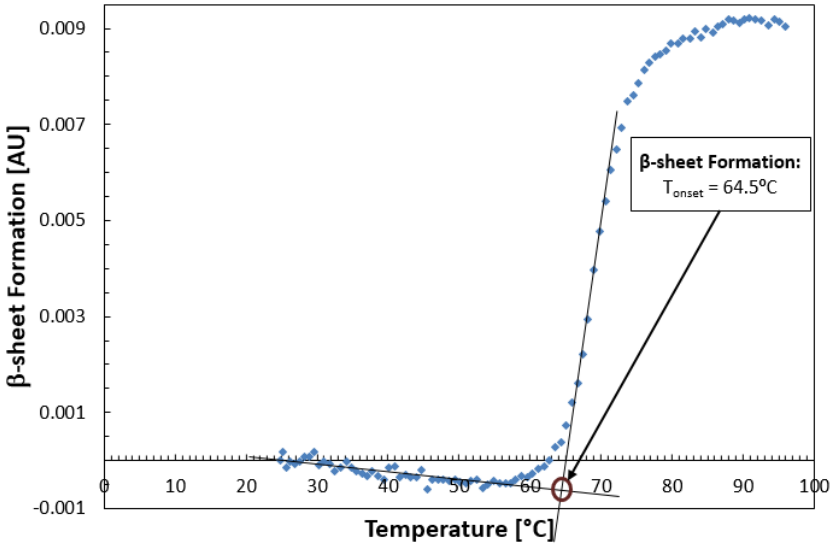

Appendix Figure 25: Denaturation Onset Calculation

This graph shows the temperature range of the experiment from 25 – 95ºC. Also, it shows how spectra were recorded every 1ºC change. Finally it lays out how the onset of denaturation was calculated.

Conclusion:

The above description shows how to calculate the onset of denaturation. First, the first spectrum is subtracted from all of the subsequent spectra. Second, the second derivative is taken of the difference spectra. Third, this second derivative is inverted by multiplying by minus one. Fourth, a baseline is drawn beneath the β-sheet curve which is centered around 1620cm^{-1}. Fifth, the area between each curve and the baseline is calculated and plotted against the temperature at each of the spectra. Sixth, tangent lines are drawn on the just made plot to determine the onset of denaturation which is the intersection of the tangent lines.

APPENDIX F: Explanation of MATLAB Code

Background:

In order to efficiently process spectra to determine denaturation onset, a MATLAB code was developed.

Purpose:

The purpose of this appendix is to explain how the MATLAB code works and how to use it.

Explanation:

The MATLAB code can be broken into five main parts:

- Starting the MATLAB script
- Retrieve the Amide I region (1600 – 1700cm^{-1}) from the raw data
- Calculate difference and inverse second derivative of difference
- Define baseline under which to calculate area
- Retrieve calculated areas in order to calculate denaturation onset

Starting the MATLAB script

The first portion of the MATLAB code is run by calling the function name with the title of the spectra and the number of spectra. The format for starting the program is the following:

ftiranalysis('YYMMDDR0',#)

where "YY" are the last two digits of the year, "MM" is the month, "DD" is the day of the experiment, "R" is the run number (if no number is used, this may be omitted), "0" is needed to match the title as the titles are auto-generated with four digit space with an automatic title of "YYMMDDR". One of the zeroes is supplied with "0", and the MATLAB code looks for the other three numbers with the "%03i" command. An example of running the script is the following:

```
ftiranalysis('15071610',95)
```

Appendix Figure 26: Example input MATLAB code to start script

The above example says that the run being analyzed is the first run on July 16, 2015. Also, 95 spectra were taken on the run.

Retrieve the Amide I region (1600 – 1700cm^{-1})

Next, the data from the Amide I region is read and indexed. This is done by taking the rows from 1937 to 2197 since these correspond to wavenumbers approximately 1600 – 1700 cm^{-1}. The numbers of 1937 and 2197 are used because of the resolution of 4cm^{-1} used in the measurements.

Calculate difference and inverse second derivative of difference

The next section calculates the difference and subsequent inverse second derivative of the difference spectra. The result of this is shown in Appendix Figure 27.

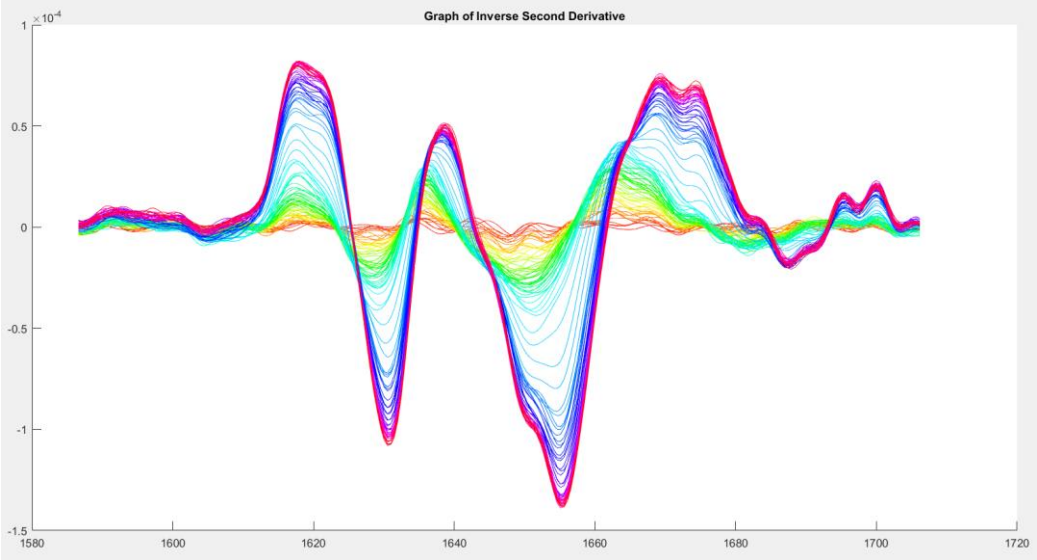

Appendix Figure 27: Inverse second derivative of difference spectra from MATLAB Code

Define baseline under which to calculate area

The MATLAB script displays the inverse second derivative plot and enables the user to select two points from which to calculate the area under the β-sheet curve. The selecting of the left side of the baseline is shown in Appendix Figure 28 below.

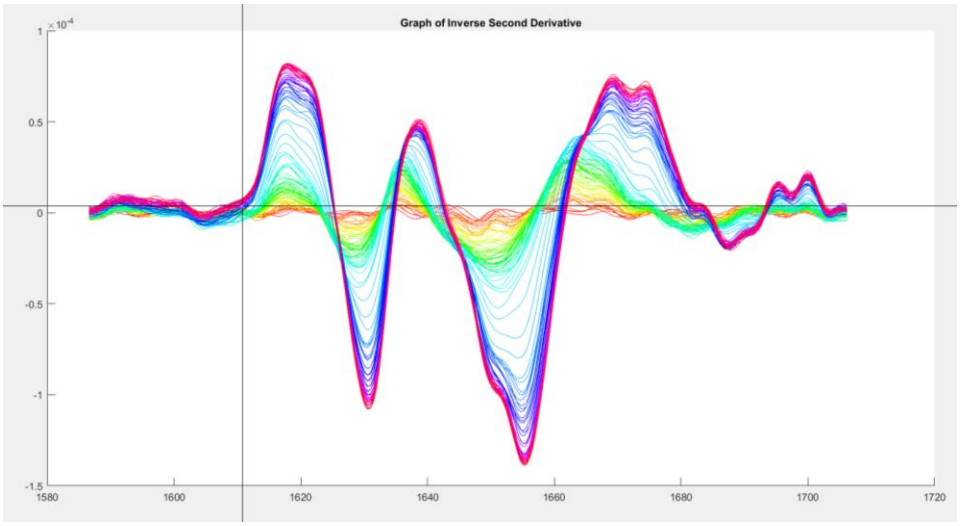

Appendix Figure 28: Left side of β-sheet curve at ~1611cm^{-1}

The right side of the baseline is indicated by Appendix Figure 29 below.

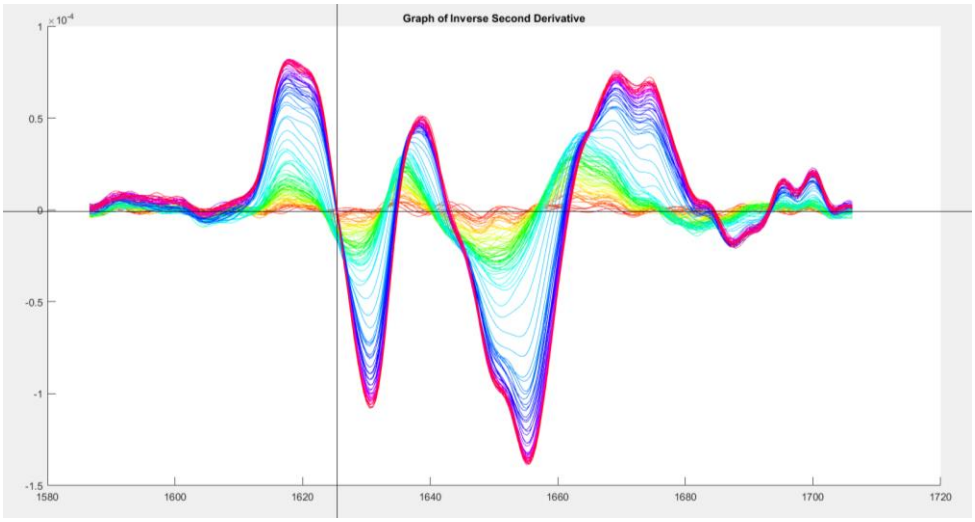

Appendix Figure 29: Indication of the right side of the β-sheet curve at ~1623cm^{-1} where the temperature is indicated by color is it varies from red-yellow-green-blue-indigo-violet with increasing temperature

Retrieve calculated areas in order to calculate denaturation onset

After selecting the baseline from which to calculate the area, a figure is output from the code. An example of this is following in Appendix Figure 30:

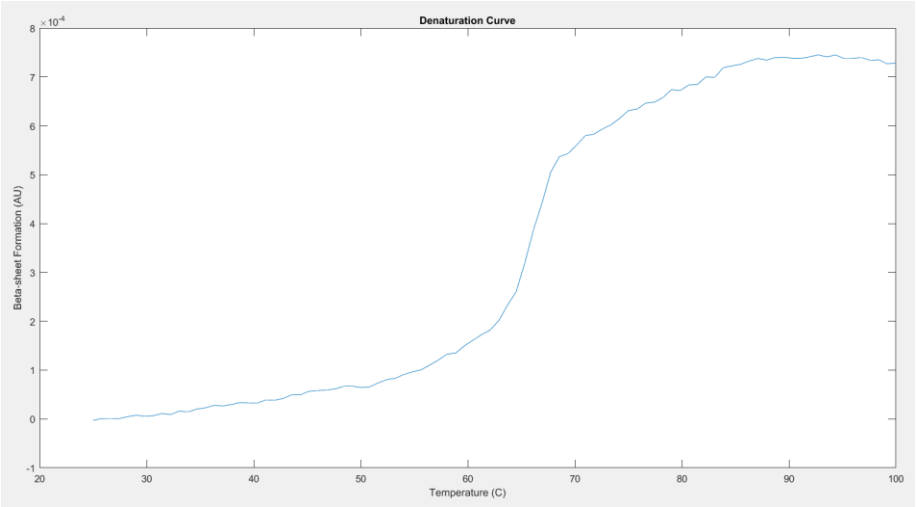

Appendix Figure 30: Output of graph by MATLAB which plots the beta-sheet formation versus temperature

The above figure graphs the calculated beta sheet formation versus pre-programmed temperature instead of the actual temperature recorded by a thermocouple. The β-sheet formation can be retrieved by looking under the Matlab folder as shown in Appendix Figure 31.

Appendix Figure 31: Location of MATLAB output folder

MATLAB Code:

```
%%FTIR Data Analysis
%7/12/15 MK, JS
%7/21/15 MK included ginput for the baseline
%Takes the raw data from the csv file (output from the Omnic Software) and
%analyzes it
function [] = ftiranalysis(filename, m) %use csv file with data
    for i = 1:m
        datafile = [filename, num2str(i, '%03i'), '.CSV'];
        alldata = csvread(datafile,1937,0, [1937, 0, 2197, 1]);
        %opens the csv file with the specified boundaries; R1, C1, [R1, C1, R2, C2]
        wavenumb = [];
        wavenumb = alldata(:,1); %creates a column of just the raw wavenumbers
        absorb = [];
        absorb = alldata(:,2); %creates a column of just the raw absorbances
        eval(['absorbance' num2str(i) ' = absorb']); %assigns the absorbance values into
variable names absorbance i
        wavenumber = wavenumb(7:255,:);
    end
% Savitzky-Golay Smoothing and Differentiation of Data
% 7/14/15 MK
% It takes the dataset and smoothes it as it take the second derivative of
% the dataset. This is written for 13-pt filter width.
        colorVec = hsv(m-1); % Generate hue-saturation-value color map for data
    for ii = 2:m
        currentabs = eval(['absorbance' num2str(ii)]);
        eval(['absorbdiff' num2str(ii - 1) ' = currentabs - absorbance1']);
        x = eval(['absorbdiff' num2str(ii-1)]);
        filtdata = zeros(249, 1);
        for n = 1:249
            filterthat = (x(n,1)*22 + x(n+1,1)*11 + x(n+2,1)*2 + x(n+3,1)*(-5) +
x(n+4,1)*(-10) + x(n+5,1)*(-13) + x(n+6,1)*(-14) + x(n+7,1)*(-13) + x(n+8,1)*(-10) +
x(n+9,1)*(-5) + x(n+10,1)*2 + x(n+11,1)*11 + x(n+12,1)*22)/1001;
            filtdata(n) = filterthat;
        end
        eval(['filterdata' num2str(ii - 1) ' = filtdata*(-1)']);
        y = eval(['filterdata' num2str(ii-1)]);
        hold on;
        plot(wavenumber, y, 'Color', colorVec(ii-1,:)); % Plot and change the color for
each line
        title('Graph of Inverse Second Derivative') % Displays the title of the graph
    end
    hold on;
    [P,Q] = ginput(2); % Prompts to graphically input two points
    plot(P,Q,'*'); % Plots the two points on the graph
    line (P,Q); % Draws a line between the two points
    linequation = polyfit(P,Q,1); % Gives out the linear fit equation
    hold off;
    % Defines s and t as wavenumbers and the corresponding absorbances based on the wave-
numbers between P and Q
    s = wavenumber(wavenumber >= P(1,:) & wavenumber <= P(2,:));
    sinteg = zeros(length(s),1);
    for j = 2:m
        z = eval(['filterdata' num2str(j-1)]); % takes all the filtered data
        t = z(wavenumber >= P(1,:) & wavenumber <= P(2,:)); % Takes all the filtered ab-
sorbance data within the chosen points and assigns variable t
        newt = t - linequation(:,1)*s - linequation(:,2); % Takes t and subtracts the
linear equation of the line to account for the baseline
        sinteg(j-1) = simps(s,newt); % Calculates the area under the curve using Simp-
son's Rule and stores the values in the matrix called 'sinteg'
    end
    clear plot
```

```
    tem = linspace(25,100,length(sinteg)); % Creates an evenly spaced line from 25 to 100
with however many the simpson's integration values there are
    temp = tem'; % Transposes the matrix
    plot(temp,sinteg) % Plots the graph with temperature on x-axis and simpson's integra-
tion values on y-axis
    title('Denaturation Curve') % Displays the title of the graph
    xlabel('Temperature (C)') % x-axis label
    ylabel('Beta-sheet Formation (AU)') % y-axis label
    figurename = [filename,'.jpg'];
    saveas(figure(1),figurename);  % Saves the figure1
    xcelname = [filename,'.xlsx'];
    warning('off','MATLAB:xlswrite:AddSheet');
    xlswrite(xcelname,sinteg);
end
```

APPENDIX G: ATR Characterization

Purpose: This will describe how characterized the ATR in its temperature and load response.

Appendix Figure 32: ATR Accessory in FTIR Main Machine

Load Characterization:
To characterize the load, a calibrated spring from Larson Instruments (Part No: 018-3000-0010-02) was used to test if the load gauge was operating properly. The force gauge on the ATR had a no-load offset. The two offsets were at 6N and 21N. Thus, when no load was applied, the force gauge gave a reading of either 6N or 21N.

Load Characterization Methods:
To test the load a calibrated spring was put between the base of the machine and the force applicator. Since the applicator was only 4.5mm in diameter and the spring was almost 1inch in diameter, a thin piece of aluminum (1in x 4in) was used to facilitate transferring the force from the force applicator and the spring. While compressing the spring, the force gauge was read. Additionally, the length of the compressed spring was measured. Comparing the compressed length with the free length of the spring, a compressed distance was able to be calculated. Both the force gauge and calibrated spring force vs. compressed length for comparison. This was done for both the 6N and 21N offset as shown in Appendix Figure 33 and Appendix Figure 34, respectively.

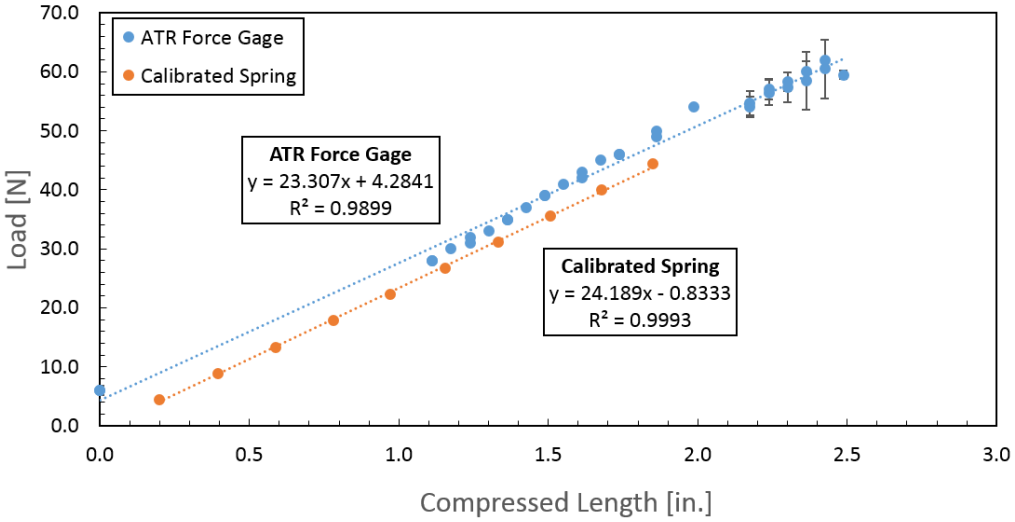

Appendix Figure 33: ATR force characterization with 6N offset

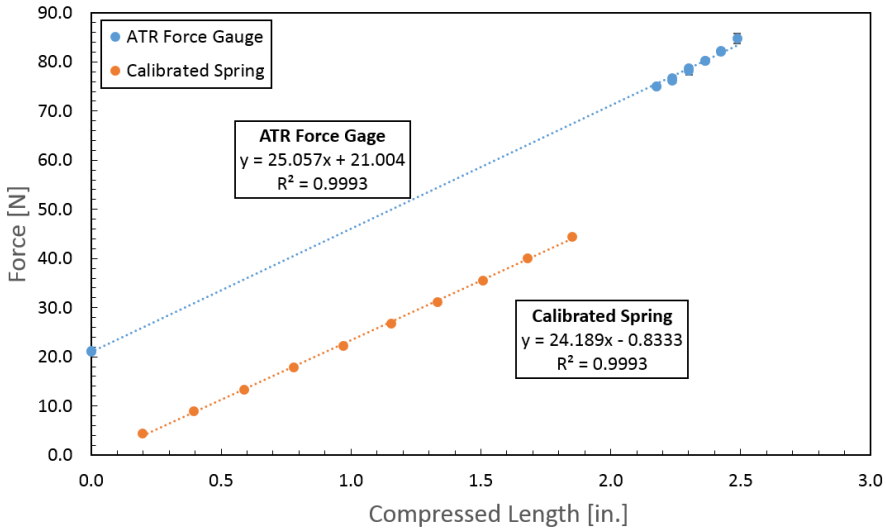

Appendix Figure 34: ATR Force Characterization with 21N offset

Force Characterization Discussion:
From the above figures, the force gauge on the ATR has a similar response to the factory calibration of the spring. This similarity is seen in that the slopes are similar especially for the 6N offset. Also, the 6N offset graph in Appendix Figure 34 shows how the force gauge overlaps with the data at compressed lengths from 1.0 – 2.0in.

Heat Characterization: Introduction
The heat characterization was completed in two parts. The first part was testing the heating rate response of the ATR device, and the second part was testing the force gauge sensitivity to being heated.

Heat Characterization: Part 1 Methods
It was found that the temperature of the sample lagged behind that of the heater. The reason for the lag is that the heaters are located below the crystal. Thus, the heat has to travel

through the diamond crystal in order to heat the sample. Appendix Figure 35 below shows the assembly of the Harrick sampling plate.

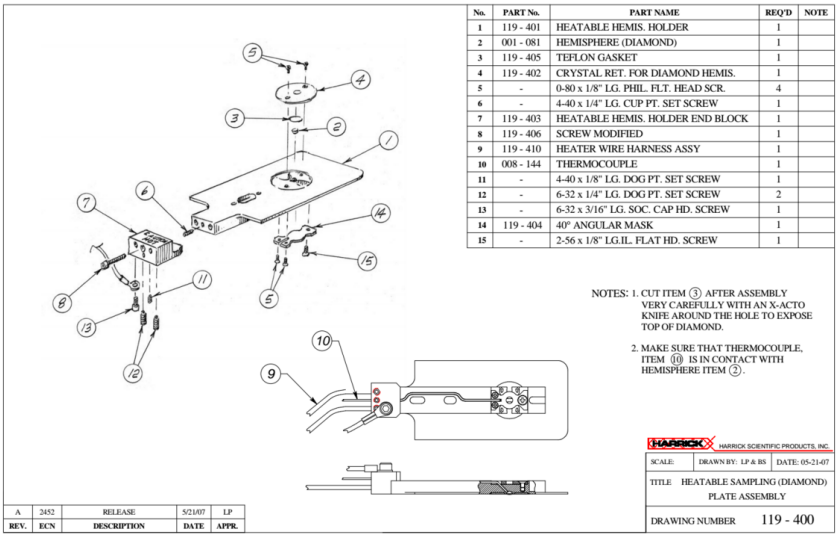

No.	PART No.	PART NAME	REQ'D	NOTE
1	119 - 401	HEATABLE HEMIS. HOLDER	1	
2	001 - 081	HEMISPHERE (DIAMOND)	1	
3	119 - 405	TEFLON GASKET	1	
4	119 - 402	CRYSTAL RET. FOR DIAMOND HEMIS.	1	
5	-	0-80 x 1/8" LG. PHIL. FLT. HEAD SCR.	4	
6	-	4-40 x 1/4" LG. CUP PT. SET SCREW	1	
7	119 - 403	HEATABLE HEMIS. HOLDER END BLOCK	1	
8	119 - 406	SCREW MODIFIED	1	
9	119 - 410	HEATER WIRE HARNESS ASSY	1	
10	008 - 144	THERMOCOUPLE	1	
11	-	4-40 x 1/8" LG. DOG PT. SET SCREW	1	
12	-	6-32 x 1/4" LG. DOG PT. SET SCREW	2	
13	-	6-32 x 3/16" LG. SOC. CAP HD. SCREW	1	
14	119 - 404	40° ANGULAR MASK	1	
15	-	2-56 x 1/8" LG.IL. FLAT HD. SCREW	1	

NOTES: 1. CUT ITEM (3) AFTER ASSEMBLY VERY CAREFULLY WITH AN X-ACTO KNIFE AROUND THE HOLE TO EXPOSE TOP OF DIAMOND.

2. MAKE SURE THAT THERMOCOUPLE, ITEM (10) IS IN CONTACT WITH HEMISPHERE ITEM (2).

HARRICK SCIENTIFIC PRODUCTS, INC.

SCALE:	DRAWN BY: LP & BS	DATE: 05-21-07
TITLE	HEATABLE SAMPLING (DIAMOND) PLATE ASSEMBLY	
DRAWING NUMBER	119 - 400	

REV.	ECN	DESCRIPTION	DATE	APPR.
A	2452	RELEASE	5/21/07	LP

Appendix Figure 35: ATR Sampling Plate

The heaters are below the crystal where the sample is located. This can be seen in Appendix Figure 36.

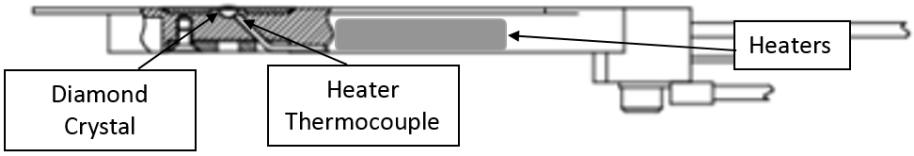

Appendix Figure 36: Enlarged view of sampling plate

When running a denaturation experiment, both the heater and tissue temperature were recorded. The tissue temperature was recorded by using a thermocouple between the diamond crystal and tissue. Additionally, a Teflon-insulated cap was used to insulate the force applicator from the heating. Finally, the tissue was sealed with silicon grease in order to maintain the moisture content of the sample. The setup is shown below in Appendix Figure 37.

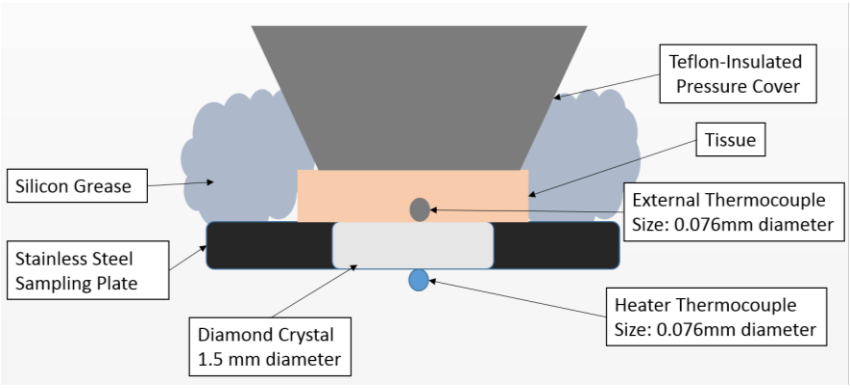

Appendix Figure 37: ATR Tissue Setup

Heat Characterization: Part 2 Methods

To test the effect heat has on the force value, the force value was recorded in addition to the heater temperature. Also, no load was initially placed with the applicator. A heating rate of 2.5ºC/min was used, and the heating range was 25 – 108ºC.

Heat Characterization: Part 1 Results

The above setup was used, and several different heating rates were set for the heater: 2.0, 2.2, 2.4, and 2.5ºC/min. Both the heater and sample response is shown in Appendix Figure 38 at a heating rate of 2.0ºC/min.

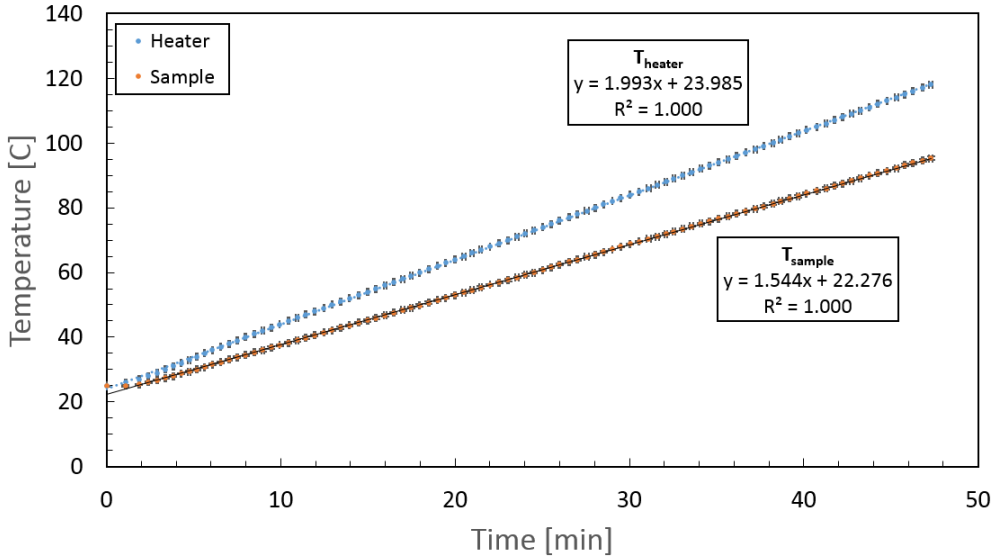

Appendix Figure 38: ATR Response of 2.0ºC/min (n = 3)

Additionally, the same type of process was done for a heating rate of 2.2ºC/min as is shown in Appendix Figure 39.

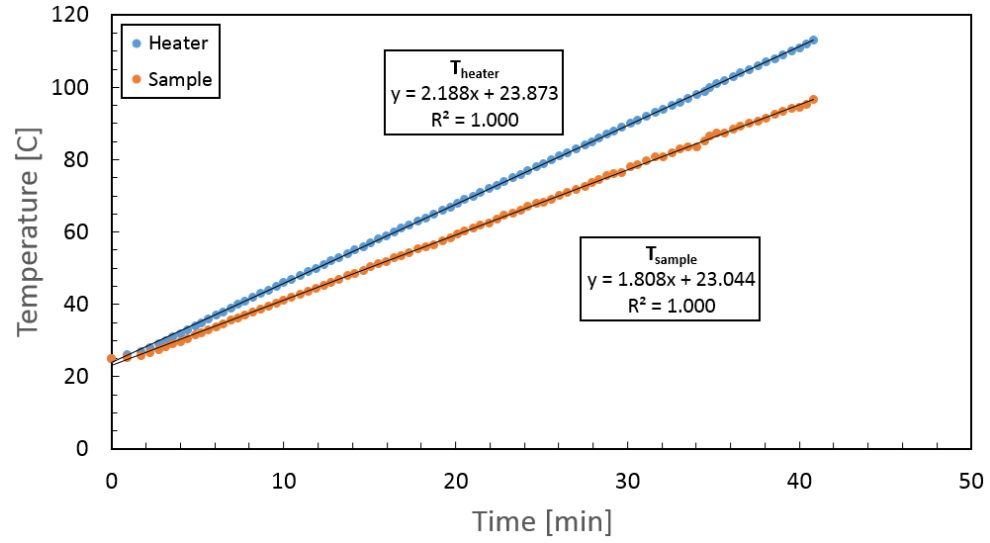

Appendix Figure 39: ATR Response of 2.2ºC/min (n = 1)

Again, this experiment was completed at a heating rate of 2.4ºC/min as shown below in Appendix Figure 40.

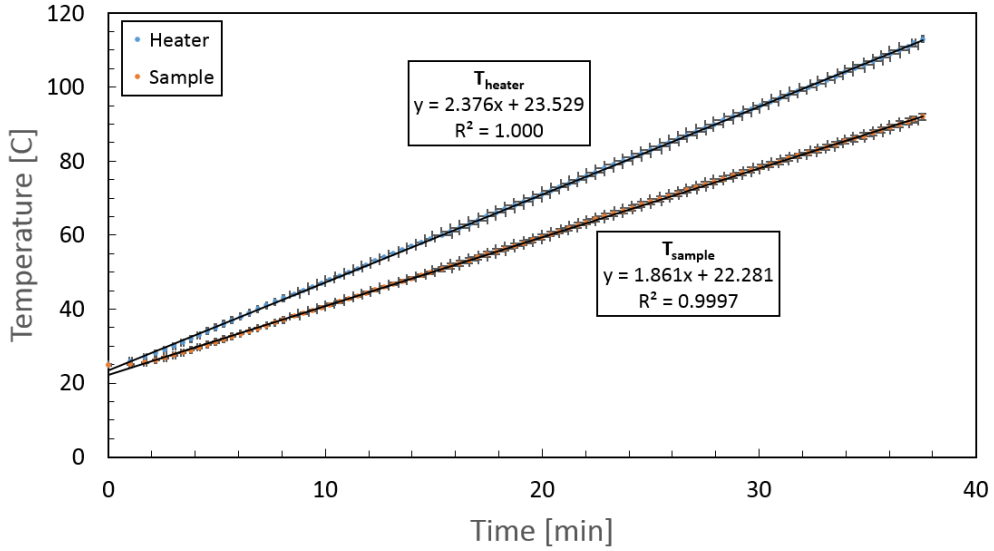

Appendix Figure 40: ATR Response of 2.4ºC/min (n = 4)

Finally, the experiment was performed mainly at a heating rate of 2.5ºC/min which is shown below in Appendix Figure 41.

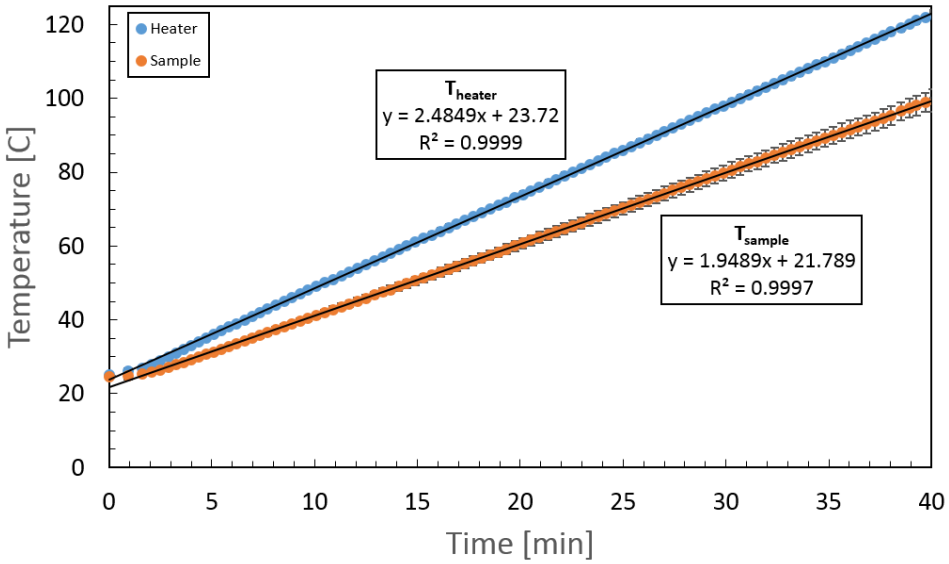

Appendix Figure 41: ATR Response of 2.5ºC/min (n = 25)

Heat Characterization: Part 2 Results

The temperature was plotted against temperature, and the result is shown in Appendix Figure 42.

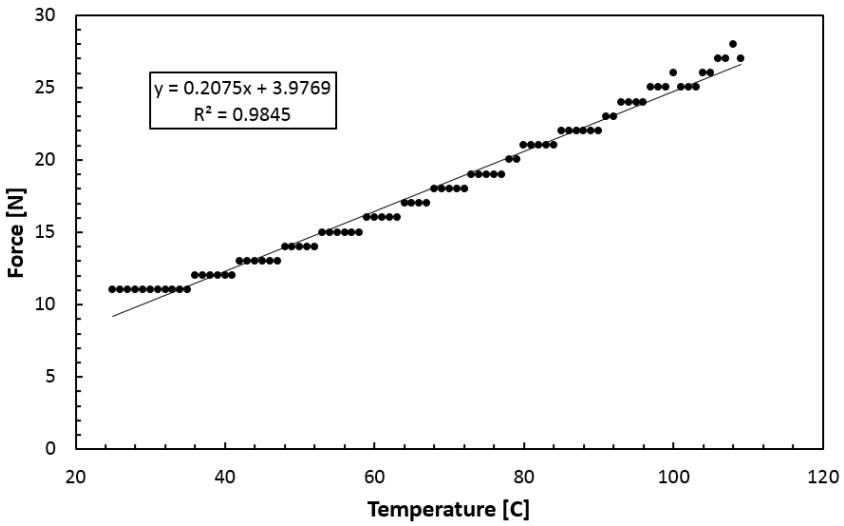

Appendix Figure 42: Force vs Temperature

This experiment has only been performed once, but this confirms a large influence of temperature on the force applicator of the ATR.

APPENDIX H: Effect of Sample Thermocouple on Pressure Measurements

Background:

Denaturation measurements were made with the application of load, but the denaturation onset did not seem to change. Further investigation revealed that using a thermocouple absorbed the effects of the load.

Purpose:

The purpose of this appendix is to demonstrate that using a thermocouple in the described setup throws-off denaturation onset measurements as the thermocouple bears the load instead of the tissue in question.

Protocol:

Denaturation measurements were completed with and without an additional thermocouple. This additional thermocouple was used to characterize the temperature response of the tissue. The ATR accessory was controlled with a thermocouple below the diamond crystal. The additional thermocouple was placed between the diamond crystal and the tissue in order to observe the temperature response. A picture of this setup is seen below in Appendix Figure 43.

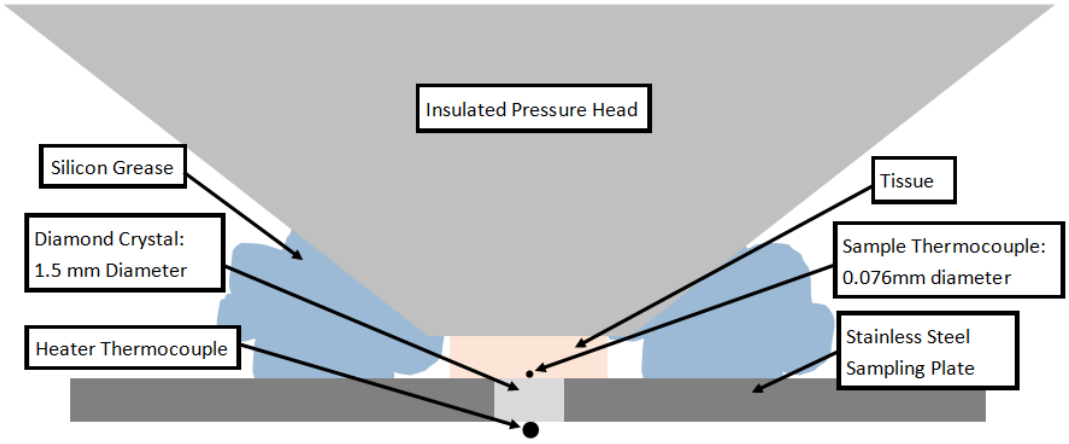

Appendix Figure 43: ATR setup of Denaturation Measurements

Denaturation measurements were initially made with loads of 2N. After making several measurements at this load, the load was increased to 10N and 20N to see what the effect the load had on the denaturation onset.

Results:

The results of 0N load without using an additional thermocouple are shown with loads of 10N and 20N with the use of an additional thermocouple in Appendix Figure 44.

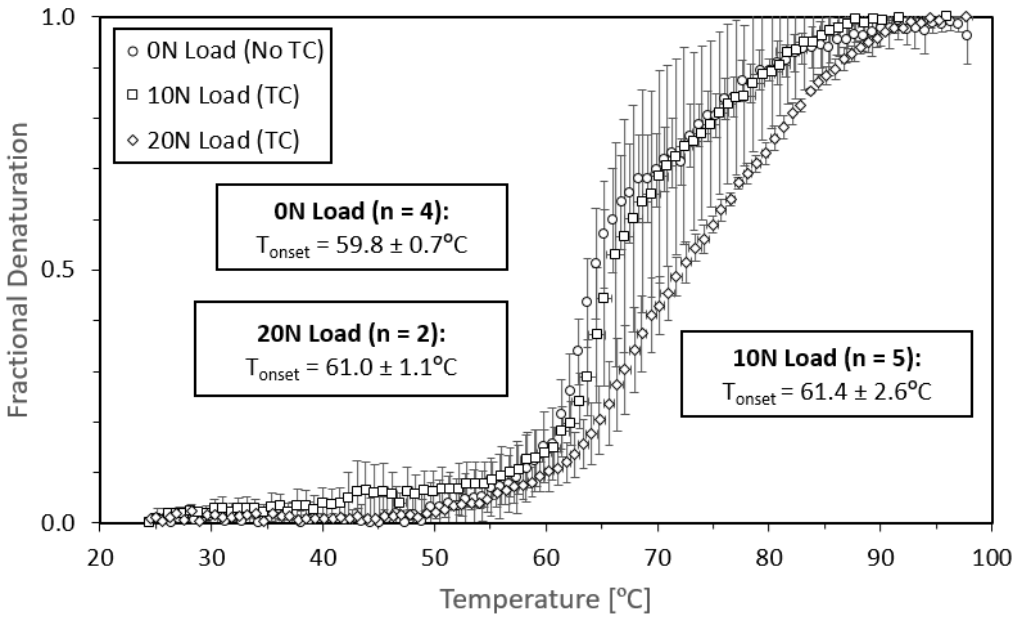

Appendix Figure 44: Effect of load on denaturation onset with the use of an additional thermocouple. The legend with the (TC) indicates the use of an additional thermocouple between the diamond crystal and the tissue.

The above figure shows that the denaturation onset was not significantly changed as the load was increased with the use of an additional thermocouple.

Conclusion:

Understanding that the thermocouple was bearing most of the load instead of the tissue prompted the removal of using the thermocouple in subsequent denaturation measurements. Since the sample temperature follows closely with the heater temperature, a calibration curve between the sample temperature and the heater temperature was determined by taking the average of six (n = 6) runs. This calibration curve was used in the place of using an additional thermocouple.

APPENDIX I: Denaturation Onset Between DSC and FTIR

Introduction: Determining the onset of denaturation has been done in the literature for both Differential Scanning Calorimetry (DSC) and Fourier Transform Infra-Red (FTIR) Spectroscopy. Representative paper for DSC denaturation onset is by Wang, et al. [75], and a representative paper for FTIR onset is by He, et al. [77].

Purpose: This appendix will show that denaturation onset has been determined different ways for both FTIR and DSC. Also, the denaturation onset as calculated by DSC and FTIR have been compared differently.

1. Tangent Line Method:

In order to calculate the denaturation onset, tangent lines are placed along different slopes. The intersection of these lines is taken to be the denaturation onset. This has the advantage of being able to readily process data. A drawback, however, is that this process is subject to a high degree of variability as each person may think differently on where the tangent lines should be placed. Wim Wolkers, who is a professor at Leibniz Institute at Hannover, is user of this method. This method is seen in papers of Venkatasubramanian, et al. [67] and Wang, et al. [75]. This method will be described as follows.

The tangent line method is used for both DSC and FTIR. The steps for the process are the following:

- **Step 1:** Place tangent lines on places of changing slope
- **Step 2:** Calculate intersection of tangent lines

1.1 FTIR Example from Wang, S. 2014. BBA

The FTIR spectra is shown below in **Appendix Figure 45**.

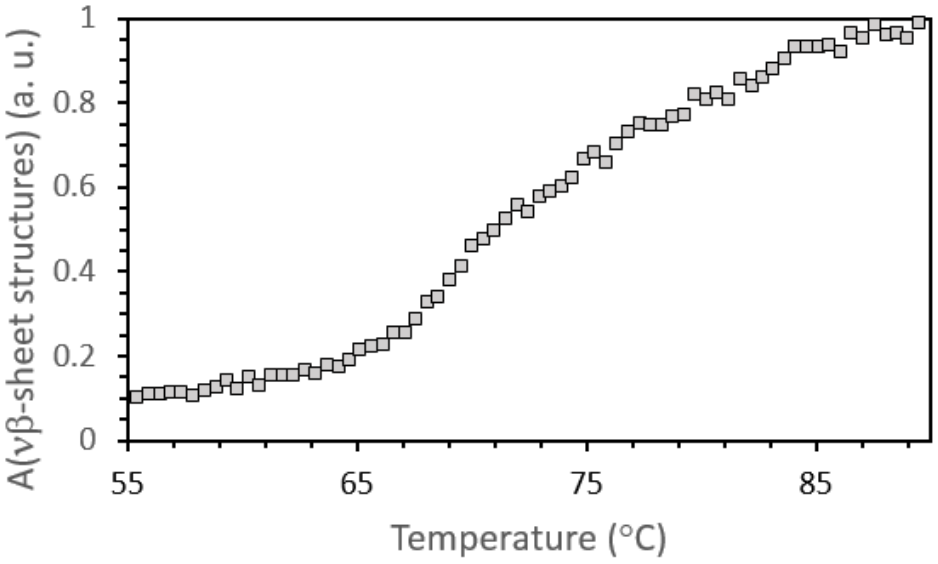

Appendix Figure 45: FTIR fractional denaturation curve of decellularized heart valve leaflets

Appling Step 1, the tangent lines are placed as follows in Appendix Figure 46.

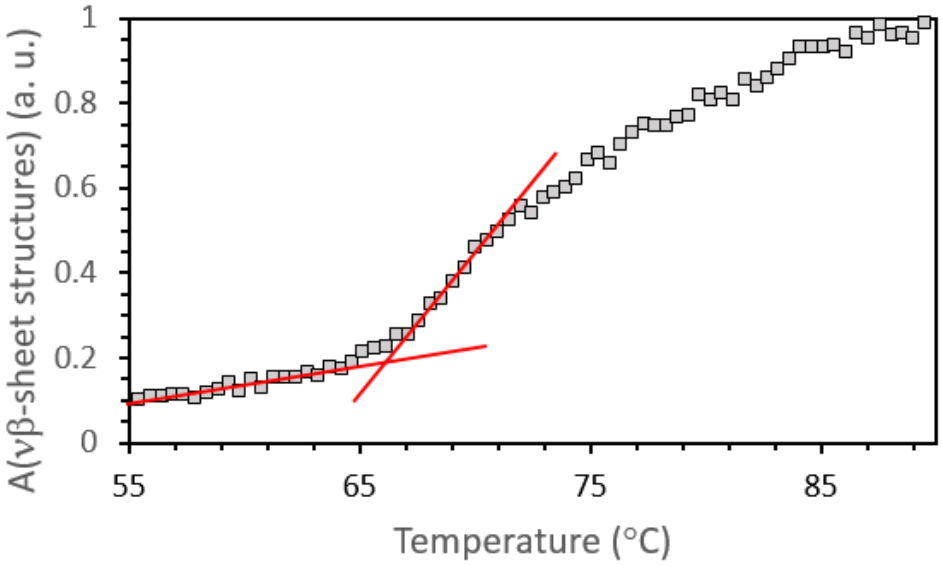

Appendix Figure 46: Denaturation plot with tangent lines

After placing the tangent lines, the onset is to be interpreted. This is shown below in Appendix Figure 47.

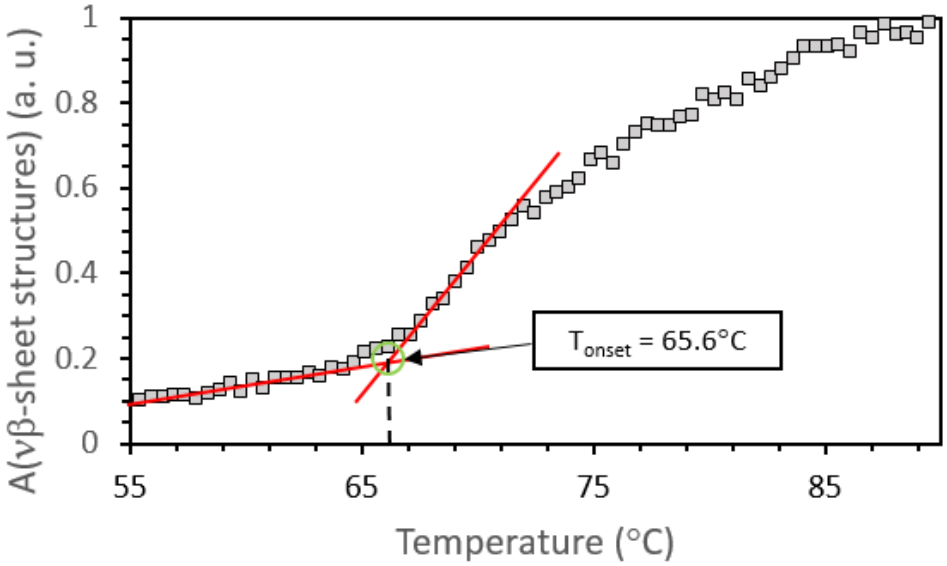

Appendix Figure 47: Denaturation onset determination

1.2 DSC Example from Wang, S. 2014. BBA

Similarly, in order to calculate denaturation onset by the tangent line method, one applies the tangent lines directly to the excess heat scan. The tangent lines applied to the DSC scan is shown in Appendix Figure 48.

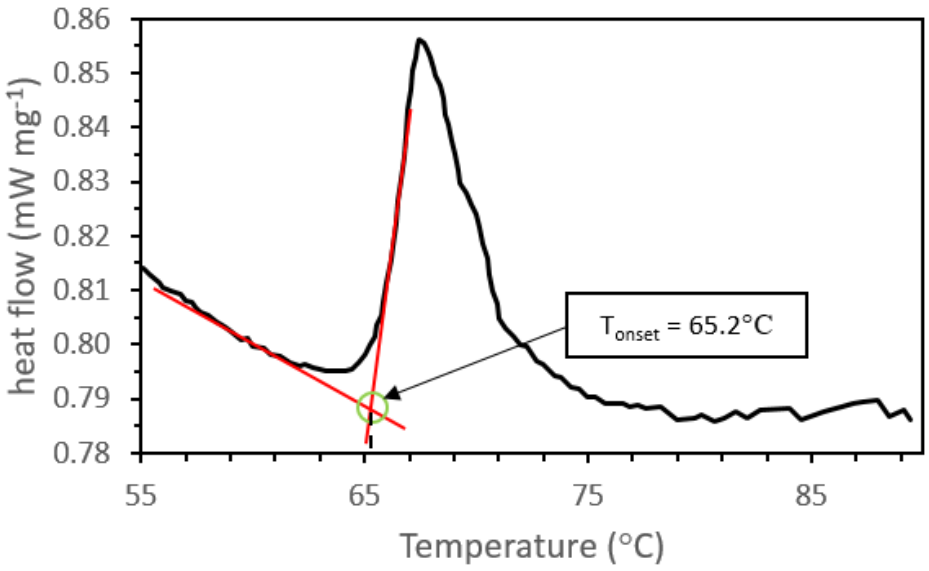

Appendix Figure 48: Tangent lines applied to DSC scans

The variation of the tangent line is show in the above calculated onset of 65.2ºC, but the author measured denaturation onset of 65.5ºC.

2. Derivative Method

The derivative method is another way that has been used to calculate denaturation onset. Instead of using tangent lines to calculate onset, it calculates the derivative of the FTIR fractional denaturation onset and the onset is determined to be when the derivative is greater than zero after 37ºC [83]. Appendix Figure 49 from Qin, et al. shows a fractional denaturation curve being transformed into a derivative plot from which one may extract the onset of denaturation which is just where the derivative is greater than zero.

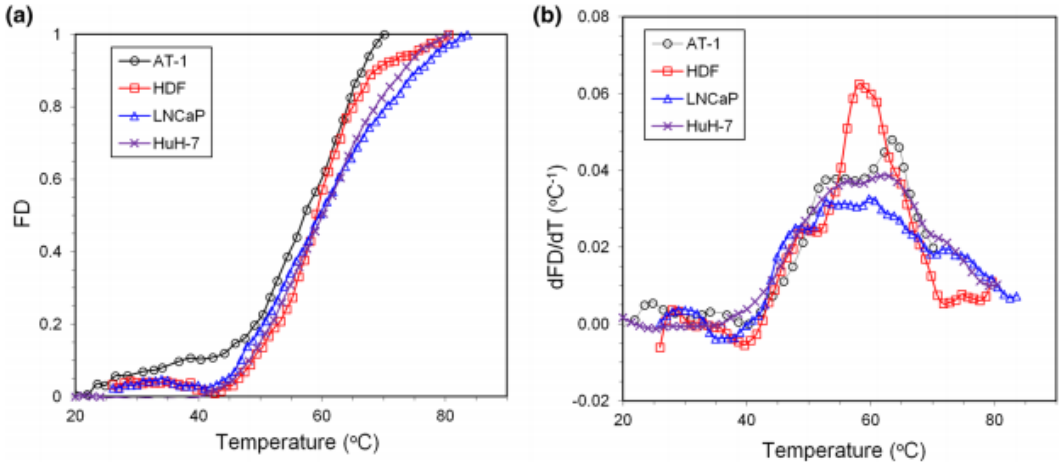

Appendix Figure 49: Panel (a) is the fractional denaturation (FD) curve. Panel (b) is the derivative of the beta-sheet formation with respect to temperature.

In Supplemental 1 of Qin, et al., Qin shows four examples of denaturation onset using the derivative method in Appendix Figure 50.

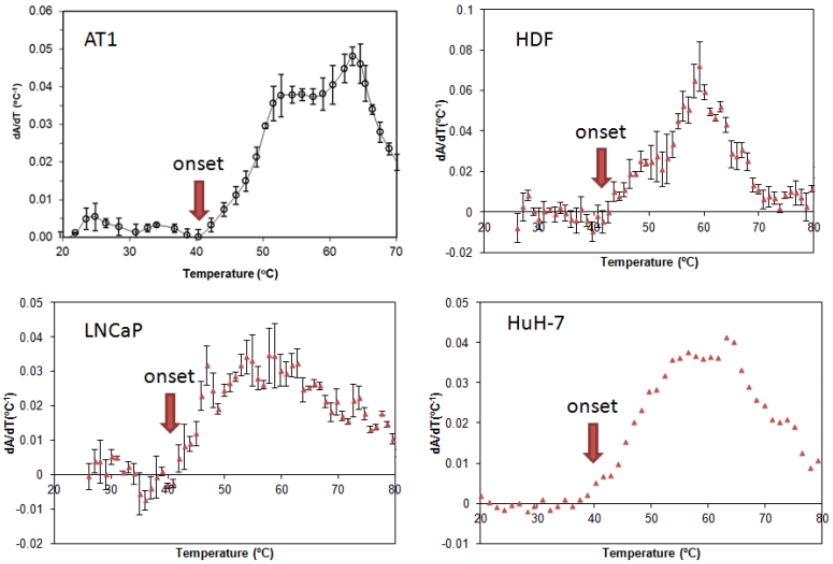

Appendix Figure 50: Denaturation onset determination via derivative method taken from Supplemntal 1 of Qin, et al.

3. DSC and FTIR Comparison

Both DSC and FTIR have been used as ways to calculate denaturation onset. This section will discuss how DSC and FTIR have been compared. Also, they hypothesis of this section is that it matters how you measure the denaturation onset depending on how one analyzes both FTIR and DSC.

3.1 Test Case 1: Wang, S. 2014. BBA Comparison of FTIR fractional denaturation with DSC scan

In this paper, Wang compares both FTIR and DSC seemingly by the tangent line method since this method yielded very close denaturation onset temperatures as to what was reported in the paper. For reference, the graph is shown below in Appendix Figure 51.

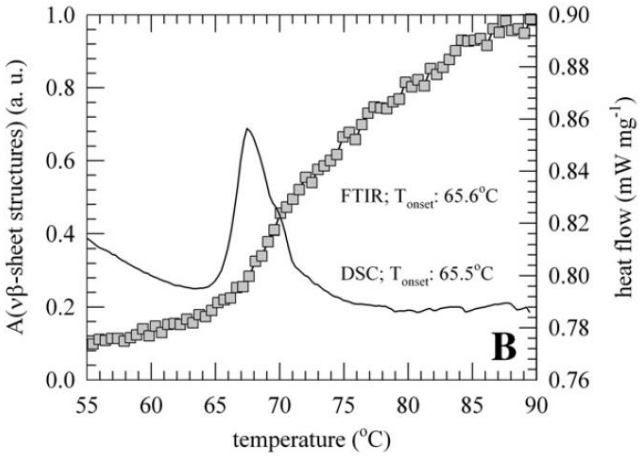

Appendix Figure 51: Comparison of FTIR fractional denaturation with DSC scan from Wang, S. 2014. BBA

The above figure claims a close relation between the denaturation onset coming from FTIR and DSC.

3.2 Test Case 2: He, X. 2004. ABME – Comparison of derivative of FTIR fractional denaturation with DSC scan

This paper keeps the DSC scan as in Section 3.1, but it takes the derivative of the FTIR curve with respect to temperature. This is shown below in Appendix Figure 52.

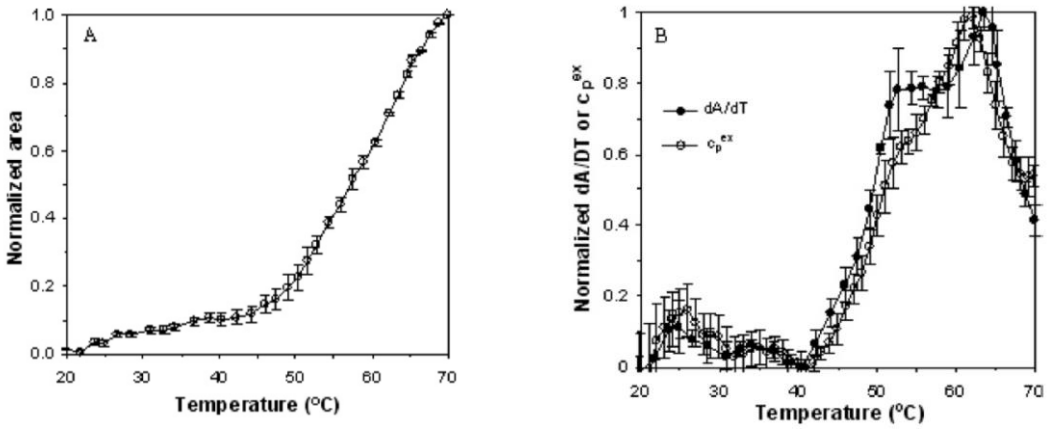

Appendix Figure 52: Panel (A) shows the fractional denaturation curve of FTIR. Panel (B) shows the derivative of fractional denaturation compared with the DSC scan. Both pictures are from He, X. 2004. ABME. The paper notes that the onsets are at 40.3ºC and 41.4ºC for the FTIR and DSC, respectively.

The paper says that the derivative of the fractional denaturation matches the excess specific heat scan quite well.

From the first test case, a comparison was made between FTIR fractional denaturation and DSC scan. Also, the second case compares the derivative of the fractional denaturation and the DSC scan. The next section will reverse the comparison for both cases and make denaturation comparison. So, the first case will be changed to the derivative of the FTIR fractional denaturation curve and the DSC scan. Furthermore, the second case will compare the FTIR fractional denaturation curve with the DSC scan.

3.3 Re-process of Test Case 1: Comparison of Wang, S. 2014 BBA data with He, X. 2004. ABME methods

This section will analyze the Wang data by the methods used by He in which He compared the derivative of fractional denaturation with the DSC scan. See Appendix Figure 53 below for the comparison of denaturation onset in Wang's analysis and He's analysis. Data was retrieved from Wang by use of PlotDigitizer, and the derivative was taken using a 9-point derivative factor from Savitzky & Golay.

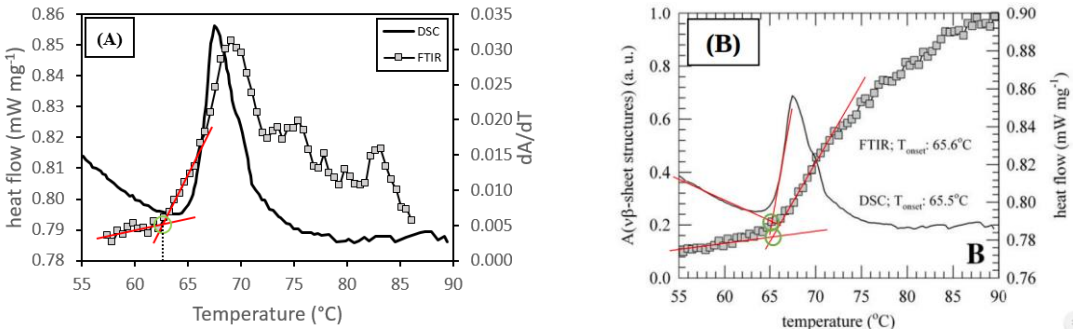

Appendix Figure 53: Panel (A) shows the Wang data processed how He, X. 2004. ABME processes it. Panel (B) shows the Wang processing. Using the derivative method for Panel (A), the denaturation onset for the FTIR changes from 65.6ºC in Panel (B) to ~62.5ºC in Panel (A).

The above graph illustrates how the denaturation onset changes by almost 3ºC (from 65.6ºC to 62.5ºC) depending on what method is used to determine the onset. The next section will re-analyze the He data by the methods used by Wang.

3.4 Re-process of Test Case 2: Comparison of He, X. 2004. ABME data with Wang, S. 2014. BBA methods

This section will analyze the He data by comparing the FTIR fractional denaturation curve with the DSC scan. The comparison is shown in Appendix Figure 54. Again, data was retrieved via PlotDigitizer.

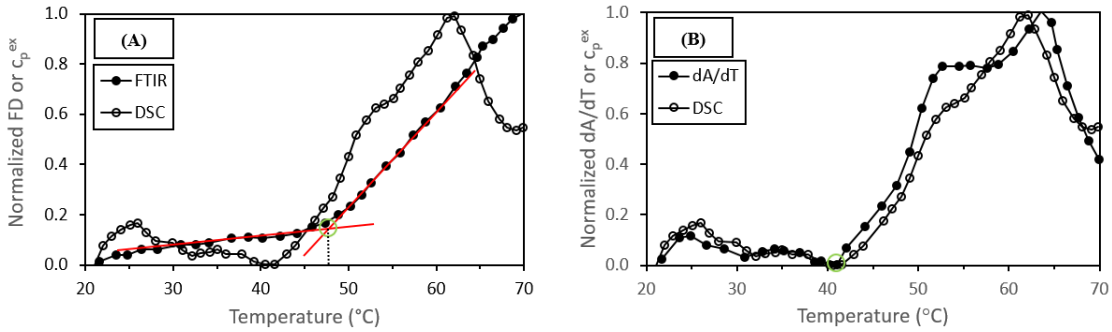

Appendix Figure 54: Panel (A) shows the denaturation onset comparison that is done in the Wang paper. Panel (B) shows the denaturation onset comparison that is done in the He paper. Panel (A) shows a denaturation onset of ~47.5ºC using the tangent line method for the FTIR whereas Panel (B) shows a denaturation onset of ~41ºC.

The above graph shows a starker contrast when processing the He data the way Wang does. The difference in denaturation onset is 6ºC between the respective methods.

3.5 Comparison of Miles rat tail tendon DSC data and FTIR rat tail tendon done here

The reason for doing all of this data processing came about when I was trying to compare my FTIR data on rat tail tendon with the literature, namely DSC work done by Miles in 1995. Appendix Figure 55 below compares two methods of analyzing the presented FTIR work in this paper with Miles DSC data.

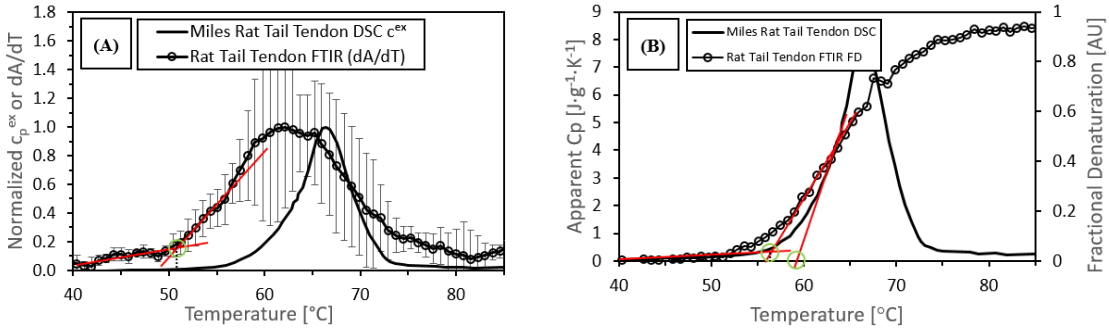

Appendix Figure 55: Panel (A) has the comparison that is done in the He paper. Panel (B) compares the data as presented in the Wang paper.

The data shown above in Appendix Figure 55 shows a contrast in the determination of denaturation onset. For example, Panel A gives an onset for the FTIR data of ~51ºC using the tangent line method. In Panel B, the denaturation onset is ~56ºC which is much closer to Miles onset of ~59ºC as calculated by the tangent line method.

Conclusion

This Appendix was to show that the way one processes data will change the denaturation onset temperature depending on how one processes the data, whether it be by using the derivative method or tangent line method.

APPENDIX J: Difference in Second Derivative Plots for Pressure Runs

Background:

Reporting fractional denaturation can be a bit misleading as denaturation onset is defined as an increase in β-sheet formation with a simultaneous decrease in α-helix formation [83].

Purpose:

The purpose of this appendix is to show how the inverse second derivative plots change when applying pressure to the sample. This will be shown by displaying what a normal second derivative plot looks like and contrasting it with those generated by pressure.

Inverse Second Derivative Plot: 0N Load with Heating Rate

For tissue with no load, the an example of the second derivative plot looks like the following in Appendix Figure 56.

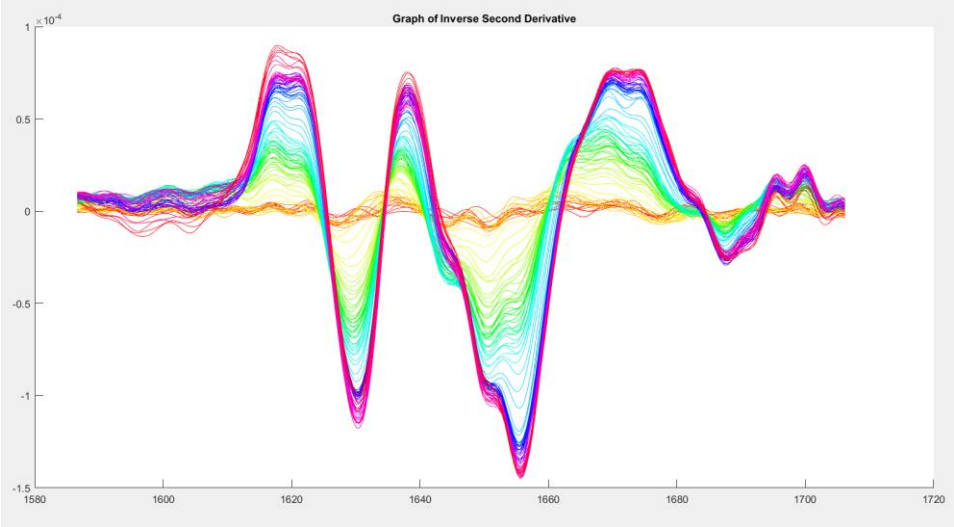

Appendix Figure 56: Inverse second derivative plot on Run 3 of July 16, 2015 which used carotid artery with no load. It should be noted that the primary β-sheet formation is centered at 1620cm^{-1}. Also, the α-helices is centered at 1650cm^{-1} [78].

Inverse Second Derivative Plot: 10N Load with Heating Rate

For tissue with 10N load with no thermocouple, a representative second derivative plot is shown below in Appendix Figure 57.

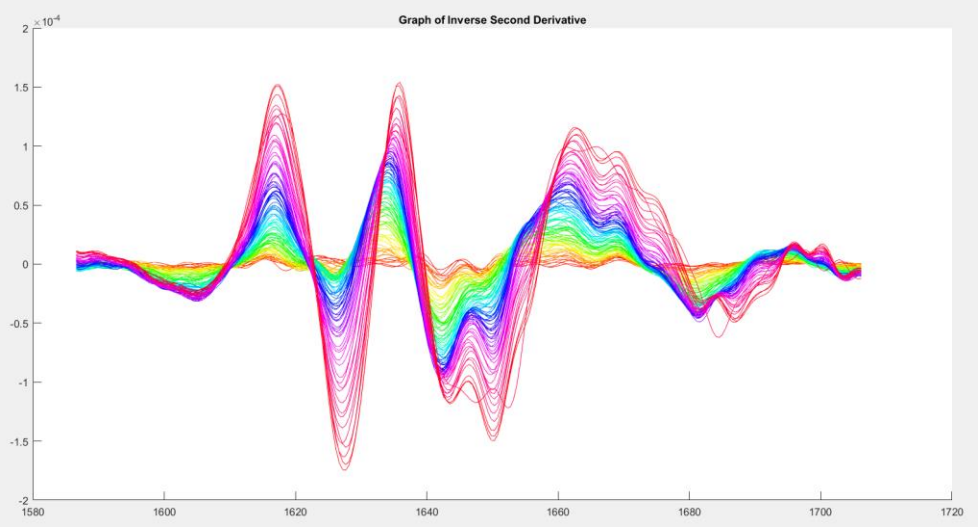

Appendix Figure 57: Inverted second derivative plot with 10N load on sample. This picture corresponds to Run2 on July 22nd, 2015. This plot looks similar to the 0N plot above as it has the similar curves centered at 1620cm^{-1} and 1650cm^{-1} which correspond to β-sheet and α-helics, respectively.

Inverse Second Derivative Plot: 20N Load with Heating Rate

Also, the second derivative plot of carotid artery with 20N of load is shown below in Appendix Figure 58.

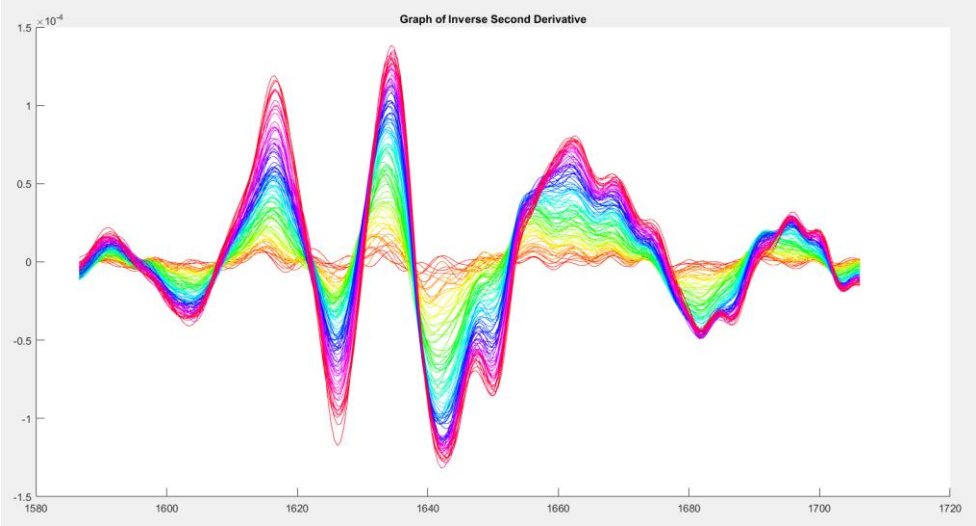

Appendix Figure 58: This plot corresponds to Run2 on July 24th, 2015. This plot of the second derivative of 20N is also similar to that of 0N and 10N which contains clearly defined curves centered at 1620cm^{-1} and 1650cm^{-1}.

Inverse Second Derivative Plot: 50N Load with Heating Rate

Also, tissue experiencing 50N of load with a heating rate is shown in Appendix Figure 59.

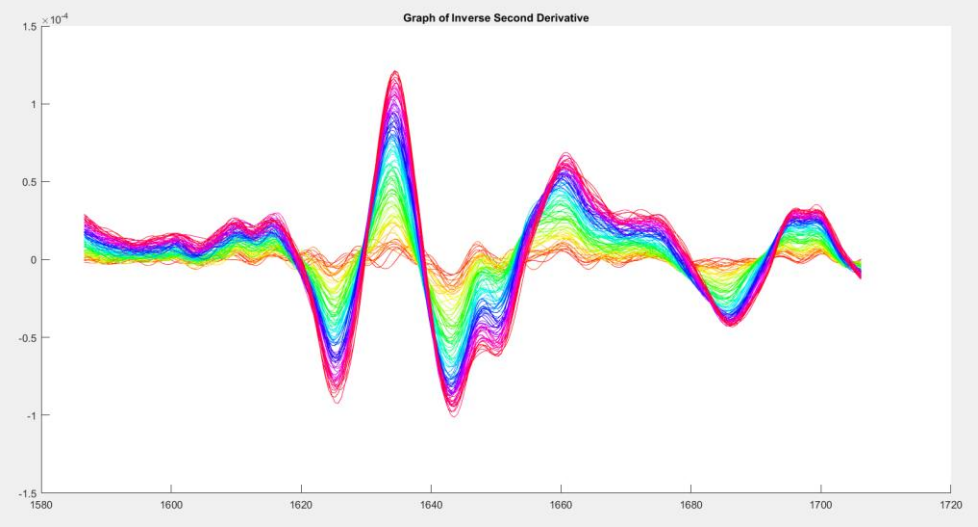

Appendix Figure 59: Inverse second derivative plot of 50N load with heating rate. This plot corresponds to Run1 of September 19th, 2015. This plot contains most of the familiar curves, but the curve centered at 1620cm^{-1} is at least half the size of the previous loads.

Inverse Second Derivative Plot: 0N Load with no Heat

Also, Appendix Figure 60 shows the inverse second derivative plot with 0N load and no heat applied.

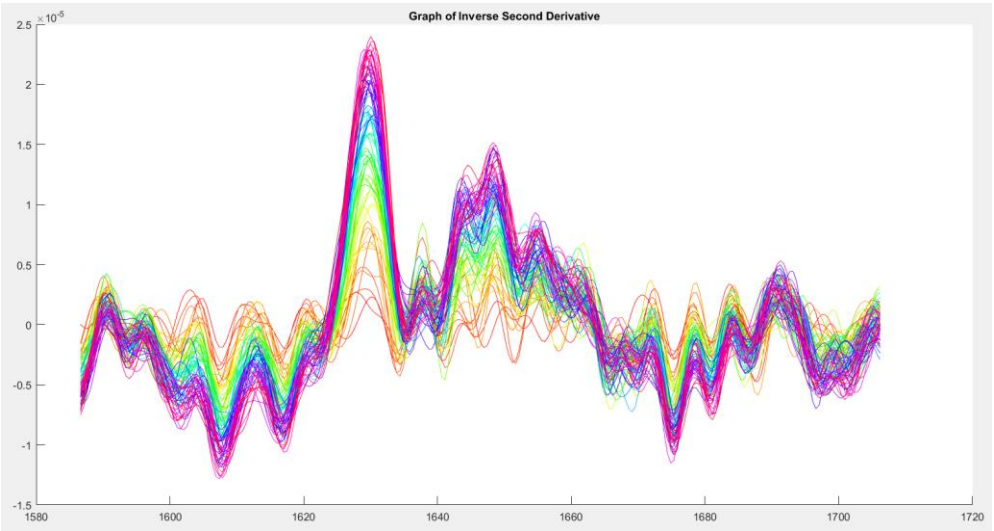

Appendix Figure 60: Inverse second derivative plot of 0N with no heat. This plot was Run 2 on August 20th, 2015. No distinguishable peaks are seen in the above graph to accurately determine any denaturation occurring.

Inverse Second Derivative Plot: 10N Load with no Heat

Next, the inverse second derivative plot of 10N load with no heat is shown in Appendix Figure 61.

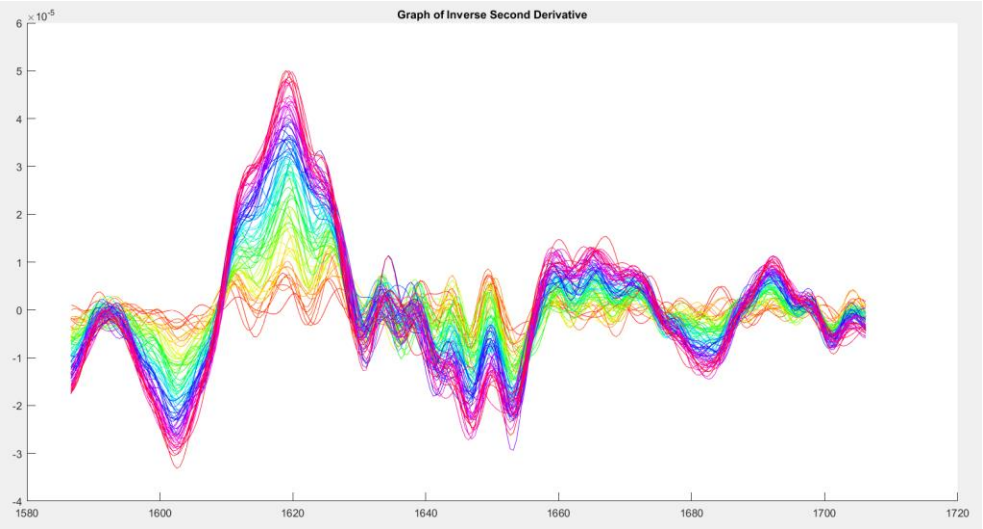

Appendix Figure 61: Inverse second derivative plot with 10N load with no heat. This plot was taken on Run1 on August 27th, 2015.

Inverse Second Derivative Plot: 20N Load with no Heat

Next, the inverse second derivative plot of 20N load with no heat is shown below in Appendix Figure 62.

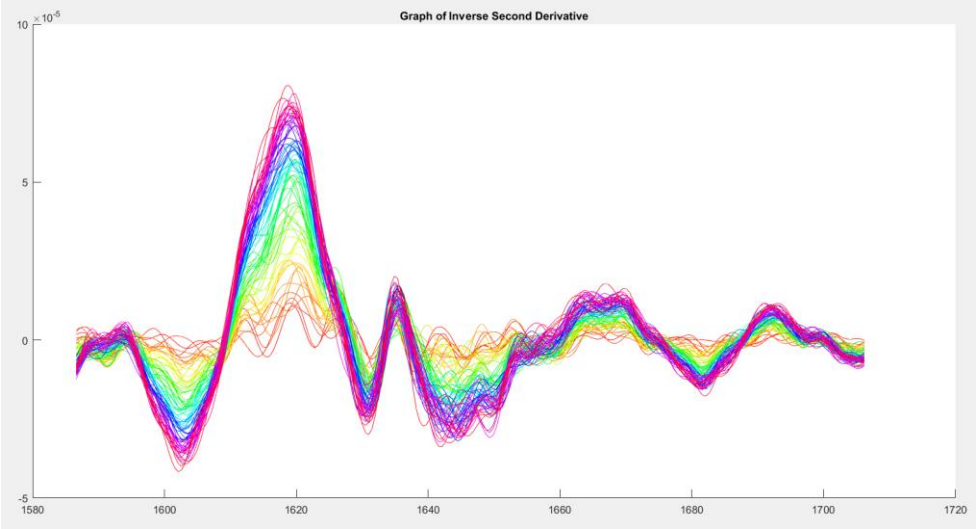

Appendix Figure 62: Inverse second derivative plot with 20N load with no heat. This plot was taken on Run2 on August 28th, 2015.

Inverse Second Derivative Plot: 50N Load with no Heat

Finally, the inverse second derivative plot was taken with a 50N load with no heat in Appendix Figure 63.

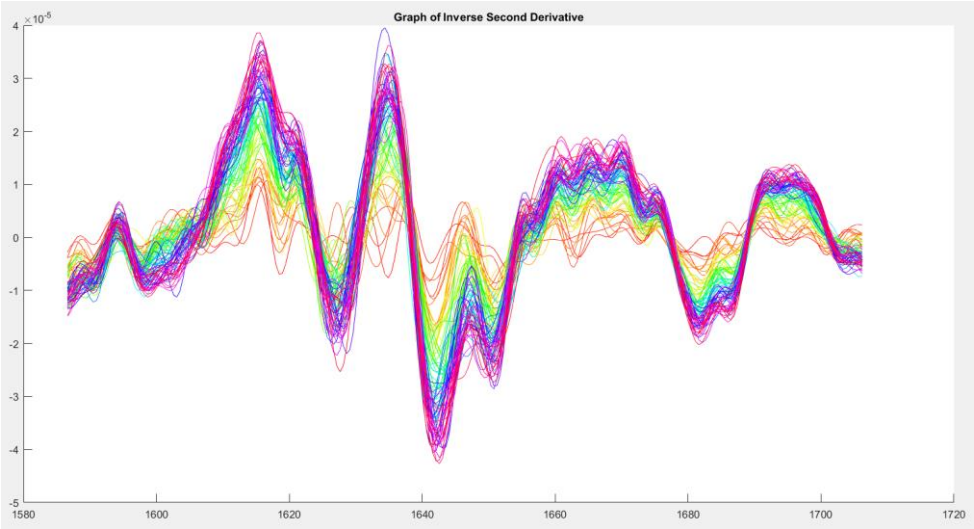

Appendix Figure 63: Inverse second derivative plot with 50N load with no heat. This plot was taken on Run2 on September 16th, 2015.

Conclusion:

This appendix is to show that the second derivative plots change depending if pressure or temperature is applied to the sample. With no pressure and temperature applied, the curves are barely distinguishable. However, one has to be careful in determining what qualifies for β-sheet to name the term fractional denaturation in a plot.

APPENDIX K: FTIR Point Measurement Timeline

Introduction: In order to determine the effects of pressure and temperature on tissue, FTIR with the ATR accessory was performed on tissue that went under treatments that were tested for mechanical strength as the 140ºC;50lb;30s, 140ºC;20lb;30s, 100ºC;50lb;30s, and 100ºC;20lb;30s.

Purpose: The purpose is to determine what molecular changes occur with the Thermal Jig treatments.

Timeline: The timeline started with measuring fresh tissue. After that, the thermal jig parameters were measured for comparison.

1. MAY 20 – 21, 2015: Fresh Measurements

Purpose:

The first set measurements was to measure how arteries looked fresh on FTIR spectra.

Protocol:

The arteries were harvested on May 18th and received on May 20th at UMN. Upon receiving arteries, they were soaked in D_2O at least one hour. For FTIR measurements, the arteries were measured under the following conditions:

- Wet with small force (2N)
- Blotted with small force
- Wet with large force (50N)
- Blotted with large force.

Also, the weight before and after blotting tissue was taken. Measurements were taken on May 20th – 21st.

Measurements Summary:

The protocol above was followed. More details can be found in Joel's Notebook III pages 53 – 57. Weight measurements and sample FTIR spectra is shown below in Appendix Figure 64.

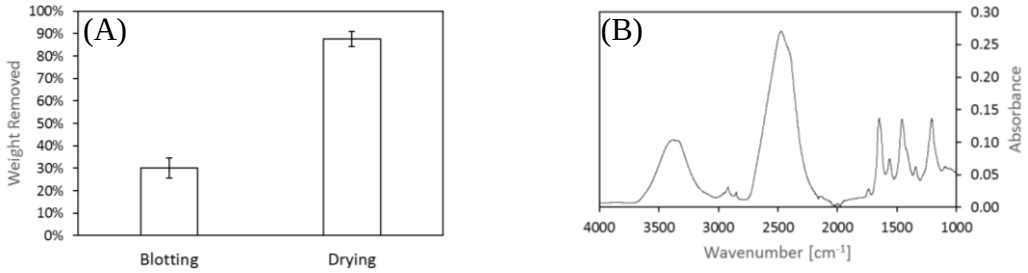

Appendix Figure 64: Panel (A) shows weight removed from blotting with ten (n = 10) samples compared to weight removed from drying tissues with four (n = 4) samples. Two

samples were completed on May 21st and two were completed on Feb 2nd. The drying details can be found in Joel's Notebook II on page 45 and Notebook III on page 58. Panel (B) shows a sample FTIR spectra of fresh blotted tissue under 2N of force.

Conclusions:

The weight reduction by blotting at 30.1 ± 4.4% is very similar to that measured when sealing arteries for burst pressure. Thus, the process seems to be similar. Next measurements will be of arteries subjected to treatment of 140ºC;50lb;30s.

2. MAY 22 – 23, 2015: 140ºC;50lb;30s and 100ºC;50lb;30s

Purpose:

The purpose of these measurements is to test arteries with ATR before and after fusion to see if any change is detected.

Protocol:

The arteries were harvested on May 20th and received on May 22nd. Testing was completed on May 22nd and 23rd.

Arteries were soaked in 0.9% w/v D_2O solution with NaCl for 1 hour. Test arteries on wet, blotted, and fused state. Each of this testing is done at a load of 2N to ensure the artery has proper contact with the crystal.

Measurement Summary:

Heaters were set to 150ºC. Ten (n = 10) arteries were sealed at 140ºC;50lb;30s and four (n = 4) arteries were sealed at 100ºC;50lb;30s. For 140ºC treatments, the temperature was measured with the temperature controllers, and the temperature was generally within 140 ± 3ºC for the whole run. For 100ºC treatments, the heaters were set to 100ºC, and the temperature was generally within 100 ± 4ºC for the whole run. Details on testing and weight measurements can be found in Joel's Notebook III on pages 59 – 64. Summary of data tested is shown below in Appendix Figure 65.

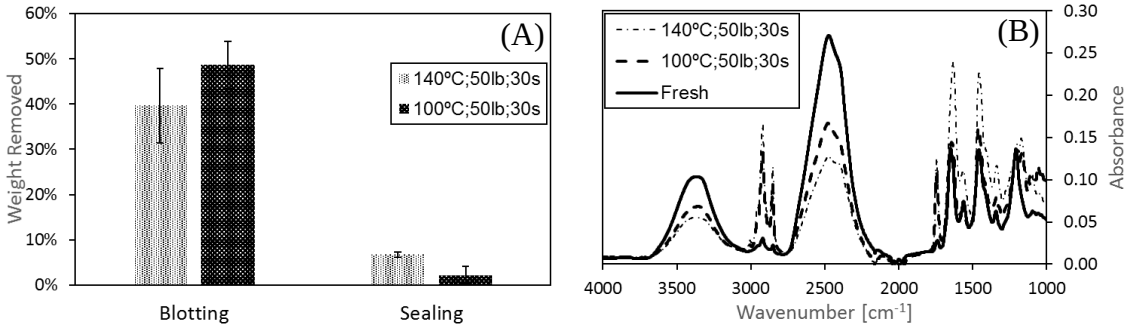

Appendix Figure 65: Panel (A) shows the summary of weight removal from blotting and sealing from treatments of 140ºC;50lb;30s (n = 10) and 100ºC;50lb;30s (n = 4). Panel (B) shows a representative spectra of fresh, 140ºC;50lb;30s, and 100ºC;50lb;30s FTIR spectra.

Conclusions:

From the weight measurements, more weight was removed from blotting under the 100ºC;50lb;30s treatment, but the difference was not significant. For the sealing, the weight removed was significantly higher under the 140ºC;50lb;30s treatment as compared to the 100ºC;50lb;30s treatment. Next measurements will focus on treatments of 140ºC;20lb;30s and 100ºC;20lb;30s.

3. MAY 28 – 29, 2015: 140ºC;20lb;30s, 100ºC;20lb;30s, 100ºC;50lb;30s

Purpose:

The purpose of these measurements is to test arteries with ATR before and after fusion to see if any change is detected.

Protocol:

The arteries were harvested on May 26th and received on May 28th. Testing was completed on May 28th and 29th.

Arteries were soaked in 0.9% w/v D_2O solution with NaCl for 1 hour. Test arteries on wet, blotted, and fused state. Each of this testing is done at a load of 2N to ensure the artery has proper contact with the crystal.

Measurement Summary:

Six (n = 6) arteries were sealed at 100ºC;20lb;30s, five (n = 5) arteries were sealed at 140ºC;20lb;30s, and five (n = 5) arteries were sealed at 100ºC;50lb;30s. For 140ºC treatments, the temperature was set to 150ºC. Temperature was initially at 145ºC. After 10s, the temperature settled down and stayed within 140 ± 3ºC for the whole run. For 100ºC treatments, temperature was initially at 95ºC. After 7s, the temperature stayed within 100 ± 4ºC for the whole run. Details on testing and weight measurements can be found in Joel's Notebook III on pages 65 – 70. Summary of data tested is shown below in Appendix Figure 66.

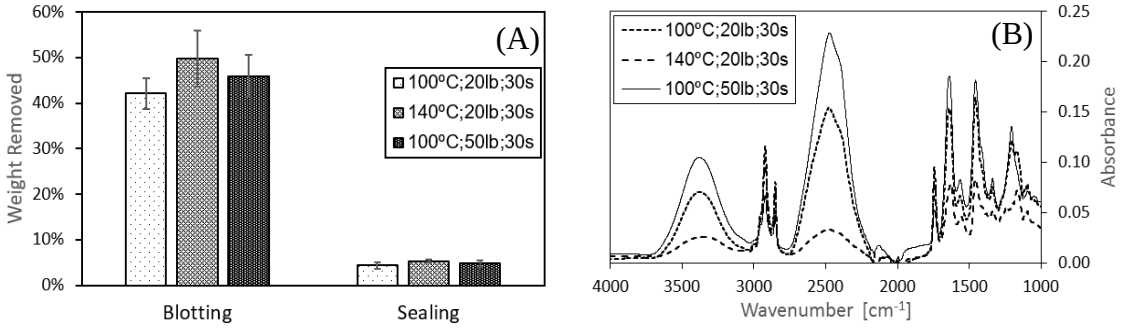

Appendix Figure 66: Panel (A) shows the weight removal by different sealing parameters in blotting and sealing with five (n = 5) samples for each artery as one sample from 100ºC;20lb;30s had weight data that did not make sense. Panel (B) shows a representative of the FTIR spectra of each treatment.

Conclusions:

For the weight removal, the blotting and sealing are similar for the three treatment levels. For the FTIR spectra, one can tell that a significant amount of water has been removed from the 140ºC;20lb;30s sample as the O-H stretch at 3300cm^{-1} is much lower than the other two treatments. More testing will be done to bring sample sizes to ten for each of the treatments.

4. JUN 10 – 11, 2015: 140ºC;20lb;30s, 100ºC;20lb;30s, 100ºC;50lb;30s

Purpose:

The purpose of these measurements is to increase the sample size of point measurements for parameters of 140ºC;20lb;30s, 100ºC;20lb;30s, and 100ºC;50lb;30s to ten.

Protocol:

The arteries were harvested on Jun 8th and received on Jun 10th. Testing was completed on Jun 10th and 11th.

Arteries were soaked in 0.9% w/v D_2O solution with NaCl for 1 hour. Test arteries on wet, blotted, and fused state. Each of this testing is done at a load of 2N to ensure the artery has proper contact with the crystal.

Measurement Summary:

Five (n = 5) arteries were sealed at 100ºC;50lb;30s, four (n = 4) arteries were sealed at 140ºC;20lb;30s, and three (n = 3) arteries were sealed at 100ºC;20lb;30s. For 140ºC treatments, the temperature was set to 150ºC. Temperature was initially at 145ºC. After 10s, the temperature settled down and stayed within 140 ± 3ºC for the whole run. For 100ºC treatments, temperature was initially at 95ºC. After 8s, the temperature stayed within 100 ± 3ºC for the whole run. Details on testing and weight measurements can be found in Joel's Notebook III on pages 71 – 77. Summary of data tested is shown below in Appendix Figure 67.

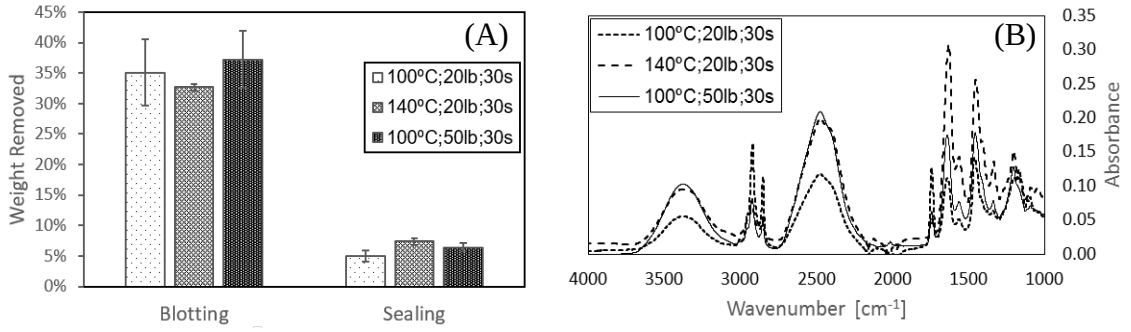

Appendix Figure 67: Panel (A) shows the amount of weight removed for the three sealing parameters for blotting and sealing. Panel (B) shows the representative spectra for each treatment.

Conclusions:

A few more samples need to be collected in order to fill the quota for 100ºC;20lb;30s and 140ºC;20lb;30s. Otherwise, latest testing suggests that the 140ºC;20lb;30s seems to remove more water from sealing than 100ºC;20lb;30s and 100ºC;50lb;30s. These results will have to be pooled with previous testing and test for statistical significance.

5. JUN 17 – 18, 2015: 140ºC;20lb;30s, 100ºC;20lb;30s, and 100ºC;30s

Purpose:

The purpose of these measurements is to finish the sample size of point measurements for parameters of 140ºC;20lb;30s and 100ºC;20lb;30s. Also, samples were tested by only applying constant temperature of 100ºC to the tissue without any weight except that of the top plate.

Protocol:

The arteries were harvested on Jun 15th and received on Jun 17th. Testing was completed on Jun 17th and 18th.

Arteries were soaked in 0.9% w/v D¬2O solution with NaCl for 1 hour. Test arteries on wet, blotted, and fused state. Each of this testing is done at a load of 2N to ensure the artery has proper contact with the crystal.

Measurement Summary:

One (n = 1) artery were sealed at 100ºC;20lb;30s, and one (n = 1) arteries were sealed at 140ºC;20lb;30s. For the temperature only measurements, five (n = 5) arteries were treated at 100ºC;30s. For 140ºC treatments, the temperature was set to 150ºC. The temperature stayed within 140 ± 3ºC for the whole run. For 100ºC treatments, temperature was initially at 94ºC. After 6s, the temperature stayed within 100 ± 3ºC for the whole run. Details on testing and weight measurements can be found in Joel's Notebook III on pages 78 – 81. Summary of data tested is shown below in Appendix Figure 68.

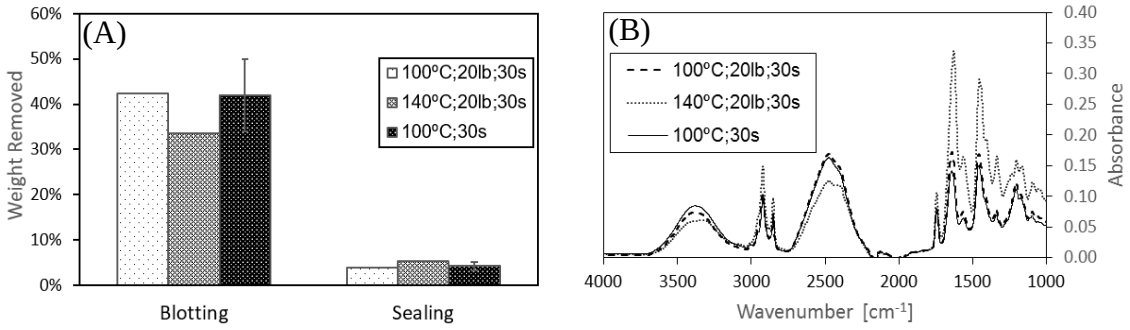

Appendix Figure 68: Panel (A) shows the weight removed from the three different treatment methods. Panel (B) shows representative spectra from each of the treatment methods.

Conclusions:

More data will be taken at temperature only settings.

6. JUN 19 – 20, 2015: 100ºC;30s and 140ºC;30s

Purpose:

The purpose of these measurements is to finish the sample size of point measurements for parameter of 100ºC;30s and start on parameter 140ºC;30s. These experiments were completed by treating the tissue without any weight except that of the top plate.

Protocol:

The arteries were harvested on Jun 17th and received on Jun 19th. Testing was completed on Jun 19th and 20th.

Arteries were soaked in 0.9% w/v D_2O solution with NaCl for 1 hour. Test arteries on wet, blotted, and fused state. Each of this testing is done at a load of 2N to ensure the artery has proper contact with the crystal.

Measurement Summary:

Five (n = 5) samples were tested for both the 100ºC;30s and 140ºC;30s parameter. For the 100ºC treatment, the temperature was initially at 96ºC. After 6 seconds, the temperature reached and stayed at 100 ± 3ºC. For the 140ºC treatment, the temperature was initially at 145ºC. After 15 seconds, the temperature reached and stayed within 140 ± 4ºC. More details can be found in Joel's Notebook III on pages 82 – 86. Summary of data tested is shown below in Appendix Figure 69.

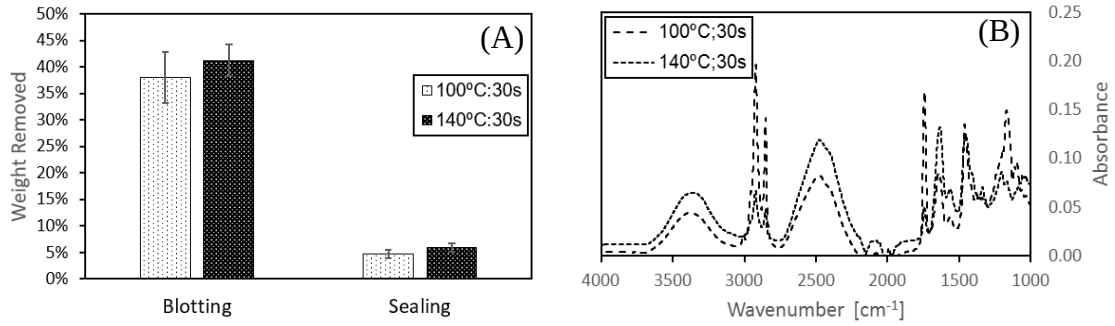

Appendix Figure 69: Panel (A) shows a summary of weight measurements coming from parameters 100ºC;30s and 140ºC;30s. Panel (B) shows example spectra from the treatment parameters.

Conclusions:

Only five more measurements need to be taken at the treatment level of 140ºC;30s. This will conclude the point measurements.

7. JUN 24, 2015: 140ºC;30s

Purpose:

The purpose of these measurements is to finish the sample size of point measurements for parameter of 140ºC;30s. These experiments were completed by treating the tissue without any weight except that of the top plate.

Protocol:

The arteries were harvested on Jun 22nd and received on Jun 24th. Testing was completed on Jun 24th.

Arteries were soaked in 0.9% w/v D2O solution with NaCl for 1 hour. Test arteries on wet, blotted, and fused state. Each of this testing is done at a load of 2N to ensure the artery has proper contact with the crystal.

Measurement Summary:

Five (n = 5) arteries were treated with 140ºC;30s. For the 140ºC treatment, the temperature was initially at 147ºC. After 12 seconds, the temperature reached and stayed at 140 ± 3ºC. More details are recorded in Joel's Notebook III on pages 87 – 89. Data results can be found in Appendix Figure 70.

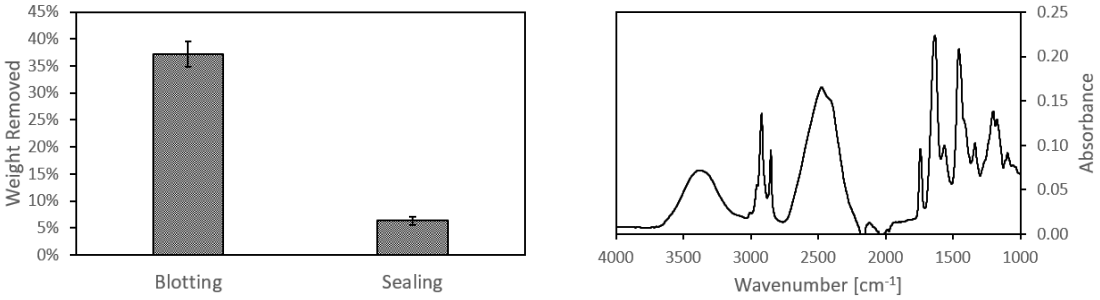

Appendix Figure 70: Panel (A) shows the weight data from 140ºC;30s with five samples. Panel (B) shows a representative spectrum.

Conclusions:

Combining all of the weight measurements, the comparison of weight loss can be seen in Appendix Figure 71 below.

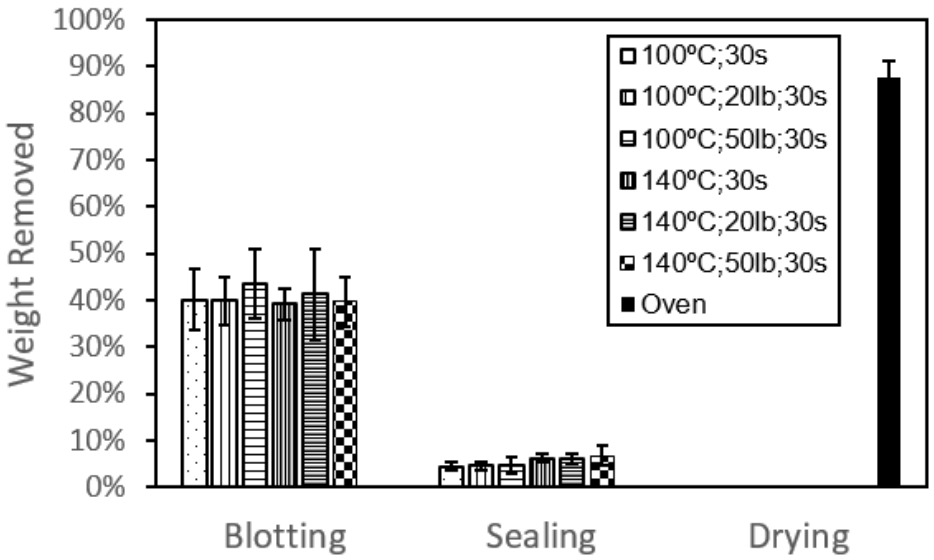

Appendix Figure 71: Summary of weight measurements with treatment parameters of 100ºC;30s (n = 10), 100ºC;20lb;30s (n = 9), 100ºC;50lb;30s (n = 14), 140ºC;30s (n = 10), 140ºC;20lb;30s (n = 10), 140ºC;50lb;30s (n = 10), and drying in the oven (n = 4).*)*